Contributions to indoor broadband power-line communications : channel modeling and data rate optimization

Kassim Khalil

Numéro d'ordre: 15/24

Université de Valenciennes et du Hainaut-Cambrésis

THÈSE DE DOCTORAT

présentée à

L'Université de Valenciennes et du Hainaut-Cambrésis

Pour l'obtention du grade de

DOCTEUR EN ÉLECTRONIQUE

École doctorale: Sciences Pour l'Ingénieur (SPI)

Laboratoire, Groupe de recherche: Institut d'Électronique, de Micro-Électronique et de Nanotechnologie/Département d'Opto-Acousto-Électronique (IEMN/DOAE), Groupe COMNUM

par

Kassim KHALIL

Contributions à l'étude des communications numériques sur le réseau électrique à l'intérieur des bâtiments : modélisation du canal et optimisation du débit

Soutenue le 7 juillet 2015 à Valenciennes, devant le jury composé de:

Rapporteurs:
- Thierry CHONAVEL, *Professeur, Télécom Bretagne*
- Fabienne UZEL-NOUVEL, *Maître de Conférences HDR, Université de Rennes*

Examinateurs:
- Hassan RABAH, *Professeur, Université de Lorraine* (président du jury)
- Nicolas GINOT, *Maître de Conférences HDR, Université de Nantes*
- Marc GAZALET, *Professeur, Université de Valenciennes*
- Mohamed GHARBI, *Maître de Conférences, Université de Valenciennes*

Directeurs de thèse:
- Patrick CORLAY, *Maître de Conférences HDR, Université de Valenciennes*
- François-Xavier COUDOUX, *Professeur, Université de Valenciennes*

Numéro d'ordre: 15/24

Université de Valenciennes et du Hainaut-Cambrésis

THÈSE DE DOCTORAT

présentée à

L'Université de Valenciennes et du Hainaut-Cambrésis

Pour l'obtention du grade de
DOCTEUR EN ÉLECTRONIQUE

École doctorale: Sciences Pour l'Ingénieur (SPI)

Laboratoire, Groupe de recherche: Institut d'Électronique, de Micro-Électronique et de Nanotechnologie/Département d'Opto-Acousto-Électronique (IEMN/DOAE), Groupe COMNUM

par

Kassim KHALIL

Contributions to indoor broadband power-line communications: Channel modeling and data rate optimization

Soutenue le 7 juillet 2015 à Valenciennes, devant le jury composé de:

Rapporteurs:
– Thierry CHONAVEL, *Professeur, Télécom Bretagne*
– Fabienne UZEL-NOUVEL, *Maître de Conférences HDR, Université de Rennes*

Examinateurs:
– Hassan RABAH, *Professeur, Université de Lorraine* (président du jury)
– Nicolas GINOT, *Maître de Conférences HDR, Université de Nantes*
– Marc GAZALET, *Professeur, Université de Valenciennes*
– Mohamed GHARBI, *Maître de Conférences, Université de Valenciennes*

Directeurs de thèse:
– Patrick CORLAY, *Maître de Conférences HDR, Université de Valenciennes*
– François-Xavier COUDOUX, *Professeur, Université de Valenciennes*

To my parents

Remerciements

En préambule, je souhaite adresser tous mes remerciements aux personnes qui m'ont apporté leur aide, qui ont ainsi contribué à l'élaboration de ce mémoire et m'ont soutenu depuis le début.

Tout d'abord, j'exprime ma profonde gratitude envers mes directeurs de thèse, Monsieur François-Xavier COUDOUX et Monsieur Patrick CORLAY, de m'avoir fait bénéficier de leurs expertises, pour leurs soutien sans faille, leurs aides précieuses, leur bonne humeur et leurs disponibilités.

Je remercie Monsieur Marc GAZALET pour sa contribution très importante à ce travail ainsi que pour la qualité de ses explications et son enthousiasme. Je tiens à remercier également Monsieur Mohamed GHARBI pour ses nombreux conseils, sa bonne humeur, sa disponibilité, et pour toute son aide.

Mes sincères remerciements s'adressent aussi aux rapporteurs Madame Fabienne UZEL-NOUVEL, Maître de Conférences HDR à l'INSA de Rennes et Monsieur Thierry CHONAVEL, Professeur à Telecom Bretagne, ainsi qu'aux examinateurs Monsieur Hassan RABAH, Professeur à l' Université de Lorraine et Monsieur Nicolas GINOT, Maître de Conférences HDR à l'Université de Nantes, qui m'ont fait le grand honneur d'évaluer ce travail.

Je tiens à remercier Hossep ACHDJIAN pour les bons moments partagés pendant toute la thèse et pour ses encouragements sans faille.

Un merci à Basma BOURAOUI pour la bonne ambiance du travail au bureau et les nombreux moments partagés.

Je tiens à remercier également Othmane ALAOUI pour les bon moments passés ensembles, pour son aide et son soutien.

Je remercie, de façon plus générale, tous les membres, les enseignants-chercheurs, les doctorants de l'IEMN-DOAE qui j'ai pu échanger et travailler; tout spécialement Khadija, Salah Eddine, Mourad, Yamen, Amina, Linda, Abedlmajid, Jamal, Karl, Kais, Sarah, Lamyae, Laid, Bada, Zeinab, Ali, Hassan, Sandy, Daher, Sélima, Sofiane.

Évidemment, ces remerciements ne seraient pas complets sans la mention de ma famille. Un grand merci à mes parents, ma mère Zeinab ROUMIEH et mon père Ibrahim KHALIL

pour m'avoir donné le goût des études, pour leur amour inestimable, leur confiance, leurs sacrifices et pour leur appui sans faille. Merci à mes frères et ma sœur pour leur complicité et leur présence malgré la distance qui nous sépare.

Table of Contents

Abstract

In recent years, the electrical network has become an essential candidate for high-speed data transmission inside buildings. Many solutions are currently underway in order to optimize these technologies known under the name of in-home Power-Line Communications (PLC). Multiple-Input Multiple-Output (MIMO) technique has recently been transposed into power-line networks for which different signal feeding possibilities can be considered between phase, neutral and earth wires. In this thesis, we propose two original contributions to indoor broadband PLC. The first contribution concerns the MIMO-PLC channel modeling. Based on a Single-Input Single-Output (SISO) parametric channel model presented in the literature, we propose a MIMO one by considering a new parameter which characterizes the spatial correlation. The proposed model enables an accurate description of the spatial correlation of European MIMO PLC field measurements. The second contribution is related to the impulsive noise present in power-line networks which constitutes a major problem in communications systems. We propose an outage capacity approach in order to optimize the average data rate in Orthogonal Frequency Division Multiplexing (OFDM) systems affected by impulsive noise. First, we study the channel capacity as a function of a noise margin provided to the transmitted symbols. Then we determine the analytical expression of the outage probability of an OFDM symbol in terms of the noise margin, by studying in detail the interaction between the noise impulse and the symbol. Based on the two aforementioned relations, we deduce the outage capacity. Then we propose an approach that enables to maximize the average system data rate. Finally, we present the results in the particular case of indoor broadband PLC in the presence of impulsive noise.

Résumé

Au cours de ces dernières années, le réseau électrique est devenu un candidat incontournable pour la transmission de données à haut débit à l'intérieur des bâtiments. De nombreuses solutions sont actuellement à l'étude afin d'optimiser ces technologies connues sous le nom Courants Porteurs en Ligne (CPL) ou PLC (Power-Line Communications). La technique MIMO (Multiple-Input Multiple-Output) a été tout récemment transposée au réseau filaire électrique pour lequel différents modes d'alimentation peuvent être envisagés entre la phase, le neutre et la terre. Dans le cadre de cette thèse, nous proposons deux contributions originales à l'étude des communications numériques sur le réseau électrique à l'intérieur des bâtiments. La première contribution concerne la modélisation du canal MIMO-PLC. En repartant d'un modèle du canal paramétrique SISO (Single-Input Single-Output) connu dans la littérature, nous proposons un modèle du canal MIMO en considérant un nouveau paramètre caractérisant la corrélation spatiale. Le modèle proposé permet de représenter fidèlement la corrélation spatiale des mesures effectuées à l'échelle européenne. La deuxième contribution concerne le bruit impulsif présent sur le réseau électrique domestique qui constitue un problème majeur dans les systèmes de communications. Nous proposons une méthode basée sur la notion de capacité de coupure afin d'optimiser le débit moyen dans les systèmes OFDM (Orthogonal Frequency Division Multiplexing) soumis aux bruits impulsifs. D'abord, nous étudions la capacité du système en fonction d'une marge de bruit fournie aux symboles transmis. Ensuite, nous déterminons l'expression analytique de la probabilité de coupure (outage) d'un symbole OFDM en fonction de cette marge, en étudiant de manière détaillée l'interaction entre l'impulsion de bruit et le symbole. A partir de ces deux calculs, nous déduisons la capacité de coupure. Puis, nous proposons une approche qui maximise l'espérance mathématique du débit reçu. Finalement, nous présentons les résultats obtenus dans le cas particulier d'une transmission à haut débit sur PLC en présence de bruits impulsifs.

List of Figures

List of Tables

Acronyms

AWGN Additive White Gaussian Noise

BER Bit Error Rate

BG Bernoulli Gaussian

CDF Cumulative Distribution Function

CIR Channel Impulse Response

CM Common Mode

CTF Channel Transfer Function

DSL Digital Subscriber Line

DFT Discrete Fourier Transform

EHF Extremely High Frequency

FEC Forward Error Correction

FFT Fast Fourier Transform

HD High Definition

HD-PLC High-Definition Power-Line Communication

HPAV HomePlug AV

HF High Frequency

IEEE Institute of Electrical and Electronics Engineers

i.i.d. Independent and identically distributed

IFFT Inverse Fast Fourier Transform

ITU International Telecommunication Union

ITU-T International Telecommunication Union - Telecommunication Standardization Sector

KS Kolmogorov-Smirnov

LAN Local Area Network

MAC Medium Access Control

MIMO Multiple-Input Multiple-Output

MTL Multiconductor Transmission Line

MF Medium Frequency

N Neutral

OFDM Orthogonal Frequency Division Multiplexing

P Phase

PDF Probability Density Function

PE Protective Earth

PLC Power-Line Communications

PSD Power Spectral Density

PHY Physical layer

QAM Quadrature Amplitude Modulation

RCS Ripple Carrier Signaling

RX Receiving socket

SHF Super High Frequency

SISO Single Input Single Output

SVD Singular Value Decomposition

SLF Super Low Frequency

SNR Signal-to-Noise Ratio

THF Tremendously High Frequency

TWACS Two-Way Automatic Communications System

TX Transmitting socket

UHF Ultra High Frequency

UPA Universal Powerline Association

ULF Ultra Low Frequency

UNB Ultra Narrowband

VHF Very High Frequency

VLF Very Low Frequency

WF Water Filling

Introduction

Power-Line Communication (PLC) is a technology that enables delivering information over existing power cables which are originally designed for electrical power transmission. PLC systems are now being developed as an alternative to conventional wireless and wired communication systems, because of its low cost, widespread presence and flexibility of use. Over the years, having started from very low bit rate applications, such as home automation and automatic meter reading, PLC has emerged as a potential solution for in-home broadband communications. Today's broadband PLC technologies can support data rates up to 1 Gbps [1]. However, the power-line medium has not been devised for communication purposes and constitutes a challenging environment for reliable and high-speed data communications. It is characterized by several differences from other wired media such as high channel attenuation, high noise level and the presence of various loads (of different impedances) that are connected to the in-home outlets giving rise to a random aspect which needs to be well characterized. These challenges have recently made this technology a hot topic in communication area.

The power-line channel is very harsh and noisy transmission environment that is very difficult to model. It is frequency-selective, time varying and is impaired by colored background noise and impulsive noise. In addition, the structure of the electrical grid differs from country to country and also within a country and the same applies for indoor wiring practices [2]. A complete PLC channel consists of the Channel Transfer Function (CTF) and channel noise. An accurate description of CTFs for PLC network topologies is of great interest and importance in the development and testing of digital communication algorithms. However, the considerable variability of PLC networks makes this task quite difficult. Therefore, one of the main challenges is to model the PLC CTFs. In this regard, a random CTF generator for a Single-Input Single-Output (SISO) configuration has been presented in the literature [3]. The procedure was applied to a set of measured channels that were interestingly divided into nine classes in [4] according to their channel capacities. On the other hand, a characterization of the channel noise has been presented in the literature where five classes of additive noise are distinguished [5]. Among these additive noises, the asynchronous impulsive noise is the most

detrimental one since it may occur at irregular intervals and contains considerable energy. It drastically affects high-speed communications, in such a way that complete symbols or even bursts of symbols cannot be decoded by the receiver. Another challenge, therefore, is to provide reliable communications in the presence of such kind of noise.

The ever growing demand for high speed data services has led to the emergence of Multiple-Input Multiple-Output (MIMO) techniques in PLC systems. MIMO communication is used in systems provided with multiple transmission and reception antennas, with the aim of increasing data rates and communications reliability. The applicability of MIMO signal transmission in PLC networks arises from the fact that in most developed countries the domestic electrical wiring is made up of three wires, namely the Phase (P), Neutral (N) and Protective Earth (PE). The conventional PLC systems use only the P-N port obtained from P and N wires to transmit and receive data, and are called SISO systems. If the unused PE wire is utilized, the three wires can form three transmission and reception ports P-N, P-PE and N-PE to create MIMO-PLC communication. Over the past few years, many investigations have been undertaken relating to the MIMO techniques in PLC, and large-scale measurement results on MIMO power-line channel have become available. Notably, in [6], a detailed channel analysis of a MIMO-PLC system from a measurement campaign conducted in six European countries covering the frequency range up to 100 MHz has been presented.

In this thesis, we propose original contributions to the channel modeling and data rate optimization for indoor broadband power-line communications. The contributions are twofold. First, we propose a MIMO random CTF generator for indoor broadband PLC based on the aforementioned SISO configuration. We consider a MIMO channel as the superposition of correlated SISO channels so we attempt to describe a MIMO channel using the nine classes obtained with the SISO configuration. An additional parameter, related to the correlation factor, has to be taken into account. We show that when this parameter is obtained from probabilistic distribution with properly chosen standard deviations for each of the nine classes, the European MIMO PLC field measurements can be accurately reproduced by the random channel generator.

Second, we propose an outage capacity approach in order to optimize the average data rate in OFDM systems affected by impulsive noise, and more specifically by asynchronous impulsive noise. To this end, we first study the channel capacity of OFDM systems affected by impulsive noise, by adding a noise margin (or useful power reserve) to the transmitted symbols. The system declares an outage if the energy of the impulsive noise contained in an OFDM symbol exceeds the added noise margin. Then, by studying in detail the overlap between the noise impulse and the symbol, we determine the analytical expression of the outage probability of an OFDM symbol in terms of the noise margin. From these two calculations, we deduce the outage capacity of the system. Based on the obtained

outage capacity, we further propose an approach that enables to determine the optimal noise margin required to maximize the average data rate. As a particular case, we consider the characteristics of impulsive noise specific to indoor broadband PLC. We show that the optimal noise margin is zero. This means that, from an information theory point of view, the maximum average data rate is achieved if none of the impulsive noise affected symbols are recovered.

The remainder of this thesis is organized as follows: Chapter 1 presents a brief introduction of indoor broadband MIMO PLC, the context of our study. The state-of-the-art study on the CTF and channel noise characterization and modeling approaches is presented in Chapter 2. Based on the SISO random CTF generator presented in the literature, Chapter 3 proposes an extension to MIMO one. In Chapter 4, we first illustrate the detrimental effect of impulsive noise on the BER system performance. Then, we present an information theory-based approach in order to ensure maximum data rate transmission in OFDM systems affected by impulsive noise, and its application to indoor broadband PLC. Finally, we conclude and give some perspectives for future work.

CHAPTER 1

Broadband Indoor MIMO Power-Line Communications

1.1 Introduction

In-home (indoor) power-line networks are attracting a great deal of attention since they offer an interesting compromise between wireless and wired network solutions. In fact, using existing home power lines for data transmission enables a ubiquitous broadband network to be exploited offering potentially robust, viable, high-speed and cost-effective solutions. Moreover, power-line communications can benefit from new digital signal processing and communication techniques to increase the transmission efficiency. Recently, MIMO technology has been applied to PLC with the aim of increasing the channel capacity, by making use of the PE wire in addition to the P and N wires.

This chapter provides a brief introduction to broadband indoor MIMO PLC systems, the context of our study. Firstly, a brief historical development of PLC is provided. Then, an overview on PLC systems is presented. Finally, MIMO for PLC is investigated which will further constitute a basic subject of this thesis.

1.2 Brief Historical Development of PLC

Like most of the innovations where the necessity is the underlying reason of their existence, the need of better controlling, maintaining and protection of the electrical power grid were important drivers for the appearance of PLC. In fact, the ability to transmit the information across the same pair of wires as are used for electrical power distribution grid has long been a goal. The idea of PLC has a long history that started from the early 1900s, when the first patents were made in this area [7–10]. Since that date, utility companies around the world have been using this technology for remote metering and load control, using at first narrowband PLC solutions operating in low frequency band (from 9 to 140 kHz) that achieved data rates ranging from few hundred bps to a few kbps [11]. Since the 1920s, the carrier-frequency transmission of voice has begun over high-tension lines for the purpose of operations management, monitoring and limitation, and removal of failures [9]. Since the 1930s, the Ripple Carrier Signaling (RCS) has been used over the medium and low-voltage lines to control peak events at demand side by issuing control signals to switch off heavy duty appliances [9]. This solution has been quite successful, especially in Europe, so it has been extended to include other applications related to "home automation" that allow controlling various in-home devices like illumination, heating, elevator, and so on. Overall, several innovative schemes related to remote transmission over power lines were made from early 1900s to 1980s, mainly due to the enormous evolution of electronics. By the late 1980s and early 90s, sophisticated error control coding techniques were proposed and implemented in a PLC modem hardware [7].

The tremendous revolution of digital communications in the 1990s, combined with the evolution of internet and related services and the developments in electronics have played an important role in renewing and increasing the interest in PLC [7]. Indeed, the high cost of the traditional access networks, which represent approximately 50 % of the investments in the total network infrastructures [12], presented PLC as a serious alternative technology for telecommunication service delivery for the so-called "last mile" connectivity, denoted as "access PLC", as the infrastructures already exist. Access PLC networks can be realized using the medium and low-voltage power lines that feed homes as transmission medium, and can be used as a Local Area Network (LAN). This last application of the PLC technology is referred to as indoor PLC. As a result, indoor broadband PLC appeared as a response to the growing need of high speed communications over power lines, which can achieve significant higher data rates compared to those offered by the narrowband PLC systems.

Despite the main advantages inherent in indoor broadband PLC technology, it faces a number of serious challenges related to the harsh nature of the power-line medium. These challenges have recently made this technology a hot topic in communication area. Since the late 1990s, an increased effort has been put into characterization of PLC channels [13]. As a result, an international symposium dedicated to PLC was established in 1997; this is the International Symposium on Power-Line Communications and its applications (ISPLC), which became an official conference of the Institute of Electrical and Electronics Engineers (IEEE) communication society in 2006 [2]. Moreover, more and more tracks on the subject of PLC have emerged in several well-known international electrical engineering conferences (e.g. global communication conference). Simultaneously, an increased attention has been put from both the industry and research community to develop specifications and a global standard for high-speed communication over the power cables. Nowadays, indoor broadband PLC are specified by the standards that will be discussed in Section 1.4.

1.3 An Overview on PLC Systems

PLC is a technique that allows the transfer of digital information through the classical power lines. It profits from the already installed power-line infrastructures for data communication purposes. After years of development, the technology to deliver high-speed data over the existing electric power distribution grid has emerged. This technology is referred to as broadband PLC which uses medium- and low-voltage power lines to provide telecommunication services (data, Internet, telephone, fax, etc) to individual subscribers in homes or businesses. In fact, PLC technologies have exploited a wide available frequency band, which can be grouped according to the International Telecommunication Union (ITU) into ultra-narrow-, narrow- and broad-bands, and which will be discussed in Section 1.3.3. The principle of functioning of broadband PLC is based on modulating low-energy/high-frequency data signals to the alternating electric current and transmitting them through the same wire that carry the low frequency electricity to buildings. Data signals thus propagate over the electrical installations and can be received and decoded remotely.

As PLC uses the electrical installations as transmission medium, it is of interest to provide an overview of the electrical installation networks in terms of operation voltages of power lines. The electrical power systems can be divided into three voltage levels as illustrated in Figure 1.1:

- High voltage power-lines, with voltages in the range from 110 to 380 kV, form a long-distance electric energy transportation network. They serve for the long-distance transport of energy from the power station to the big customer, and are usually implemented

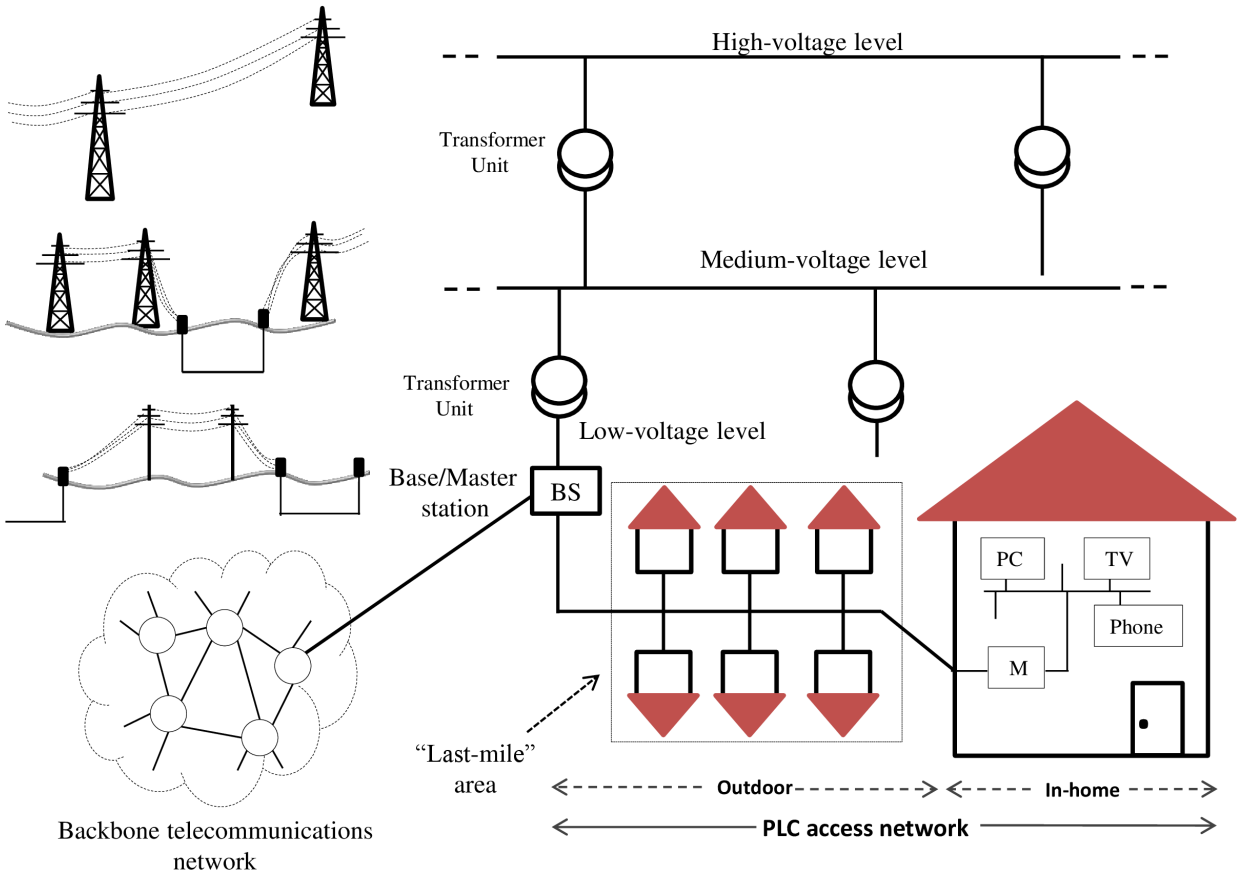

FIGURE 1.1: Structure of power supply and PLC access networks derived from [12].

in the form of three-phase current overhead lines.

- Medium voltage power-lines, with voltages in the range from 10 to 30 kV, bring electrical power into cities, towns, and villages. They can span distances from 5 to 25 km, and are realized as both overhead and underground networks.
- Low voltage power-lines, with voltages from 110 to 400 V, ensure the final distribution to customer premises over distances up to a few hundred meters. Low voltage networks are also implemented as both overhead in rural areas and underground in urban areas.

The three power-line levels are interconnected to each other by means of transformers, designed in such a way that the energy loss is as low as possible at the frequency (50 or 60 Hz).

Broadband PLC systems fall into two broad categories: in-home PLC systems and last-mile (or access PLC) systems (see Figure 1.1). Access PLC uses electrical transmission lines to deliver high-speed broadband services from service suppliers to homes and offices. On

the other hand, in-home PLC applications occur within a single building (house, apartment block or office building) and use the power grid inside the building as a LAN. Initially, considerable attention has been given to the utilization of low-voltage distribution lines as a last-mile technology. However, strong competition from Digital Subscriber Lines (DSL) and cable services has discouraged the deployment of outdoor PLC systems in most developed countries. Paradoxically, this high penetration of DSL services has encouraged the emergence of indoor PLC. In the following, further details on the PLC access networks and in-home PLC networks will be provided.

1.3.1 PLC Access Networks

PLC access networks are low-voltage power supply networks used for data transmission for the last mile access. An example of the architecture of the PLC access network is depicted in Figure 1.1, which mainly consists of a transformer unit and a number of power supply cables that connect the end users to the low-voltage network. The transformer unit allows the interconnection of the low-voltage network with medium- and high-voltage networks. In order to be able to convey telecommunication data, PLC last mile access has to be connected to backbone telecommunication networks by the means of base/master stations that may provide several communication interfaces with various backbones technologies such as DSL, optical fiber networks, etc. The PLC subscribers are connected to the low-voltage network via an electrical power meter unit, denoted "M" in Figure 1.1 or plug to any in-home socket in the electrical network. In the first case, the subscribers within a house or a building are connected to the PLC modem using another communications technology such as DSL and wireless local area networks. In the second case, the in-home electrical installation are used as a LAN, which is referred to in-home PLC technology.

1.3.2 In-home PLC Networks

In-home PLC systems use the already existing electrical infrastructure inside a home as data transmission medium. In this way, the in-home backbone connecting all digital electronic devices within a private house (or flat) can be used as a PLC LAN. This exploitation enables new and highly convenient networking functioning without needing additional cables. Typical devices existing in private homes such as computers, high definition (HD) TVs, telephones, video devices, console games, printers, and so on can be connected and communicate via an access point to the PLC network. Nowadays, in-home PLC technology can be considered as one of the best solutions for providing home automation services like automatic light control, security observation and heating control [12].

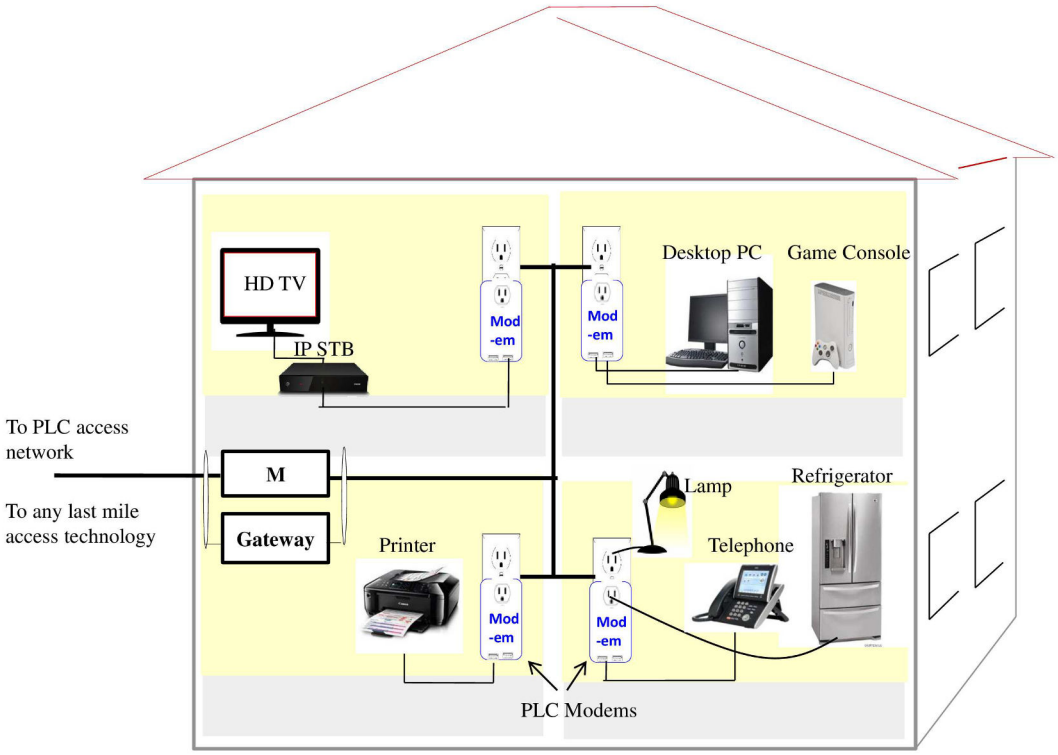

FIGURE 1.2: Typical structure of an in-home PLC network.

A typical structure of an in-home PLC network is depicted in Figure 1.2. As can be seen from the figure, the network devices are connected via PLC modems, which are connected directly to the wall power supply sockets (outlets). In-home PLC networks can be connected to a PLC access network profiting from additional metering services such as remote meter reading and energy management. It can also be connected to any last mile access technology allowing the end users to profit from liberalized telecommunication market [12]. A gateway (see Figure 1.2) is used to separate between the in-home PLC network and the PLC access network avoiding problems related to the different natures of the two networks. In addition, it allows the communication between in-home PLC modems, and between the internal devices and the outdoor PLC network.

1.3.3 PLC Frequency Bands

As agreed upon by the ITU, the frequency bands can be represented as in Figure 1.3, where the band name abbreviations stand for super low, ultra low, very low, low, medium, high, very high, ultra high, super high, extremely high and tremendously high, respectively. PLC technologies, until now, have exploited a wide available frequency band to enable low- and high-speed data transmission over the power lines. They can be grouped into three

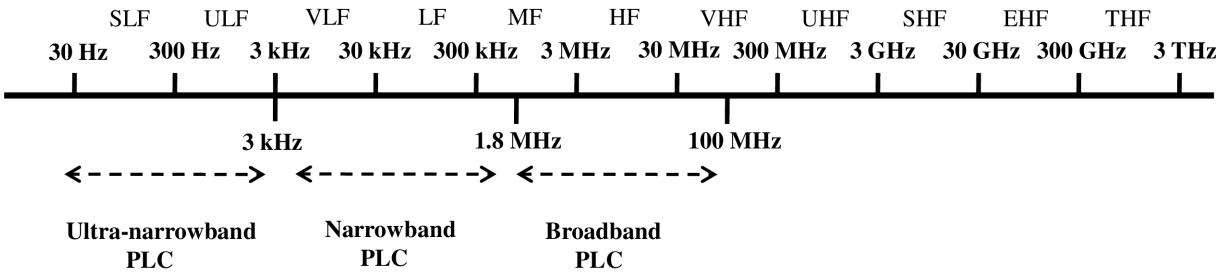

FIGURE 1.3: ITU frequency bands and their usage in PLC.

categories according to the data transmission band as shown in Figure 1.3 [11, 13]:

1. Ultra Narrowband (UNB)-PLC technologies which offer very low data rate (<100 bps) in the ULF ($0.3-3$ kHz) band or in the upper part of the SLF ($30-300$ Hz) band. An historical example of UNB-PLC is the RCS. More recent examples are the automatic meter reading, turtle system and the Two-Way Automatic Communications System (TWACS).

2. Narrowband (NB)-PLC technologies operate in the VLF/LF/MF bands (3-500 kHz), which include the European comité européen de normalization ($3-148.5$ kHz) band, the U.S. federal communications commission ($10-490$ kHz) band, the Japanese association of radio industries and businesses ($10-450$ kHz) band and the Chinese ($3-500$ kHz) band [13]. Two subgroups can be distinguished from NB-PLC technologies:

   a) Low data rate: includes single carrier modulation-based technologies that offer data rates of a few kbps. Examples of these technologies are devices conforming to the following recommendations: International Organization for Standardization (ISO)/International Electrotechnical Commission (IEC) 14908-3 (also known as LonWorks), IEC 61334-3-1, Insteon, X10, HomePlug C&C, SITRED, Ariane Controls etc.

   b) High data rate: involves technologies that offer data rates ranging between tens of kbps and around 500 kbps. These technologies are today based on Orthogonal Frequency Division Multiplexing (OFDM). Typical examples of these technologies are those devices included in the family of the ongoing standard projects: International Telecommunication Union - Telecommunication Standardization Sector (ITU-T G.hnem), IEEE 1901.2, Powerline Related Intelligent Metering Evolution (PRIME) and G3-PLC.

3. Broadband (BB)-PLC technologies operate in the MF/HF/VHF bands (1.5-250 MHz)

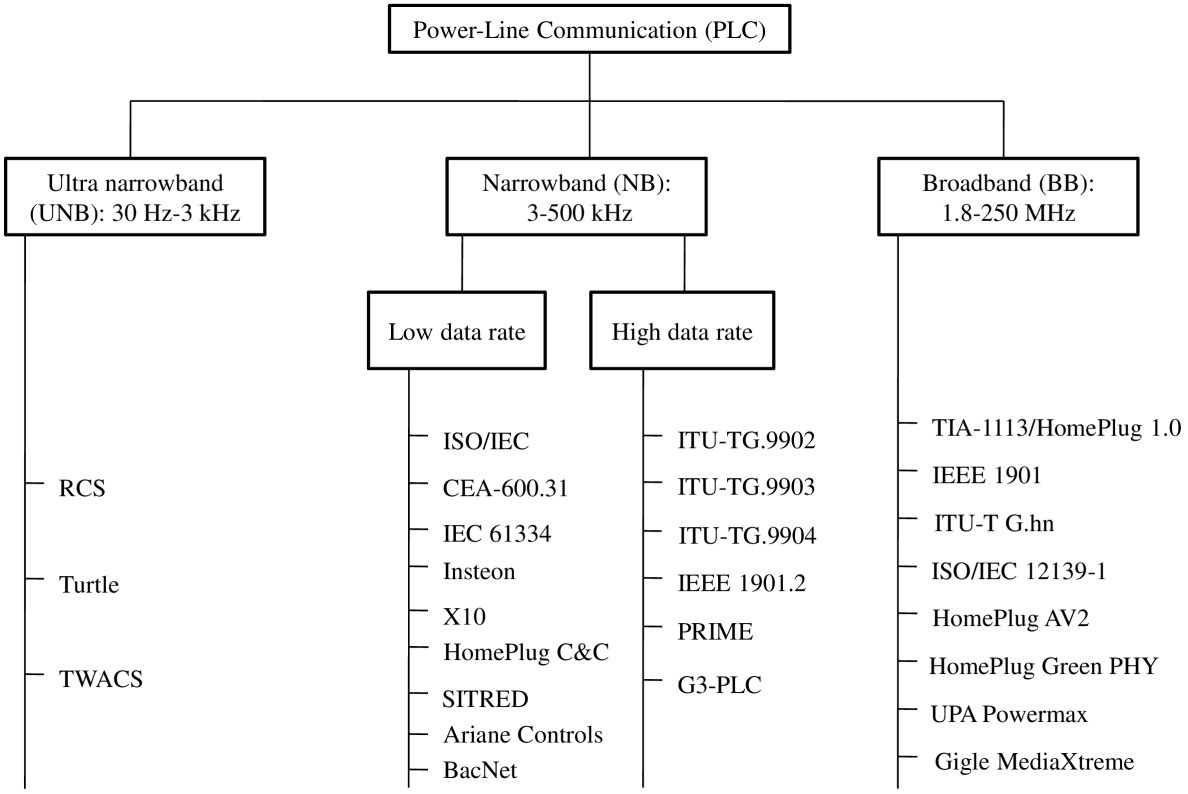

FIGURE 1.4: Overview of the UNB-, NB- and BB-PLC standards and specifications derived from [13].

with physical layer (PHY) data rates ranging from several Mbps to several hundred of Mbps. Typical examples BB-PLC technologies are devices conforming to the TIA-1113 (HomePlug 1.0), IEEE 1901, ITU-T G.hn (G.9960/G.9961), HomePlug AV2, HomePlug Green PHY, Universal Powerline Association (UPA) Powermax, and Gigle MediaXtreme.

Many efforts have been made in order to standardize communications over power lines, notably by the IEEE and the ITU-T. An overview of the UNB-, NB- and BB-PLC standards and specifications is depicted in Figure 1.4 [13]. In the next section, we will give an overview of the latest standardization efforts in IEEE and ITU-T on broadband PLC, the context of our study.

1.4 Broadband PLC Specifications and Standards

With the growing interest in broadband communication over power lines, several industrial groups have been involved in the development and the standardization of broadband

PLC products. In the last decade, broadband PLC chipsets came to the market are mainly based on specifications supported by consortia such as the HomePlug Powerline Alliance (HomePlug), the HomeGrid Forum, the UPA and the High-Definition Power-Line Communication (HD-PLC) Alliance. The chips operate in the band from around 2 to 86 MHz, and in some cases, optionally up to 300 MHz, and allow data rates around 200 Mbits [13].

In order to ensure that the broadband PLC systems are widely successful, the IEEE and the ITU-T started work on such next-generation standards, namely the IEEE 1901 [14] and ITU-T G.hn [15], respectively. The HomePlug and the HomeGrid Forum played a significant role in the development of these standards. Next, we provide a brief summary of the major discussion groups and the proposed specifications, as well as the standards.

HomePlug Powerline Alliance

An industrial organization that now comprises more than 75 companies, was formed in 2000 to set up specifications for indoor broadband communications over power lines, and presently covers the access networks and the command and control of home platforms. Until now, it has released three specifications for broadband in-home PLC [16]. The first release of HomePlug in June 2001, called HomePlug 1.0.1, with raw data rates up to 14 Mbit/s, was followed in July 2005 by a second release called HomePlug AV (HPAV) [17] (the letters "AV" stand for "Audio-Video"). The HPAV system, supporting raw data rates up to 150 Mbit/s, employs adaptive OFDM over a bandwidth from 1.8 to 30 MHz. To meet market needs, the HomePlug published in 2012 the HomePlug AV2 specification (HPAV2) which delivers gigabit-class bandwidth, while remaining fully interoperable with the other HomePlug technologies [18]. The HPAV2 defined new features at both PHY and medium access control (MAC) layers that improved the performance of AV2 power-line modems by improving coverage and robustness of communication links. We report some of the new PHY-layer features as follows [18]:

- MIMO signal processing, by considering the three available electrical wires for communications.
- Additional frequency spectrum from 30 to 86 MHz beyond the frequency used for HomePlug AV.
- Higher-order quadrature amplitude modulation (QAM) (up to 4096-QAM) and higher code rates (8/9 code rate).

HomeGrid Forum

HomeGrid Forum [19] was formed to promote a home network technology family of standards developed under the ITU-T, namely G.hn. The initial phase was to contribute to the development of the ITU standards, and educate the market about the potential of G.hn. This Forum supports the adoption and deployment of a new generation of local networks based on different types of home wires such as telephone wiring, coaxial cables and power lines. It ensures the compliance and interoperability between the wired medium technologies.

HD-PLC

HD-PLC [20] was established in September 2007 as an alliance of voluntary groups. It aims to expand the use of the HD-PLC technology and to improve communication compatibility among products employing HD-PLC. Adoption of HD-PLC is increasingly promoted as a number of companies have already launched HD-PLC-based products, such as Panasonic, Sony, Mitsubishi [20].

Universal Powerline Association (UPA)

UPA Alliance founded in 2004 has about twenty members and aims to promote the PLC technology in the world of telecommunication. It released specifications related to three aspects of PLC technology: the UPA coexistence specification, the UPA access specification, and the UPA digital home specification v1.0 [21]. In 2010, the UPA suspended its activities due to financial problems.

IEEE 1901

In 2005, the IEEE communication society lunched the IEEE 1901 programme to develop a global standard for high-speed communication over power lines. The IEEE 1901 standard was finally approved and published in December 2010. It uses HomePlug AV as baseline technology but extends the bandwidth up to 50 MHz, allowing up to 500 Mbps data rates at the physical layer. In addition to the Fast Fourier Transform (FFT) OFDM scheme used in HPAV networks, the IEEE 1901 defines, as an option, an alternative modulation technique, called wavelet OFDM defended by the HD-PLC consortium. The FFT-PHY layer uses 1974 carriers between 1.8 and 50 MHz with a carrier spacing of 24.414 kHz. The use of frequencies greater than 30 MHz is optional. Certain carriers in the range $1.8 - 30$ MHz are used for amateur radio broadcasts leaving 917 active carriers that can be used for data transmission [13].

ITU-G.hn

In 2006, the ITU-T commenced work on the G.hn standards to develop a next-generation home networking technology with transceiver capable of operating over any wired medium within homes such as co-axial, phone lines and power lines. The development of Gh.n are HomeGrid forum backed specifications, which includes the following ITU-T standards [13]:

- G.9960: specifies the G.hn's PHY layer, was approved at the end of 2008;
- G.9961: specifies the G.hn's data link layer, was approved in June 2010;
- G.9963 (G.hn MIMO): includes MIMO for PLC, was approved in December 2011.

G.hn standards use the OFDM modulation where the parameters such as the number of subcarriers and subcarrier spacing are defined per each media (power lines, phone lines or coaxial cables). For example, in the context of PLC, three transmission bands with a frequency spacing of 24.4140625 kHz are specified: bandwidth of 25 MHz with 1024 subcarriers, 50 MHz with 2048 subcarriers, and 100 MHz with 4096 subcarriers.

1.5 MIMO for PLC

MIMO technology constitutes a major step in the design of wireless communication systems, and is already at the core of several wireless standards such as IEEE 802.11n, WiMAX and LTE [22,23]. By exploiting additional spatial channels, MIMO techniques deliver significant performance enhancements in terms of data transmission rate and interference reduction. Compared to their related SISO solutions, they can offer a fundamental increase in the channel capacity without requiring additional transmit power or bandwidth. SISO communication utilizes a single channel for data transmission, whereas a MIMO system is composed of M transmitters and N receivers and exploits $N \times M$ spatial channels, as shown in Figure 1.5. The additional channels, which can be exploited using techniques such as space-time coding, enable more reliable and high-speed communication.

The power-line channel has long been regarded as a SISO channel based on two conductors. However, by utilizing the three-wire installations exist in many countries worldwide, MIMO techniques can also be applicable in PLC.

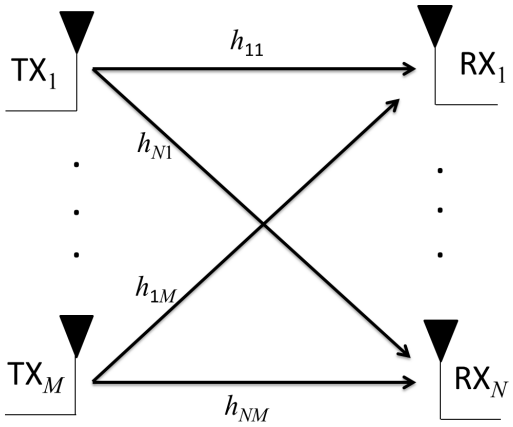

FIGURE 1.5: A MIMO communication system.

1.5.1 SISO PLC Channel

PLC systems available today are called SISO since they use only a single transmission channel between two outlets. This is the differential-mode channel between the phase (or live) and neutral wires, as illustrated in Figure 1.6. Figure 1.7 presents an example of real CTF (magnitude) of a SISO PLC link in the frequency range up to 100 MHz [24]. As can be noted from the figure, the PLC channel is highly frequency-selective. For details on the PLC channel characterization, please refer to Chapter 2.

The encoding scheme which is used by most of the broadband PLC providers to modulate high data rate signals over the power lines is OFDM. OFDM modulation divides a high data rate stream into multiple low data rate streams that are then transmitted at different frequencies to the receiver. Indeed, the basic idea of OFDM is to divide the available spectrum into several orthogonal subchannels (or subcarriers) that are sufficiently flat compared to the channel coherence bandwidth. In this case, each subcarrier can be modulated separately which makes OFDM robust against frequency-selective fading scenarios (and also narrowband interference) due to simple channel equalization. In the following, a theoretical background on the capacity of broadband SISO PLC channels is given.

We consider a broadband PLC signal of a set of frequencies in the range $[f_{min}, f_{max}]$. OFDM technique transforms a frequency-selective channel into a large number of independent Additive White Gaussian Noise (AWGN) subchannels. For a SISO channel transmission composing of one feeding (transmitting) port and one receiving port, the relation between the received signal $r(f)$ and transmitted signal $s(f)$ is given by:

$$r(f) = h(f)s(f) + n(f), \tag{1.1}$$

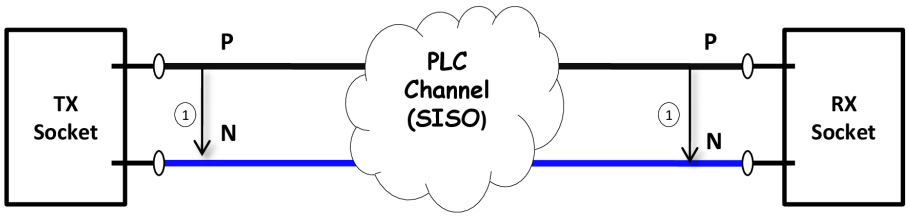

FIGURE 1.6: SISO-PLC channel.

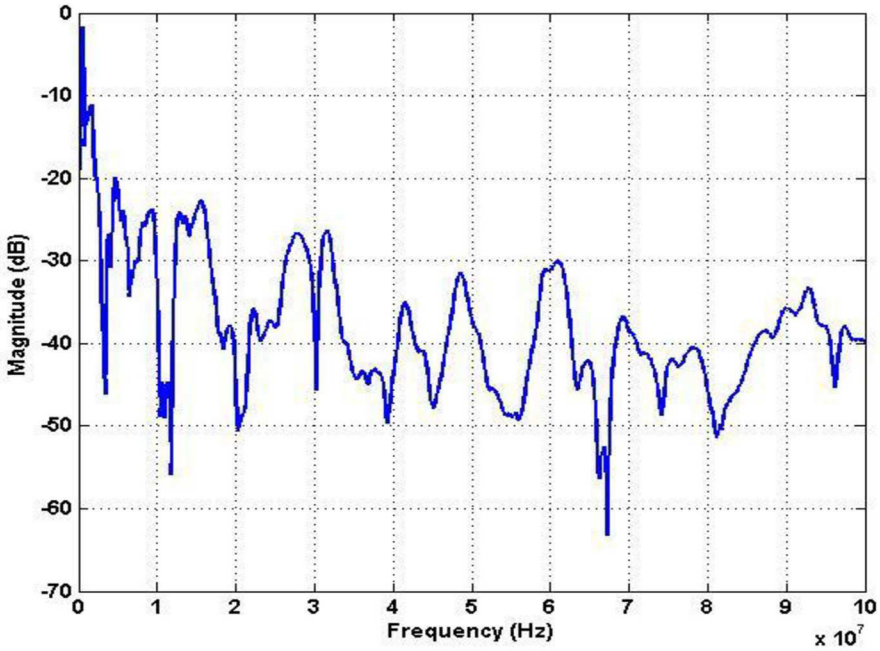

FIGURE 1.7: Measured SISO PLC CTF [24].

where $h(f)$ is the SISO CTF defined for all frequencies f and $n(f)$ represents the received noise. Based on Shannon's theory [25], theoretical limits of data rates over AWGN channels can be computed. The capacity of a single-carrier SISO channel with a Signal-to-Noise-Ratio (SNR) γ, denoted as C_{SISO}, is given by:

$$C_{SISO} = B \cdot \log_2(1+\gamma) \quad [\text{bits/s}], \tag{1.2}$$

where B is the signal bandwidth in Hz. In the case of multi-carrier (OFDM) transmission with L carriers defined at frequencies from f_1 to f_L with subcarrier frequency spacing Δf, Eq. (1.2) becomes:

$$C_{SISO} = \Delta f \cdot \sum_{k=1}^{L} \log_2(1 + \gamma(f_k)) \quad \text{[bits/s]}. \tag{1.3}$$

For a given Power Spectral Density (PSD) $P(f)$ in W/Hz and a noise PSD $N(f)$ at the receiver defined in W/Hz, Eq. (1.3) can be further detailed as

$$C_{SISO} = \Delta f \cdot \sum_{k=1}^{L} \log_2 \left(1 + \frac{P(f_k)|h(f_k)|^2}{N(f_k)}\right) \quad \text{[bits/s]}. \tag{1.4}$$

The optimum power allocation of the subcarriers that maximizes the channel capacity is achieved by the well-known waterfilling (WF) algorithm. Further details on WF algorithm is given in Chapter 4, where an outage capacity approach for impulsive noise-affected OFDM systems is proposed.

Despite high channel attenuation and severe multipath effects, the channel capacity limit calculated for indoor broadband PLC, taking only the background noise into consideration, promises very high data rates over these channels [26–29].

1.5.2 MIMO PLC Channel

The availability of three wires, namely P, N and PE, in the power-line infrastructure in European countries, the U.S., and many other countries worldwide gives rise to MIMO technology that can also be applied to PLC. Utilizing the three electrical wires provides more feeding and receiving options. Figure 1.8 shows the PLC-MIMO channel for three-wire installations with differential signal feeding between the wires. MIMO are applicable due to the fact that signals transmitted from one pair of wires are visible on the three possible receiving pairs of wire. This is due to crosstalk between adjacent wires caused by the electromagnetic coupling. Three different feeding options are available: P-N, N-PE and P-PE. However, the sum of the three transmitted signals must be equal to zero, in accordance with Kirchhoff's rule. Thus only two out of the three possibilities can be used independently. On the receiving side, due to parasitic components in couplers, the third possibility and an additional fourth possibility, which is the common mode (CM) path, are available and contribute additional performance [18, 30]. In fact, unbalanced parasitic capacities from installations or devices to ground cause a CM current returning to the source. Thus, CM signals are created unintentionally in unbalanced networks. The CM reception path could be used at devices equipped with a large metal plate like the backplane of today's HD-TV screens [31]. If the MIMO-PLC receiver is able to sense CM signals, the MIMO channel matrix expands to a 2×4 MIMO system. Figure 1.9 illustrates CTFs (magnitude) measured

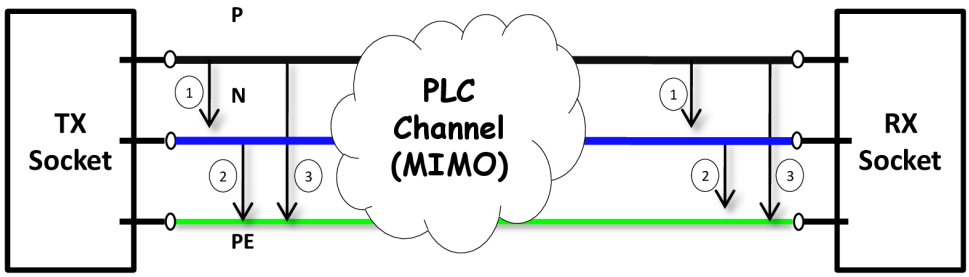

FIGURE 1.8: MIMO-PLC channel.

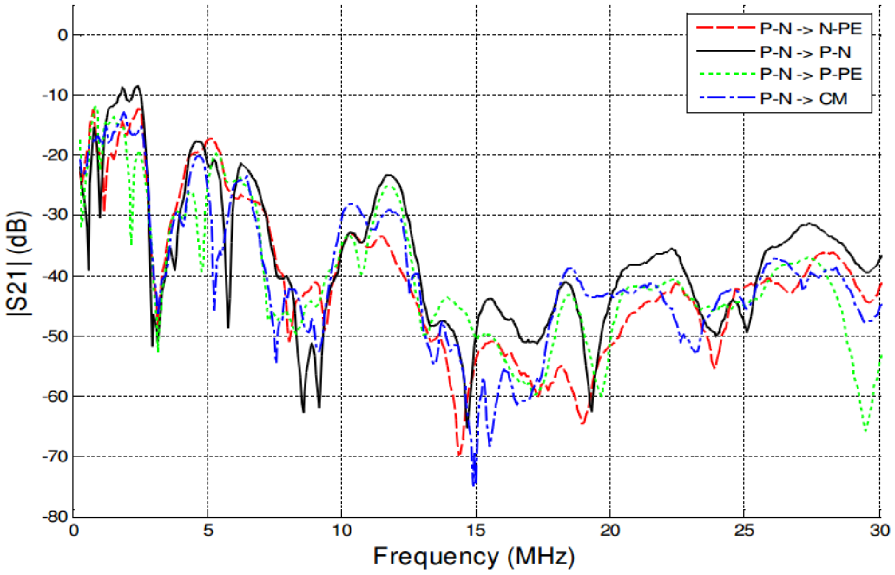

FIGURE 1.9: Measured MIMO PLC CTF [32].

in [32], where the P-N path is chosen as feeding port and the signal is measured at all possible receiving ports. Due to crosstalk between adjacent wire, the signal transmitted from the P-N port (or any feeding port) is visible on the three receiving ports, as well as the CM. The CTF shapes in Figure 1.9 are similar due to the strong coupling between the individual paths.

Figure 1.10 depicts a MIMO-PLC channel configuration with P, N and PE, as well as a schematic coupler design at the transmitter and receiver. Coupling devices used to transmit and receive the PLC signal are not independent from the channel characteristics. MIMO couplers should be designed in such a way as to produce as little additional coupling between the three wires as possible to ensure the maximum diversity between the MIMO paths. Two MIMO coupler options, namely the triangular and star coupler styles, are presented in Figure1.10:

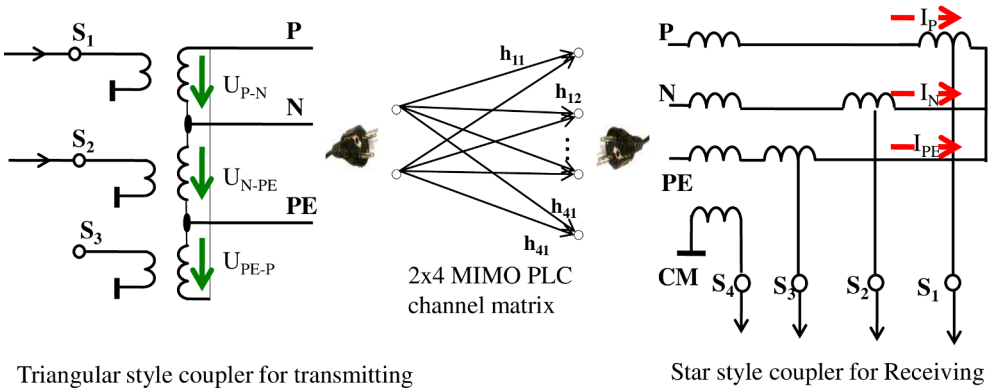

FIGURE 1.10: MIMO PLC channel: different feeding and receiving options.

- *Star style coupler for receiving*
  The star probe (or longitudinal coupler) has the benefit of providing a simple way to measure the CM signals. The sum of the currents I_P, I_N and I_{PE}, added at the center of the star probe (see figure1.10), must be zero. It can be noticed that the star probe has four signal connectors marked with S_1 to S_4. Further details on CM signals and how they are created using star style couplers may be found in [30, 31]. The star style coupler is preferred for the receiver due to the possibility of receiving CM signals.
- *Triangle style coupler for transmitting*
  The triangle style probe (or transversal coupler) has the benefit of not creating any CM signal when used for feeding. For this reason, it is preferred for the transmitter as it avoids feeding CM signals into the mains. In fact, the sum of the 3 voltages U_{P-N}, U_{N-PE} and U_{PE-P} is zero. Hence, there is no simple way to receive CM signals using a triangle style coupler.

Eigenmode Decomposition of PLC Channel Matrix

For a MIMO transmission composed of M transmitters and N receivers of each frequency f, the system can be summarized by a $N \times M$ channel matrix $\mathbf{H}(f)$ as follows:

$$\mathbf{H}(f) = \begin{bmatrix} h_{11}(f) & h_{12}(f) & \cdots & h_{1M}(f) \\ h_{21}(f) & h_{22}(f) & \cdots & h_{2M}(f) \\ \vdots & \vdots & \ddots & \vdots \\ h_{N1}(f) & h_{N2}(f) & \cdots & h_{NM}(f) \end{bmatrix}, \tag{1.5}$$

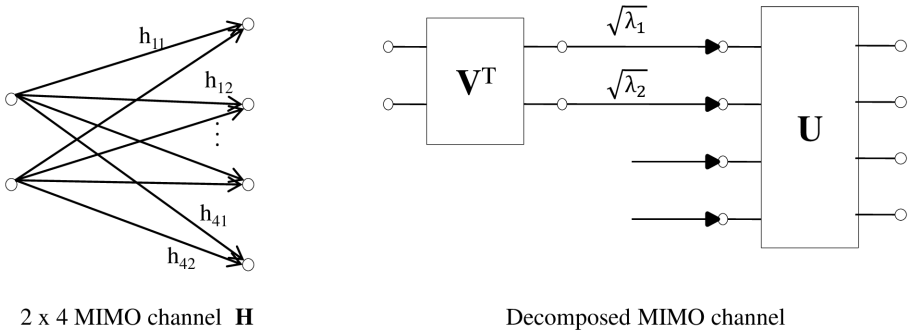

FIGURE 1.11: Decomposition of the MIMO channel into two parallel SISO channels.

where $h_{nm}(f)$ are the complex CTF coefficients from the m^{th} transmitter to the n^{th} receiver ($m = 1,..,M$; $n = 1,..,N$). Theoretically, the MIMO channel matrix $\mathbf{H}$ (for the sake of clarity we omit the index f) can be decomposed into R parallel and independent SISO branches by means of the Singular Value Decomposition (SVD) [33]:

$$\mathbf{H} = \mathbf{U}\mathbf{S}\mathbf{V}^T \tag{1.6}$$

with

$$\mathbf{S} = \text{diag}(\sqrt{\lambda_1}, ..., \sqrt{\lambda_R}) = \begin{bmatrix} \sqrt{\lambda_1} & 0 & 0 \\ 0 & \ddots & 0 \\ 0 & 0 & \sqrt{\lambda_R} \end{bmatrix}, \tag{1.7}$$

R is rank of $\mathbf{H}$, which is the minimum of the number of transmitters and receivers, i.e., $R = \min(M, N)$. $\mathbf{S}$ is a diagonal matrix of diagonal entries $\sqrt{\lambda_i}$ with $i = 1, .., R$, which are the singular values of $\mathbf{H}$; or in other words, λ_i are the eigenvalues of the "square" channel matrix $\mathbf{H}\cdot\mathbf{H}^T$, where $(\cdot)^T$ is the conjugate-transpose operator. $\mathbf{U}$ and $\mathbf{V}$ are unitary matrices, that is, $\mathbf{U}^{-1} = \mathbf{U}^T$ and $\mathbf{V}^{-1} = \mathbf{V}^T$. The dimension of $\mathbf{U}$ and $\mathbf{V}$ are $N \times R$ and $M \times R$, respectively. In the context of PLC, since the maximum number of feeding and receiving ports is $M = 2$ and $N = 4$ respectively, up to 2×4 MIMO is possible. In this case, the SVD of the MIMO-PLC channel results in two independent and parallel SISO channels ($R = 2$) with attenuations $\sqrt{\lambda_1}$ and $\sqrt{\lambda_2}$. The 2×4 MIMO-PLC channel matrix and its decomposition in singular values are shown in Figure 1.11. Note that the multiplication of the diagonal matrix $\mathbf{S}$ in Eq. (1.6) by the unitary matrices $\mathbf{U}$ and $\mathbf{V}$ does not change the total energy of $\mathbf{S}$. Thus, the sum of the eigenvalues λ_1 and λ_2 represents the total gain of the MIMO-PLC channel $\mathbf{H}$.

MIMO PLC Channel Capacity

Based on the SVD, the MIMO-PLC channel can be seen as two independent and parallel SISO channels of gains λ_1 and λ_2 (see Figure 1.11). Therefore, the channel capacity can be obtained as an extension of the SISO-PLC channel capacity, given in Section 1.5.1 Eq. (1.4), to the sum of the two channel capacities of the independent SISO channels as follows:

$$C_{MIMO} = \Delta f \cdot \sum_{k=1}^{L} \sum_{i=1}^{R=2} \log_2 \left(1 + \frac{P(f_k)\lambda_i(f_k)}{R \cdot N(f_k)} \right) \quad \text{[bits/s]}. \tag{1.8}$$

In should be noted in Eq. (1.8) that the noise vector at the receiver is assumed to be uncorrelated and that the noise power is the same for all receive ports. It should also be noted that the available signal power is divided by $R = 2$ as the available power is shared between the R independent channels. This is usually considered for comparison purposes with SISO case. Note that the MIMO signal PSD is limited by a constraint due to the electromagnetic interference properties of the low-voltage distribution network.

Several MIMO-PLC channel capacity computations can be found in literature [6, 34–38]. It is proved that the MIMO technique in PLC is effective in increasing the capacity by approximately a factor of two in comparison with SISO-PLC systems [34, 35].

MIMO PLC Channel Correlation

The singular values not only give information on the gain of the MIMO paths but also indicate the spatial correlation between them. The spatial correlation in (dB) can be measured through the parameter κ_{dB} as follows [6]:

$$\kappa_{\text{dB}} = 20 \times \log_{10} \left(\frac{\sqrt{\lambda_1}}{\sqrt{\lambda_2}} \right). \tag{1.9}$$

Note that without loss of generality, the first singular value $\sqrt{\lambda_1}$ is assumed to be larger than the second one $\sqrt{\lambda_2}$. By definition, when the channel is completely correlated, κ_{dB} in Eq. (1.9) approaches infinity. In fact, in this case the rank R of the channel matrix $\mathbf{H}$ is equal to one, which means $\lambda_2 = 0$, since all entries of the channel matrix have the same value. On the other hand, when the channel is completely uncorrelated, $\kappa_{\text{dB}} = 0$. The higher the κ_{dB} ratio, the larger the singular value spread between the two streams is, indicating a high spatial correlation.

In order to investigate the MIMO-PLC spatial correlation, channel measurements in six European countries have been conducted in frequencies up to 100 MHz [6]. The scattering

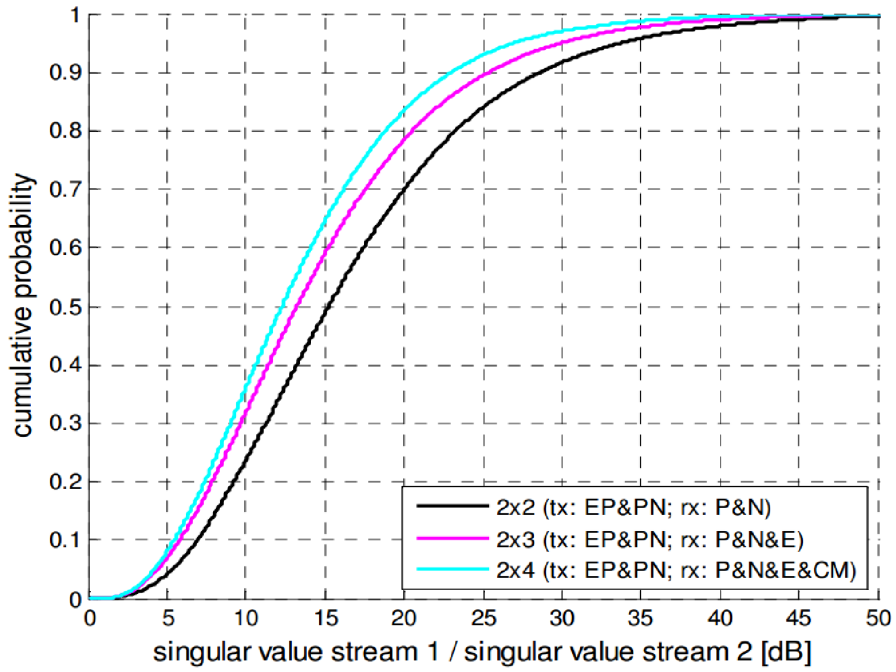

FIGURE 1.12: MIMO-PLC channel spatial correlation from measurements in [6].

parameter S21 of MIMO PLC channels was recorded at 34 locations, where a total number of 4,588 CTFs was measured. The κ_{dB} ratio is calculated for each measurement and frequency f, which results in a total number of 7,345,388 values, before calculating the commutative distribution function (CDF) [1]. The obtained results for three different MIMO configurations are illustrated in Figure 1.12 [6]. It can be deduced from the figure that the value of κ_{dB} is relatively high, which indicates that the MIMO-PLC channels are correlated. The 2×2 MIMO configuration presents the highest spatial correlation. For an example of this MIMO configuration, 30% of channels have at least a factor of 100 between the largest singular value and the smaller one (cumulative probability= 0.7). 78% of channels have at least a factor of 10 (cumulative probability= 0.22). The slow slope at higher values of the cumulative probability shows that a few channels have a very high spatial correlation [6].

1.6 Conclusion

In this chapter, an overview on indoor broadband MIMO-PLC has been proposed. After providing a brief historical development of communications over power lines, a description of PLC networks as well as frequency bands was presented. Then, a brief summary of the major broadband PLC groups and specifications was given. Finally, a brief introduction to SISO

1. The cumulative distribution function of a real-valued random variable X is the function given by $F_X(x) = \mathrm{P}(X \leq x)$

and MIMO PLC channels was presented. The applicability of MIMO techniques in PLC, the channel capacity and the MIMO spatial correlation were investigated. The European MIMO-PLC channel correlation presented in this chapter will be considered in Chapter 3 to validate a MIMO channel model proposed by us. This chapter presented a brief introduction to indoor broadband MIMO PLC systems, the context of the study.

CHAPTER 2

Power-Line Channel and Noise: Characteristics and Modeling

2.1 Introduction

Advanced communication technologies have made possible the transmission of high-speed digital data over the classical indoor electrical wires. However, the power-line medium has not been devised for communication purposes and constitutes a challenging environment for reliable and high-speed data communication. Varying impedance, considerable noise, and high attenuation are the main issues [39]. Recently, MIMO techniques have become an important research field for enhancing the throughput of indoor broadband PLC systems by exploiting the additional PE wire. The development of such systems requires an accurate description of the propagation channel.

This chapter presents our state-of-the-art study on the PLC channel and noise characterization and modeling. More precisely, in Section 2.2, after a general presentation of the channel characteristics, we present the different options of PLC channel models and focus on the parametric statistical modeling approach where some of the literature models are described. Then we turn to MIMO-PLC channels, where different modeling approaches are presented. Next, in Section 2.3, the additive interference, which are roughly categorized into background noise and impulsive noise, are characterized. In particular, the different approaches used to model the asynchronous impulsive noise, which is the main source of transmission errors in PLC, are investigated. Finally, Section 2.4 concludes the chapter and

summarizes the considered system model.

2.2 PLC Channel Characterization and Modeling

2.2.1 PLC Channel Characterization

The characteristics of indoor power-line CTFs are difficult to model due to the considerable variability and complexity of PLC networks. Adequate channel models that include various classes of channel frequency responses are required to assess the performance of PLC systems. In the literature, a lot of effort has been spent to characterize and model power-line channels [3, 4, 39–43]. Unfortunately, these models have not been standardized yet, so there is no common, widely accepted channel model for in-home PLC.

One of the major challenges in PLC is to characterize and model the channel. In fact, the PLC channel suffers from frequency-dependent attenuation caused by conductor and dielectric losses. In addition, signal propagation does not only take place along a single path between the transmitter and the receiver, but additional reflections caused by impedance mismatches at line discontinuities must also be considered. The PLC channel can therefore be considered as a multi-path environment with frequency-selective attenuation. The multi-path reflections result in dispersion of the time domain signal, which can be characterized by the delay spread. The delay spread parameter represents the total time interval during which signal reflections with significant energy arrive at the destination, and is derived from the second moment of the delay power spectrum. Another important parameter that captures the frequency-selective characteristics of a channel is the coherence bandwidth. This parameter is a statistical measurement of the range of frequencies over which the channel can be considered flat. With respect to the bandwidth (or channel duration) of the transmitted signal, the value of the coherence bandwidth (or delay spread) determines the need for employing channel protection techniques such as OFDM modulation or channel coding.

Furthermore, the PLC channel generally presents a linear and periodically time variant behavior [44]. The frequency responses may vary depending on the domestic appliances connected to the network, that is, when electric appliances are plugged in or out, and switch on or off. Consequently, the transmitter and/or receiver should adapt continuously their transmission and/or detection parameters to the channel change. In this respect, an accurate description of the characteristics of the PLC channel is fundamental.

Several measurement campaigns have been undertaken in different countries to characterize the PLC channel. A channel characterization in the frequency range from several kHz up to 20 MHz was presented in [40]. Another measurement campaign was performed in U.S.

targeting the $1.8 - 30$ MHz frequency band [42]. A channel characterization up to 100 MHz based on a measurement campaign conducted in France was presented in [24, 41], where the PLC channel was classified into nine classes according to the channel capacity. Recently, a statistical characterization of the in-home PLC channel based on an experimental campaign performed in Italy in the 1.8-100 MHz frequency band has been presented [43]. The work therein aimed at refining statistical models presented in the literature, by providing comparable results with respect to other measurement campaigns. We report some of the statistical channel characteristics presented in [43]:

- the PLC channel is significantly frequency selective in the $1.8 - 100$ MHz frequency range;
- the magnitude of the channel frequency response as well as the root-mean-square delay spread can be modeled as log-normally distributed random variables;
- the average channel gain (in dB) is normally distributed with good approximation;
- experimental observations showed that the time-dependency is not pronounced in the considered frequency band. This finding was validated by other experimental results as [45], where it was shown that channel time variations are mostly experienced below 2 MHz;
- signaling above 100 MHz (and in particular up to 300 MHz) can provide achievable rate improvements. However, the spectral efficiency, i.e., the bit rate per-unit frequency, decreases significantly.

2.2.2 PLC Channel Modeling

Many contributions in the field of broadband PLC were primarily focused on modeling the channel. In general, PLC channel models can be split into two categories: bottom-up (or physical) and top-down (or parametric) models. Basically, the bottom-up approach relies on the electrical properties of the transmission line to describe the PLC CTF [46–49]. It considers the power cables as two or multi-conductor transmission line (MTL) [50], where the voltages and currents vary in magnitude and phase along the cables. Although this approach has the advantage of not needing any field measurements, it requires the perfect knowledge of the network topology in terms of cable characteristics, loads, and so on. As a consequence, a lack of knowledge in these characteristics may lead to a significant degradation of the model accuracy. On the other hand, with the top-down approach, the CTF (or impulse response) is obtained by fitting a certain parametric function with a data coming

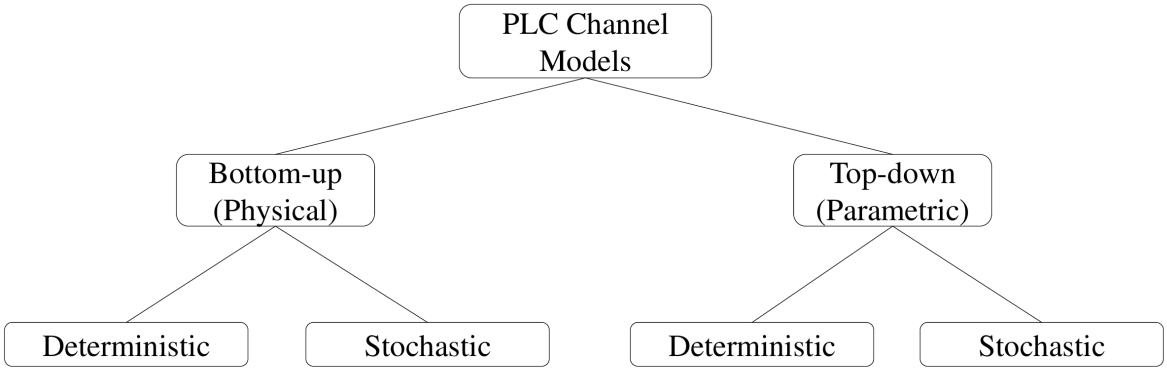

FIGURE 2.1: An illustration of the different types of PLC channel models.

from measurements [3, 4, 40, 51]. The main advantage of this approach is that it does not require knowledge of the network characteristics.

Further, within each category, it can be distinguished between deterministic and stochastic models. Figure 2.1 illustrates the different options of PLC channel models. Deterministic models actually aim at reflecting one or small set of PLC channel realizations. This approach has the advantage of being well adapted to represent deterministic network topologies, without the risk to generate unrealistic channels due to modeling inaccuracies. However, it is only able to partially describe the underlying physics of power-line signal propagation and thus has limited applicability. Also, it needs a large database to obtain good results. On the other hand, the stochastic approach enables to represent a wide range of channel realizations according to their probability of occurrence. Stochastic nature of the PLC channel arises from the variability of link topologies and wiring practices. The stochastic approach considers the global statistics of the propagation medium. Therefore, its purpose is not to reproduce exactly the CTF measured in a given topology, but rather to enable the generation of random CTFs exhibiting similar statistics with the actual channel measurements. This approach represents the wide variation of PLC channels and can be used to draw general conclusions. The main drawback of that is it requires a large amount of experimental data to reproduce the model.

In this thesis, we focus on the top-down statistical modeling approach. In the following, we describe commonly accepted channel models such as the general multipath channel model proposed by Zimmermann and Dostert [40], the nine-classes channel model proposed by France Télécom in [4, 41], and the random channel generator proposed by Tonello in [3]. Tonello's channel model in [3] is basically a statistical extension of Zimmermann's channel

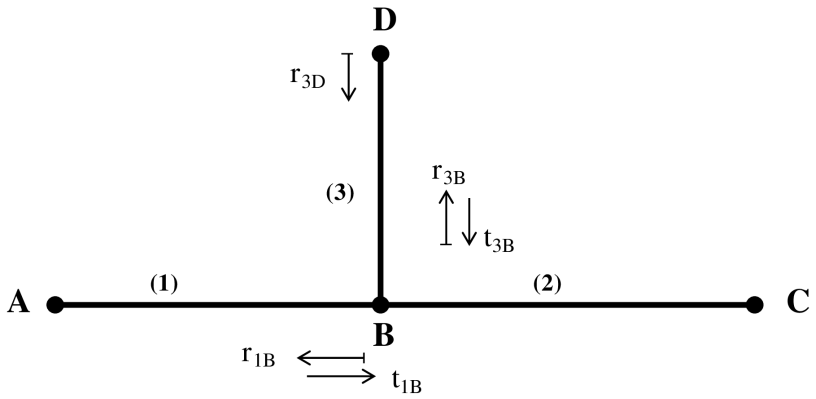

FIGURE 2.2: Simple signal propagation scenario in PLC.

model fitted to the set of the nine channel classes proposed in [4].

The Generalized Multipath Propagation Model

The generation of multiple paths in an in-home power delivery network is caused by inhomogeneities of power-line segments. In fact, in-home PLC networks are characterized by the presence of many segments and termination outlets that connect the electrical loads. In general, theses loads show different impedances compared to the characteristic impedance of power-line cables giving rise to signal reflections. In addition, numerous reflections are caused by the joints of the house service cables, house connection boxes, and the joints at series connections of cables with different characteristic impedance. As a result, the PLC channel presents a multipath scenario with frequency selective fading.

Figure 2.2 depicts a simple PLC topology that is used by Zimmermann and Dostert in [40] to analyze the echoes generated on a power-line link. This topology consists of three segments (1), (2), and (3) with the length of L_1 , L_2, and L_3 that are connected at point B. The characteristic impedance of the three segments are Z_{L1}, Z_{L2}, and Z_{L3}, respectively. A is the point at which the signal is transmitted and C is the one at which the signal is received. For the purpose of simplification, the terminal impedance at points A and B are assumed to be matched with the corresponding lines, which means $Z_A = Z_{L1}$ and $Z_C = Z_{L2}$ [40]. Thus, the signal is reflected only at points B and D. Figure 2.2 shows the reflection and transmission coefficients denoted r_{1B}, r_{3D} and r_{3B} for the reflection, and t_{1B} and t_{3B} for the transmission. All the possible propagation paths and the corresponding propagation factors g_i are given in Table 2.1; g_i represents the product of the reflection and transmission factors along the path i. Although the number of propagation paths N deduced from Table 2.1 can go up to infinity, it is reported in [40] that it is reasonable to approximate it by only

TABLE 2.1: Multipath signal propagation in a simple PLC network topology.

Path number i	Signal path	Weighting factor g_i
1	$A \rightarrow B \rightarrow C$	t_{1B}
2	$A \rightarrow B \rightarrow D \rightarrow B \rightarrow C$	$t_{1B} \times r_{3D} \times t_{3B}$
3	$\cdots$	$\cdots$
N	$A \rightarrow B(\rightarrow D \rightarrow B)^{N-1} \rightarrow C$	$t_{1B} \times r_{3D} \times (r_{3B} \times r_{3D})^{N-2} \times t_{3B}$

N_p dominant paths. Based on these analysis, an interesting model that describes the PLC channels through its multipath behavior has been proposed [40,52,53]. The general multipath model for the CTF is represented by the following equation [40]:

$$H(f) = \sum_{i=1}^{N_p} g_i(f) \cdot A(f, d_i) \cdot e^{-j2\pi f \tau_i} \tag{2.1}$$

where $g_i(f)$ is the transmission/reflection factor of path i of each frequency f which is in general complex and frequency dependent; τ_i is the delay of path i; $A(f, d_i)$ is the attenuation term caused by lossy cables which increases with frequency and propagation length, and $e^{-j2\pi f \tau_i}$ is the phase difference due to time delay. The time delay τ_i for path i is defined as:

$$\tau_i = \frac{d_i}{v_p} = \frac{d_i \sqrt{\varepsilon_r}}{c_0} \tag{2.2}$$

where ε_r is the dielectric constant, c_0 is the speed of light in vacuum, and d_i is the path length. In [40], a simplified model that uses a small number of parameters is proposed by rewriting Eq. (2.1) as follows:

$$H(f) = \sum_{i=1}^{N_p} \underbrace{g_i}_{\substack{propagation \\ factor}} \cdot \underbrace{e^{-(a_0 + a_1 f^k) d_i}}_{\substack{attenuation \\ portion}} \cdot \underbrace{e^{-j2\pi f (d_i / v_p)}}_{delay\ portion} \tag{2.3}$$

where a_0, a_1, and k are the attenuation parameters that are chosen to adapt the model to a specific network. These parameters can be obtained by fitting the model with data coming from CTF measurements.

Although this model can realistically represent a true frequency response [40], it should be noted, however, that in case of complex PLC networks it may turn out to be computationally prohibitive as each amplitude and delay associated to each path has to be estimated [54].

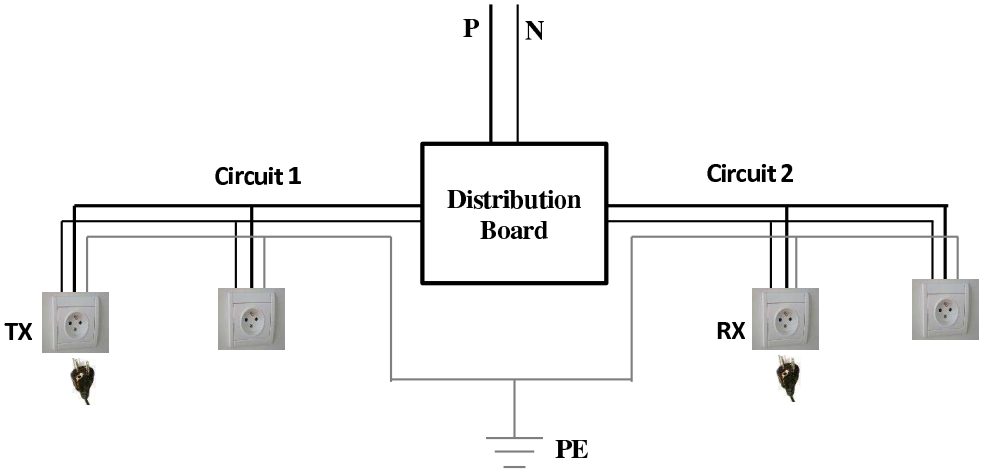

FIGURE 2.3: A typical indoor electrical network.

France Télécom's Channel Model

Adequate channel models that represent the wide variability of channel frequency responses observed in PLC are required to assess the performance of PLC systems. In this sense, an interesting approach for modeling the power-line channel is presented in [4]. The main contributions of this approach are:

1. performing a PLC channels classification according their capacities in the presence of AWGN, and providing for each class an average magnitude and phase channel model;
2. introducing the multipath characteristic of PLC channels by means of a statistically-based channel generator.

This study of characterization and modeling the PLC channel is detailed in [4, 24, 41], and is summarized here.

To characterize and model the PLC channel, Tlich et al. in [4] have conducted a measurement campaign in France over a frequency rang up to 100 MHz. A total number of 144 CTFs were measured in various indoor channel environments/sites (rural and urban, old and new buildings, apartments and houses). An important observation from the measurement results of the transfer function have been pointed out, which led to the categorization of PLC CTFs into:

- same-circuit channels, where the transmitting socket (TX) and the receiving socket (RX) are located in the same electrical circuit, i.e. they are situated in series on the same branch corresponding to one fuse in the distribution board;
- different-circuit channels, where TX and RX are located in different electrical circuits, i.e. they are separated by the distribution board.

TABLE 2.2: Channel capacities calculation parameters.

Frequency bands:	1 MHz-100 MHz
Carrier width:(Δf)	25 KHz
Number of Carriers (N):	3960
Transmitted PSD (P_s):	-50 dBm/Hz
White noise PSD (P_n):	-140 dBm/Hz

An illustrative example of communication via a different-circuit channel is presented in Figure 2.3.

For each category and site, the PLC CTFs were found to be almost identical and independent of the outlet location (peaks and notches were almost at the same frequencies). This observation led to the idea to classify the measured PLC channels according to their capacities calculated with the Shannon capacity formula described as [24]:

$$C = \Delta f \cdot \sum_{i=1}^{N} \log_2 \left(1 + \frac{P_s \cdot |H(f_i)|^2}{P_n}\right) \qquad \text{bits/s} \tag{2.4}$$

where N represents the number of carriers, Δf is the carrier spacing frequency, and P_s and P_n are the transmitted signal and noise power spectrum densities (PSDs), respectively (the two PSDs are considered to be flat). The parameters values are given in Table 2.2.

The measured channel were divided into nine classes according to their capacities. Table 2.3 summarizes the classification results in terms of measured transfer function percentages, capacity interval, and average capacity distributions [4, 24]. As shown in Table 2.3, class 1 channels have the lowest capacity; class 2 channels have a higher capacity than class 1 channels, etc. It can also be noted that most of the measured transfer functions belong to classes 3 and 2. Channels of classes 1, 8 and 9 are the less encountered ones. Note that classes 9 and 8 comprise the same-circuit channels, classes 6 to 1 consist of different-circuit channels, and class 7 represents a mixture of same and different-circuit channels [4].

For each channel class, it was found that the average frequency response is almost the same. Consequently, an average attenuation model was proposed by class. Figure 2.4 provides the analytical formulas of the average attenuation models for the nine classes and plots them.

Beside the average attenuation model, an average phase model per class was also proposed [4]. The model was derived by linearizing the median phase curve of the measured CTFs for each class. The phase models of the nine classes are depicted in Figure 2.5. As expected,

TABLE 2.3: PLC nine channel classifications.

Class	Percentage of channels	Capacity interval (Mb/s)	Average capacity (Mb/s)
1	3.49%	1000-1200	1120
2	16.78%	1200-1400	1307
3	18.18%	1400-1600	1486
4	11.88%	1600-1800	1687
5	11.88%	1800-2000	1899
6	12.58%	2000-2200	2098
7	9.79%	2200-2400	2298
8	7.69%	2400-2600	2499
9	7.69%	2600-2800	2699

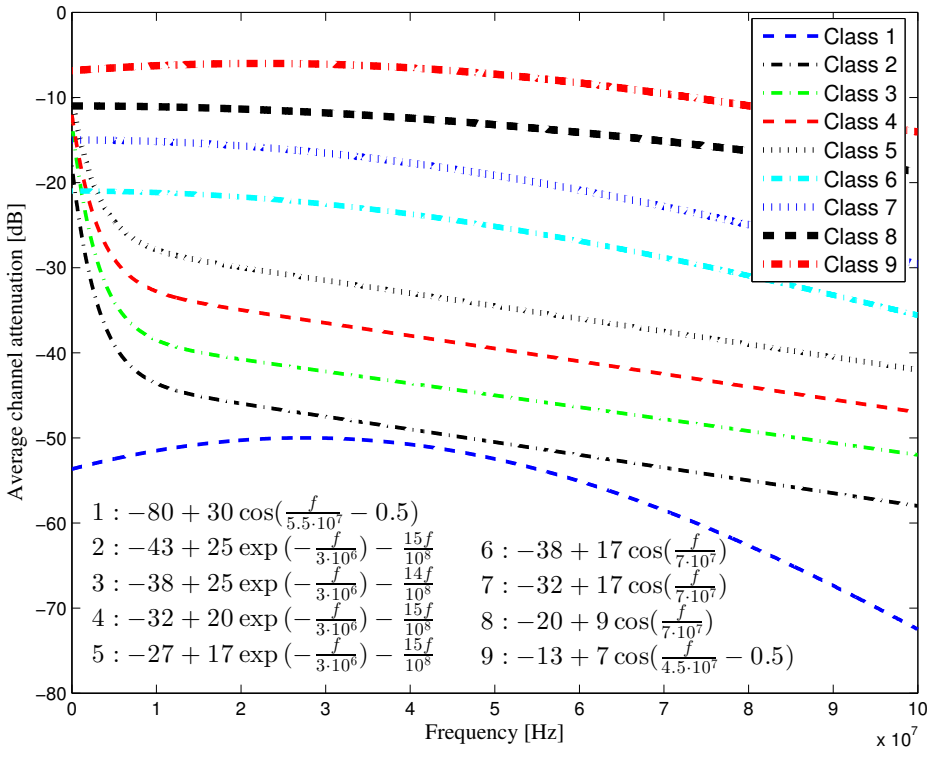

FIGURE 2.4: Gathered average attenuation models.

the higher the class number, the lower the propagation delays (classes with higher numbers contain same-circuit channels), the lower the slope of the curves.

A statistical characterization of the channel time delay spread and the channel coherence bandwidth per channel class has been done in [41]. It has been observed that the coherence bandwidth increases with respect to channel class (class 1 channels have the lowest coherence

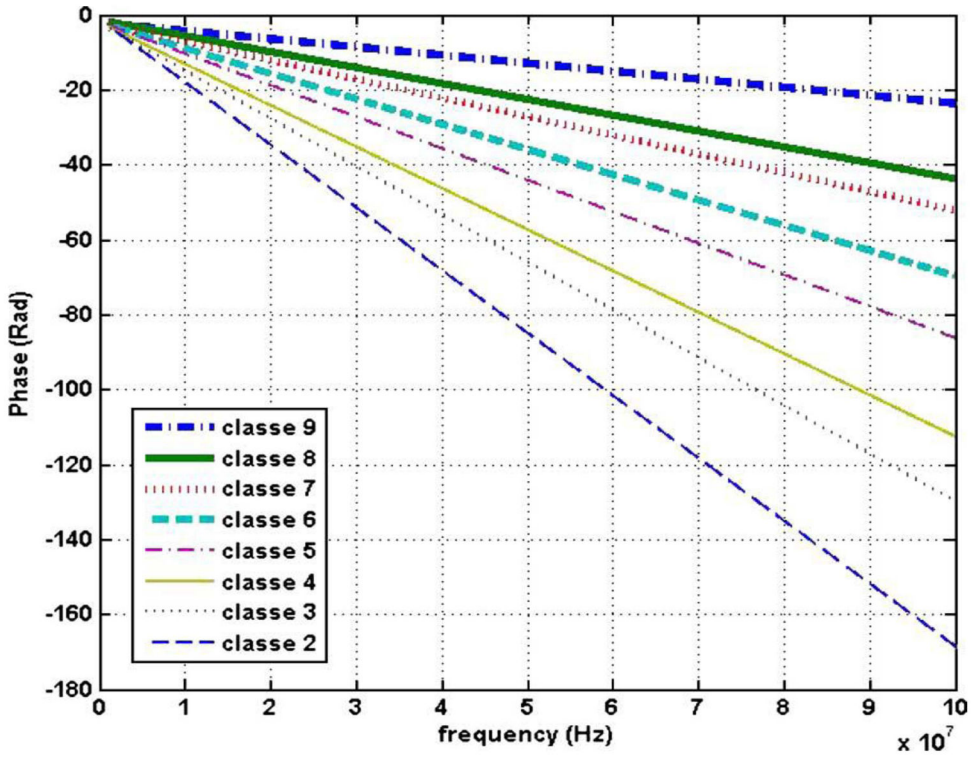

FIGURE 2.5: Average phase models for the nine channel classes [4].

bandwidth; class 2 channels have a higher coherence bandwidth than class 1 channels, etc). Similarly, it was shown that the time delay parameters decreases with respect to the channel class number.

Finally, in order to introduce multipath effects to the final PLC magnitude generator, a statistical-based channel generator was proposed based on a statistical study of magnitude peaks and notches. Also, a multipath phase generator was proposed, based on group delay nonlinearity insertion at notch frequencies [4].

Tonello's Statistical Model

As mentioned previously, it is beneficial to deal with a statistical model that allows capturing the ensemble of PLC network topologies. This is of particular interest for the design and testing of digital communication algorithms. In this sense, an interesting statistical extension of the parameters from the multipath model presented by Zimmermann and Dostert in [40] was proposed by Tonello in [55] and further developed in [24]. The mathematical function of Zimmermann's CTF model has already been presented in Eq. (2.3). The extension assumes that the multiple paths are generated by a Poisson arrival process with intensity $\Lambda\,(m^{-1})$. The maximum length of the signal path is denoted as L_{max}. In addition, the propagation

factor g_i are assumed to be real, independent, and uniformly distributed in $[-1, 1]$. Under these assumptions, the statistical expectation of the frequency domain path loss has been defined as follows [24]:

$$PL(f) = A^2 \frac{\Lambda}{3} \frac{1 - e^{-2L_{max}(a_0 + a_1 f^K)}}{(2a_0 + 2a_1 f^K)(1 - e^{\Lambda L_{max}})} \tag{2.5}$$

where the parameter A allows adding an attenuation to the Zimmermann's frequency response model of Eq. (2.3). Further explanations on the statistical extension procedure is provided in the next section.

Tonello's Random Channel Generator [3]

The statistical model proposed by Tonello in [55] has been developed in [56] and [57] to represent the channel frequency responses of the nine channel classes from [4]. Later, a refined model of [56] and [57] was proposed by Tonello et al. in [3]. The model, which proposes a random channel generation algorithm, is detailed in [3] and is summarized here.

Firstly, Tonello et al. [3] have recalled the basis of the Zimmermann's multipath propagation model based on the multipath characterization of indoor power-line networks presented in [58]. The signal at the received port is written as follows [3, 58]:

$$V_{rx} = \sum_{i=1}^{N_p} \underbrace{\left(\prod_{m=1}^{R_i} \rho_m(f) \prod_{n=1}^{T_i} \tau_n(f) \right)}_{p_i(f)} e^{-\gamma(f)\ell_i} V_{tx}(f), \tag{2.6}$$

where $V_{tx}(f)$ and $V_{rx}(f)$ denote the phasor vector of the signal at the transmitter and receiver ports, respectively; N_p is the number of paths; $\rho(f)$ and $\tau(f)$ denote the reflection and transmission coefficients account for multipath effects, respectively; R_i and T_i represent the number of reflections and transmissions coefficients, respectively; ℓ_i is the length of the i^{th} path; $\gamma(f)$ is the propagation constant which depends on the cable characteristics and, in general, is complex $\gamma(f) = \alpha(f) + j\beta(f)$. $\alpha(f)$ and $\beta(f)$ represent the attenuation and phase constants respectively, and are modeled as [40]

$$\alpha(f) = a_0 + a_1 f^K \tag{2.7}$$

$$\beta(f) = 2\pi f / v. \tag{2.8}$$

$p_i(f)$ represents the path gain which is product of the reflection and transmission coefficients. In general, the path gains are complex and smaller than one in absolute value. However, in

many cases of practical interest, the path gains can be assumed as real-valued [40]. The path gains in [3] are modeled as follows:

$$p_i(f) = g_i + c_i f^{K_2}, \tag{2.9}$$

where K_2 is the same for all the paths. Therefore, the complex channel frequency response $H(f)$ can be given from Eq. (2.6) as the ratio between the phasor of the received signal V_{rx} and the phasor of the transmitted one V_{tx}:

$$H(f) = A\sum_{i=1}^{N_p}(g_i + c_i f^{K_2})e^{-(a_0+a_1 f^K)\ell_i}e^{-j2\pi f\ell_i/\nu}, \qquad 0 \leq B_1 \leq f \leq B_2. \tag{2.10}$$

Tonello et al. [3] have then proposed to introduced some statistical properties to the above-presented transfer function model. The basic idea is to consider the model parameters as random variables that have to be described by specific distribution functions. Specifically, the parameters g_i, c_i, ℓ_i and N_p are modeled as random variables. The value of the other parameters A, a_0, a_1, K and K_2 are assumed to be constant and used for fitting with measured CTFs. Indeed, the model assumes that the reflection sources, such as joints and mismatched loads, that generate the multipath effect in PLC, are placed over a finite distance interval and are located according to Poisson arrival process with intensity $\Lambda\,(m^{-1})$. Thus, the number of paths N_p is modeled as Poisson random variable of mean ΛL, with L being the maximum network length. The path gain coefficients g_i and c_i are assumed to be independent and modeled as log-normally distributed random variables multiplied by random sign flips. The justification given for this choice is related to the fact that the path gain itself is the product of several uniformly distributed random variables which represent the transmission and reflection coefficients, and thus it can be modeled as log-normal random variables thanks to the central limit theorem. g_i and c_i have chosen with zero mean and with variances σ_G^2 and $b_0^2\sigma_G^2$, respectively. It is possible, however, to consider the path gains to be uniformly distributed as in [55]. Finally, the path lengths ℓ_i are modeled as uniformly distributed random variables in $[0, L]$, where L is constant.

In order to obtain the model parameters, Tonello et al. [3] have taken aim at the average path loss and the coherence bandwidth of the set of measured channels that were classified into nine classes and discussed previously [4]. For each class, the average path loss profile and coherence bandwidth were provided [41]. In [3], the coherence bandwidth as well as average path loss were obtained from the statistical frequency correlation function defined as:

$$\phi(f, \lambda) = E[H(f + \lambda)H^*(f)] \tag{2.11}$$

TABLE 2.4: Path gain parameter values.

Class	b_0^2	K_2
1	1.4354×10^{-6}	0.403919
$2-8$	0	–
9	2.28955×10^{-6}	0.341468

TABLE 2.5: Attenuation and multipath parameter values ($\sigma_G^2 = 1$, $\Lambda = 0.2\,path/m^{-1}$, and $v = 2 \times 10^{-8}$).

Class	A	$a_0\,(m^{-1})$	$a_1\,(s \cdot m^{-1})$	K	$L\,(m)$
1	1.3022×10^{-5}	-0.00691505	1.15712×10^{-026}	2.97983	540
2	2.8269×10^{-4}	-0.00888846	7.55014×10^{-006}	0.408174	550
3	6.7170×10^{-4}	-0.0152108	3.67885×10^{-005}	0.347786	320
4	6.3972×10^{-4}	-0.0142857	2.5219×10^{-005}	0.348188	350
5	8.3880×10^{-4}	-0.0141565	1.67181×10^{-005}	0.363295	350
6	9.5814×10^{-4}	-0.00797313	2.285×10^{-018}	1.92048	410
7	4.5819×10^{-3}	-0.0132538	1.12949×10^{-018}	2.00313	200
8	1.0964×10^{-2}	-0.0185199	9.65172×10^{-018}	1.87202	130
9	2.4856×10^{-3}	-0.0435673	2.02324×10^{-020}	2.2179	110

where $E[\cdot]$ denotes the mathematical expectation and the superscript $(\cdot)^*$ denotes the complex conjugate; λ is the lag in the frequency domain. The average path loss was derived in closed form as follows:

$$PL(f) = \phi(f,0) = \frac{|A|^2\Lambda(1+b_0^2 f^{2K_2})\left(1-e^{-2(a_0+a_1 f^K)L}\right)}{2(1-e^{\Lambda L})(a_0+a_1 f^K)}. \tag{2.12}$$

Tables 2.4 and 2.5 report the values of the model parameters resulting from the fitting procedure of the model to the nine channel classes.

Finally, in order to capture the ensemble of in-home channel variability, a composition channel has been proposed [3]. A composite channel is basically a channel that represents the wide variation of PLC channels. The nine channel classes presented in [4] is a good representative example of PLC channels. In this respect, Tonello et al. [3] have proposed a random channel generator based on the nine channel classification performed in [4]. The idea is to randomly pick channels from all the classes according to the class occurrence probability reported in Table 2.3 [4], that is

$$P_C = \{0.0349, 0.1678, 0.1818, 0.1188, 0.1188, 0.1258, 0.0979, 0.0769, 0.0769\} \tag{2.13}$$

for classes 1 to 9, respectively. A close matching between the experimental results and the simulations was found which validated the modeling approach.

2.2.3 MIMO-PLC Channel Modeling

Turning to MIMO-PLC, several investigations on MIMO channels have been made. An average capacity gain of 1.9, with respect to the SISO-PLC channel, was achieved in [35] by considering a 2×2 MIMO-PLC channel configuration. In [34], it is shown that this capacity gain increases with the number of receiving ports. For a 2×4 MIMO configuration (including CM reception as detailed in Section 1.5.2), average capacity gains that range between 2.1 and 2.6, depending on the transmitting power level, were observed.

Several bottom-up models of the three-wire transmission line of indoor PLC networks, based on the MTL theory, have been proposed [59,60]. However, the authors of these studies did not consider the three electrical wires for the purpose of MIMO communication. Only in [38, 61], the first use of the MTL theory to explicitly model the MIMO-PLC channel in a bottom-up stochastic approach is appeared [13]. The idea was based on using the stochastic topology generator presented in [49], for the SISO configuration, to define the MTL equations in the case of three-wire/MIMO communication.

On the other hand, several MIMO-PLC channel models have been proposed based on the top-down statistical approach. To this end, several measurement campaigns have been undertaken to characterize MIMO channels [6, 62–64]. In the following, we will summarize the MIMO-PLC channel models proposed from these studies as well as some channel measurements.

Canova et al. **MIMO Channel Model [36]**

The first attempt to model the MIMO-PLC channel using the top-down approach was made in [36]. This study considered a 2×4 MIMO-PLC channel, where two differential input ports are used, and up to four ports are considered at the receiver, including the CM path. The proposed MIMO-PLC channel model was based on the SISO-PLC channel impulse response (CIR) of the European OPERA project [65]. The basic idea was to introduce a random phase shift to the CIR to produce eight variants of it, and thus the 2×4 MIMO channel. In OPERA [65], four different reference models were distinguished according to the number of paths of the CIR. Table 2.6 illustrates the parameters of the multipath model proposed by OPERA for the different classes, where for each number of paths N_p, the impulse response duration T_h, the initial delay of the first path t_0 and the range $[\Phi_{min}, \Phi_{max}]$ of the

TABLE 2.6: OPERA multipath model parameters [36].

OPERA model	N_p	$T_h\,[\mu\,s]$	$t_0\,[\mu\,s]$	Φ_{min}	Φ_{max}
Good	5	0.5	0.2	0.005	0.05
fair	10	1.0	0.2	0.002	0.01
poor	15	1.5	0.5	0.0003	0.003
bad	20	2.0	0.5	0.0001	0.0005

path amplitudes are reported. Once the OPERA model is chosen, each of the eight MIMO CIRs is derived as follows [36]. The taps of the SISO CIR (reference CIR) are multiplied one-by-one by a phase factor of $e^{-j\theta}$, different for each of them, with $\theta \sim \mathcal{U}([0, 2\pi])$. Note that each of the eight variants has the same number of paths (or taps), but the amplitude of some of these taps are multiplied by a random phase factor in order to reflect the MIMO spatial correlation. Three methods to modify the taps phases were considered [36]. The idea is that the more taps are modified, the more uncorrelated the channels becomes. The correlation value R of the proposed model was computed by:

$$R = \frac{1}{\sqrt{E_1 \cdot E_2}} < h_{11}(t), h_{21}(t) >, \tag{2.14}$$

where $h_{11}(t)$ and $h_{21}(t)$ are the impulse responses of the path from ports 1 to 1 and 1 to 2, respectively; E_1 and E_2 are the energies of the two signals and $< \cdot, \cdot >$ is the inner product operator.

Hashmat et al. **MIMO Channel Model [63]**

The same approach of introducing a phase factor to obtain MIMO spatial channels from SISO one, presented in [36], was adopted in [63]. The work therein proposed a 3×3 MIMO channel model designed to fit observations from a measurement campaign conducted in France. The proposed model was based on the SISO channel model first defined by Zimmermann and Dostert in [40] and later extended statistically by Tonello in [55] (which has already been described in the paragraph Tonello's Statistical Model). The proposed MIMO channel model aimed at capturing physical features of transmission like the frequency domain path loss characteristics, the multipath fading, the median channel attenuation, and the spatial correlation of MIMO channels. The frequency domain path loss characteristics and the multipath fading are captured based on the Tonello's statistical model for the SISO link [63]. Regarding the median channel attenuation A_{med}, it is defined as follows:

$$A_{med} = \text{median}(|H(f)|) \tag{2.15}$$

where $H(f)$ is the channel matrix. This parameter is a figure of merit for the global frequency domain attenuation of a given channel [63]. It has been found that the value of A_{med} for same-circuit channels is considerably lower than the one for different-circuit channels. In addition, it has been found that the co-channels are slightly stronger than the cross-channels in the same-circuit case. In order to reflect these observations, the experimental median channel attention parameter A_{med} is added to the Zimmermann's CTF model in Eq. (2.3)). Also, statistical models of the path loss parameters a_0, a_1 and K are proposed and summarized in [63], and further detailed in [13].

Finally, in order to capture the correlation between MIMO links observed in measurements, the same formalism used in [36] is adopted to extend the Tonello's statistical transfer function model into MIMO one. Once the phase-neutral (PN-PN) link is modeled, the full MIMO-PLC channel model can be developed. The other spatial links can be modeled using an extended CTF defined as follows:

$$H(f) = A \sum_{i=1}^{N_p} g_i e^{-j\varphi_i} e^{-j(2\pi d_i/\nu)f} e^{-(a_0+a_1 f^K)d_i} \tag{2.16}$$

The idea is to assign an arbitrary additional phase φ_i to each defined path (see Eq. (2.16). The value of φ_i is selected using a uniform distribution $\mathcal{U}(-\Delta\varphi/2, \Delta\varphi/2)$. The larger the value of $\Delta\varphi$, the lower correlated the spatial channel is with respect to the PN-PN SISO path. With a value of $\Delta\varphi = 2\pi$, the model generates a minimum spatial correlation. On the other side, selecting a value of $\Delta\varphi = 0$ results in a channel that is identical to the PN-PN SISO channel. To compute the spatial correlation, the Pearson correlation coefficient [66] was considered. The proposed MIMO-PLC model reflected the multipath structure and the spatial correlation observed in experimental measurements.

Tomasoni et al. **MIMO Channel Model [67]**

Another top-down stochastic modeling approach is presented in [62], based on a statistical analysis of a set of 96 MIMO channel measurements in the $0 - 100$ MHz range recorded in five houses in North America. Firstly, each single link within the MIMO channel matrix was completely characterized through the collected statistics. Subsequently, the MIMO-PLC channel model was developed by introducing a statistical correlation following to a similar approach as in [68]. Later, a spatial correlation analysis and modeling—based on the same measurement campaign which has been considered in [62]—was made in [67]. In

this study, attention was only devoted to the spatial correlation of MIMO channels. As a result, a refined model of [62] was proposed in [67]. The authors therein analyzed the channel covariance matrices and their eigenvalues and eigenvectors. The MIMO PLC channel matrix $H(f)$ was modeled for each frequency f as follows:

$$H(f) = K(f) \cdot R_r^{1/2}(f) \cdot H^{'}(f) \cdot R_t^{1/2}(f), \tag{2.17}$$

where

$K(f)$ is a constant that introduces an overall channel gain;

$H^{'}(f)$ is a channel matrix composed of independent and identically distributed (i.i.d.) complex Gaussian variables;

$R_t(f)$ is the transmitter correlation matrix;

$R_r(f)$ is the receiver correlation matrix.

Each channel correlation matrix is modeled by its eigenvector-eigenvalue decompositions. Details on this model can be found in [67]. The proposed model enabled to obtain simulated channels that are closed to the field measurements in terms of both spatial correlation and channel capacity.

European MIMO PLC Field Measurements

A detailed channel analysis of a MIMO-PLC system from a measurement campaign conducted in six European countries covering a frequency band up to 100 MHz is presented in [6]. In this study, different MIMO configurations, including the additional fourth CM path, were investigated and compared with each other and with SISO communication. The average channel capacity of the 2×4 MIMO configuration was found to be approximately double that of SISO. A comparison of all the different MIMO configurations in terms of the channel capacity and an investigation of the spatial correlation of MIMO-PLC channels were presented [6]. An overview of this measurement campaign can be found in [64]. The measurement results of this campaign are of prime importance for the development of general MIMO-PLC channel models that reflect the entire heterogeneity of in-home PLC networks. Some results of this measurement campaign have already been presented in Section 1.5.2.

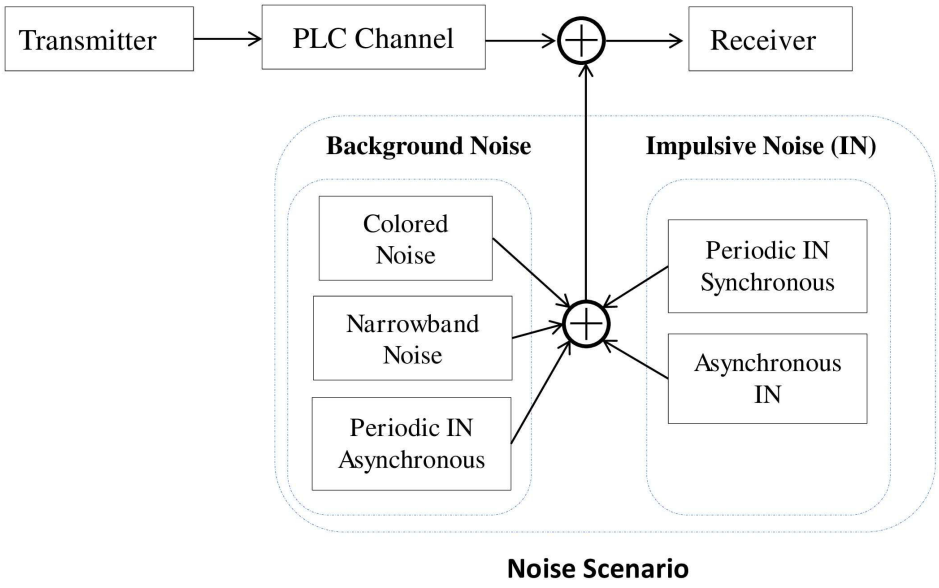

FIGURE 2.6: A typical indoor electrical network.

2.3 Noise Characterization and Modeling

In contrast to many other communication channels, noise in power-line communication cannot be described as AWGN. The interference scenario is rather complex due to the presence of different sources of disturbance. In the following, the noise characteristics and modeling approaches will be discussed.

2.3.1 Noise Characteristics

Several attempts have been made to characterize and model the different types of noise observed on indoor PLC networks [5, 69]. The noise has been divided into several classes, depending on its origin, level and physical properties. Five noise types are distinguished over broadband PLC channels in [5]: colored background noise, narrow-band noise, periodic impulsive noise asynchronous to the mains frequency, periodic impulsive noise synchronous to the mains frequency and asynchronous impulsive noise. Two main categories can be assumed from these five types as depicted in Figure 2.6 and illustrated below: background noise, which includes the first three types, and impulsive noise, which includes the last two types [5].

1. Background noise

a) *Colored background noise* is mainly caused by common household appliances like light dimmers, computers, hair dryers, and so on . It has a fairly low PSD which, however, significantly increases towards lower frequencies. The average PSD varies in the range between -140 and -125 dBm/Hz and remains stationary over periods from minutes to hours [5].

b) *Narrow-band noise* is made of continuous wave signals with amplitude modulation, mainly produced by ingress of broadcast stations operating in the short-wave and frequency-modulation bands. Other ingress noise is produced by leakage from nearby electrical or industrial equipment. The mean interference level varies with the time of the day. This type of noise usually generates strong interference over long duration in a narrow frequency bandwidth in the order of tens of kHz [13].

c) *Periodic impulsive noise asynchronous to the mains frequency* is caused by switching power supplies. The spectrum repetition rate is generally in the range from 50 to 200 kHz.

2. Impulsive noise

a) *Periodic impulsive noise synchronous to the mains frequency* is caused by the loads that work synchronously with the main, mainly by switching of rectifier diodes. They have a repetition rate of 50 or 100 Hz (60 or 120 Hz in the U.S.) and are of short duration ($10 - 100\,\mu s$).

b) *Asynchronous impulsive noise* is caused by transients due to switching within the network. The impulse duration ranges from several microseconds to a few milliseconds with a PSD that can exceed by 50 dB the level of the background noise. This kind of noise may occur at random intervals and contains considerable energy. It drastically affects high-speed communications over PLC channels, in such a way that complete symbols or even bursts of symbols cannot be decoded by the receiver. This has to be taken into account in the design of a complete and effective PLC system. Asynchronous impulsive noise is characterized by three random variables: impulse amplitude, impulse width or duration, and interarrival time. The statistical distribution of these parameters has been established through measurement campaigns [5].

Although the background noise (colored background noise, narrow-band noise and periodic impulsive noise asynchronous to the mains frequency) has a time-variant nature, it can be considered stationary since it varies very slowly over periods of seconds and minutes or sometimes even hours. On the other hand, the impulsive noise cannot be considered stationary. It is characterized by a high PSD compared with the background noise and introduces significant time variance into a communication channel [5].

The overall system noise can be modeled as the sum of the background noise, denoted as $n_b(t)$, and the impulsive noise, denoted as $n_{imp}(t)$:

$$n(t) = n_b(t) + n_{imp}(t). \tag{2.18}$$

2.3.2 Noise Modeling

This section gives a discussion on PLC noise modeling. We discuss the different noise models in the literature, starting first by presenting the background noise models and then the impulsive noise ones.

Background Noise Modeling

Background noise has been mainly characterized in the frequency domain [24, 48, 70]. Its PSD has been usually accomplished without discarding the impulsive components and the narrow-band interferences [71]. In literature, there are two methods for modeling the background noise PSD. The first one is referred to the spectrum fitting method where the measured noise PSD is fitted into certain mathematical functions of frequency with reasonable number of parameters. In this case the noise is approximated by several sources of Gaussian noise in non-overlapping frequency bands with different noise powers derived from the measured PSD [24]. The second method gives information on the random aspect of the noise at a particular frequency, it is referred to as statistical analysis method. For example, authors in [72] considered that Gaussian approximation is not a good approximation in higher frequency bands. In the following, we will describe two commonly accepted models based on the spectrum fitting method.

Esmailian et al. Background Noise Model A simple three-parameter model is presented in [48], where the noise is considered Gaussian with PSD

$$N_{n_b}(f) = a + b|f|^c \qquad \text{dBm/Hz} \tag{2.19}$$

where a, b and c are parameters derived from measurements and f is the frequency in MHz. The measurements were conducted in Canadian building in a frequency band up to 30 MHz. Two scenarios were distinguished:

1. *Worst case scenario* with the parameters (a, b, c)=(-145 dBm/Hz, 53.23, -0.337)
2. *Best case scenario* with the parameters (a, b, c)=(-140 dBm/Hz, 38.75, -0.72)

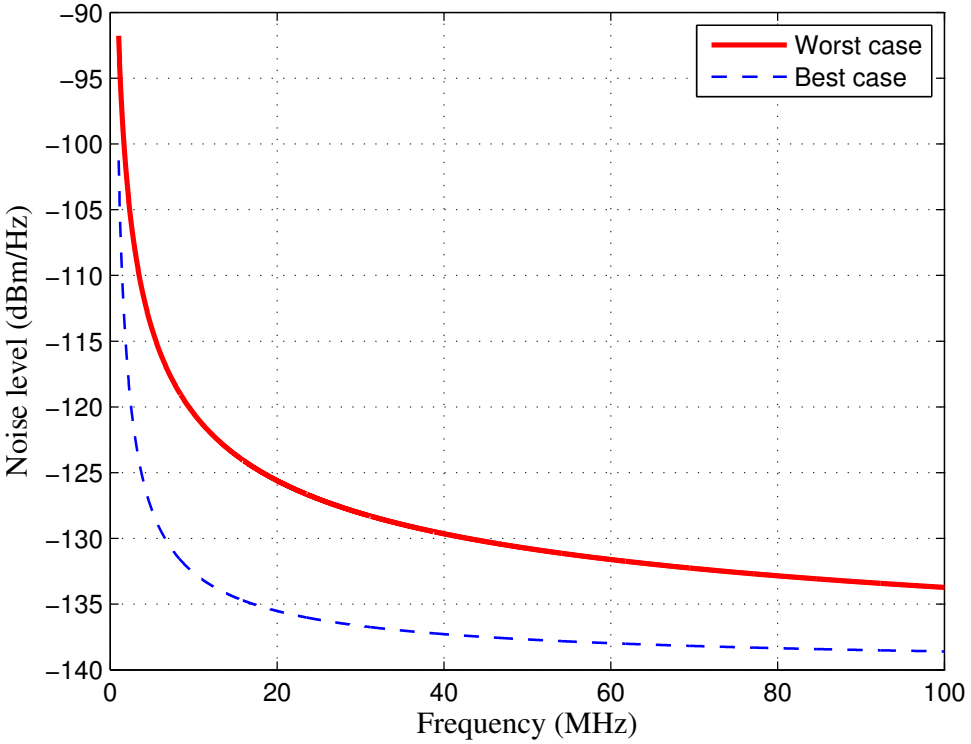

FIGURE 2.7: Worth and best cases for background noise PSD.

This model has also been found to be adequate for the measurements performed over 100 MHz bandwidth in Finland [73]. The resulting PSDs in the frequency band $1 - 100$ MHz are depicted in Figure 2.7. It can be noted from the figure that the noise PSD significantly increases towards lower frequencies.

OMEGA Background Noise Model Another simple model of the background noise is the OMEGA model proposed in [24]. This model, based on measured power-line channels, captures the typical frequency dependent character of the background noise. The general mathematical form of the OMEGA model is given by

$$N_{OMEGA} = 10 \log_{10} \left(\frac{1}{f^x} + 10^y \right) \tag{2.20}$$

where N_{OMEGA} stands for noise PSD in dBm/Hz, f is the frequency in Hz, and x and y are the noise model parameters. The x parameter controls the form of frequency dependent decay while the y parameter controls the noise floor. The values of x and y are set to 2 and -15.5 respectively in [24], which correspond to a quadratic decay and a noise floor of -155 dBm/Hz. Figure 2.8 presents a typical power-line measured noise (blue) and the

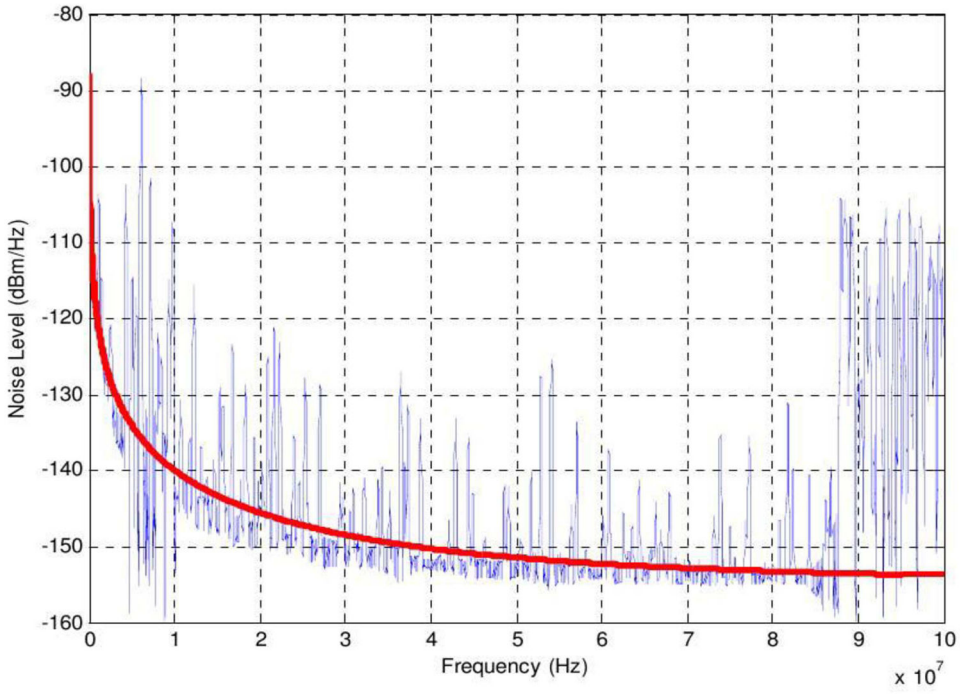

FIGURE 2.8: The OMEGA model of background noise for indoor broadband power-line channel [24].

OMEGA noise model (red) in the frequency band $0 - 100$ MHz [24], where the fitting of the model to the measures can be observed.

Impulsive Noise Modeling

The phenomenon of impulsive noise was studied by Middleton in [74], where a model for impulsive noise in communications systems was proposed. He described impulsive noise as a train of impulses, of varying duration and intensity, and of random occurrence in time. Following Middleton's noise models, many authors studied impulsive noise modeling. In this section, we focus on some probability models of impulsive noise found in the literature, which can be divided into two categories:

1. Impulsive noise models without memory, such as Middleton, Bernoulli-Gaussian, and Poisson-Gaussian noise models.

2. Impulsive noise models with memory, such as the pulse train noise model and the Markovian-based noise model.

Middleton Noise Model Middleton has developed statistical noise models which catered for noise due to both man-made and natural phenomena [75]. The most famous of these noise models is the so-called Middleton class A noise model, which has been widely accepted to model the impact of impulsive noise in communications systems. The Probability Density Function (PDF) of class A noise sample n_k is given by:

$$P_A(n_k) = \sum_{m=0}^{\infty} P_m \mathcal{N}(n_k; 0, \sigma_m^2) \tag{2.21}$$

where $\mathcal{N}(x_k, \mu, \sigma^2)$ refers to a Gaussian PDF with mean μ and variance σ^2, from which the k^{th} sample x_k is taken,

$$\mathcal{N}(x_k, \mu, \sigma^2) = \frac{1}{\sigma\sqrt{2\pi}} \exp\left(-\frac{(x-\mu)^2}{2\sigma^2}\right); \tag{2.22}$$

$$P_m = \frac{A^m e^{-A}}{m!} \tag{2.23}$$

and

$$\sigma_m^2 = \sigma_I^2 \frac{m}{A} + \sigma_G^2 = \sigma_G^2 \left(\frac{m}{A\Gamma} + 1\right) \tag{2.24}$$

where σ_I^2 is the impulsive noise variance and σ_G^2 is the background noise variance (AWGN). The parameter Γ is the Gaussian to impulsive noise power ratio. The parameter A represents the density of the impulses (of a certain width) in an observation period. The parameter A, which has become accepted as "impulsive index", therefore, can be written as $A = \eta\tau/T_0$ [76]; η is the average number of impulses per T_0, which is a unit time; τ is the average duration of each impulse, where all impulses are taken to have the same duration. As shown in Eq. (2.23), the density of impulses occurs according to a Poisson distribution. The higher is A, the closer is the class A noise to a Gaussian noise. Whereas the smaller is A, the lower is the number of impulse events. In such case, the noise corresponds to a clearly impulsive scenario. On the other hand, the parameter Γ gives an information on how strong is the impulsive noise compared to the independent Gaussian noise component. The lower is Γ, the more harmful is the impulsive noise, for a fixed parameter A. Physically, this model can be seen as a superposition of statistically independent impulsive sources that are Poisson-distributed in their arrivals in time.

Bernoulli-Gaussian Noise Model According to a Bernoulli-Gaussian (BG) impulsive noise model, the random time of occurrence of the impulses is modeled by a binary Bernoulli process and the amplitude of the impulses is modeled by a Gaussian process. The impulsive noise can thus be represented by the product of the two independent random sequences. The

impulsive sample i_k is given by

$$i_k = b_k g_k, \tag{2.25}$$

where b_k is the Bernoulli sequence with a probability of success ψ; g_k denotes the white Gaussian process with zero mean and variance σ_I^2. According to this model, the total noise seen by the receiver can be considered as a combination of two distributions: a permanent background noise (AWGN) w_k with zero mean and σ_G^2 variance, and an independent impulsive noise i_k. The total noise, denoted by n_k, is therefore given by:

$$n_k = w_k + b_k g_k. \tag{2.26}$$

The PDF of the noise n_k, assumed to be real, is given by:

$$p_{BG}(n_k) = (1-\psi)\,\mathcal{N}\left(n_k, 0, \sigma_G^2\right) + \psi\,\mathcal{N}\left(n_k, 0, \sigma_G^2 + \sigma_I^2\right), \tag{2.27}$$

where $\mathcal{N}(\cdot)$ is the Gaussian PDF already defined in Eq. (2.22). As shown in Eq. (2.27), the total noise is a stationary mixture of two Gaussian laws weighted by ψ and $1-\psi$. The two variances σ_G^2 and σ_I^2 can be related to each other by the parameter $\mu = \frac{\sigma_I^2}{\sigma_G^2}$, which represents the impulsive to Gaussian power ratio. The PDF in Eq. (2.27) thus becomes

$$p_{BG}(n_k) = (1-\psi)\,\mathcal{N}\left(n_k, 0, \sigma_G^2\right) + \psi\,\mathcal{N}\left(n_k, 0, (1+\mu)\sigma_G^2\right). \tag{2.28}$$

As clearly shown in Eq. (2.28), the BG noise model requires only two parameters, specifically ψ and μ. Based on the definition of the two parameters ψ and μ, one can notice that they are analogue to parameters A and Γ of Middleton class A model, respectively.

The BG noise model has been widely recognized as an accurate approximation of the impulsive noise for quite a few practical channels [77] including man-made impulsive noise and noise sources found in urban and military radio systems [78]. It is also used to approximate Middleton class A noise model and non-Gaussian noise environments [79].

Poisson-Gaussian Noise Model According to a Poisson-Gaussian impulsive noise model, the probability of occurrence of a number of impulsive noise events, in an interval of time of T seconds, is modeled by a Poisson process, and the distribution of the random amplitude of impulsive noise is modeled by a Gaussian process. Thus, the probability of occurrence of

k impulses in a time interval of T is given by Poisson process as follows:

$$P(k,T) = \frac{(\lambda T)^{k!}}{e^{-\lambda T}} \tag{2.29}$$

where λT represents the average number of impulses that occur in a time interval of T; λ is the mean arrival rate (probability of arrival per time unit). The λ parameter is a rate function with the following properties [80]:

$$Prob(\text{one impulse in a small time interval } \Delta t) = \lambda \Delta t \tag{2.30}$$

$$Prob(\text{zero impulse in a small time interval } \Delta t) = 1 - \lambda \Delta t \tag{2.31}$$

An assumption is made that no more than one impulse can occur in a time interval Δt. The total noise n_k seen by the receiver can be viewed as a combination of two centered (zero-mean) distributions: a permanent Gaussian background noise w_k, and an independent impulsive component i_k with time arrivals following a Poisson distribution. In terms of amplitude values in time domain, the impulsive realizations are drawn from a Gaussian distribution. i_k is thus given by

$$i_k = p_k g_k, \tag{2.32}$$

where p_k is the Poisson realization and g_k is the Gaussian sample of variance σ_I^2. The noise n_k is therefore given by

$$n_k = w_k + p_k g_k \tag{2.33}$$

and has the following PDF:

$$p_{PG}(n_k) = (1 - \lambda \Delta t)\, \mathcal{N}\left(n_k, 0, \sigma_G^2\right) + \lambda \Delta t\, \mathcal{N}\left(n_k, 0, \sigma_G^2 + \sigma_I^2\right), \tag{2.34}$$

where $\mathcal{N}(\cdot)$ is the Gaussian PDF defined in Eq. (2.22).

Pulse Train Noise Model The probability models of impulsive noise, presented previously, are commonly used in the literature for modeling the asynchronous impulsive noise in the context of indoor broadband PLC [77, 81, 82]. These models provide a closed-form and simple PDF expression that is needed in designing optimum receivers of low complexity. However, they do not represent the time behavior of the impulses observed over PLC channels and is usually generated with i.i.d. realizations. In order to better fit the physical properties of real impulsive noise, Zimmermann and Dostert have performed in [5] a thorough

analysis of the impulsive noise characteristics in both time and frequency domains. For the time domain analysis, the pulse train model $n_{pulstrain}(t)$, given below, was chosen to fully describe the impulsive noise:

$$n_{pulstrain}(t) = \sum_{k=1}^{N} A_k \cdot \text{imp}\left(\frac{t - t_{arr,k}}{t_{w,k}}\right) \tag{2.35}$$

where A_k, $t_{w,k}$ and $t_{arr,k}$ are the impulse amplitude, impulse width and arrival time, respectively; $\text{imp}(t)$ is the impulse function (or rectangular function) with unit amplitude and unit width given as follows:

$$\text{imp}(t) = \begin{cases} 0 & \text{for } |t| > \frac{1}{2} \\ \frac{1}{2} & \text{for } |t| = \frac{1}{2} \\ 1 & \text{for } |t| < \frac{1}{2} \end{cases} \tag{2.36}$$

The parameters A_k, $t_{w,k}$ and $t_{arr,k}$ are random variables whose statistical properties are investigated by measurements in [5]. Another way to describe the arrival time of impulses is through the inter-arrival time $t_{IAT,k}$ parameter, which indicates the time span between two consecutive impulses and is calculated as follows:

$$t_{IAT,k} = t_{arr,k} - t_{arr,k-1}. \tag{2.37}$$

In addition to the primary impulse parameters introduced above, namely A_k, $t_{w,k}$ and $t_{IAT,k}$ (or $t_{arr,k}$), two secondary parameters which are useful for time behavior characterization of impulsive noise, derived from the previous ones, have been introduced in [5]. The first parameter is the impulse rate

$$r_{imp} = \frac{N_{imp}}{T_{win}}, \tag{2.38}$$

which is the number of impulses N_{imp} occurring within an observation window T_{win}. The second one is the disturbance ratio given by

$$R = \frac{1}{T_{win}} \sum_{k=1}^{N_{imp}} t_{w,k}. \tag{2.39}$$

This parameter gives information about the percentage of time the transmission is corrupted by impulsive noise. Obviously, its complement allows to have a knowledge on the "impulse-free time percentage".

TABLE 2.7: Measured characteristic parameters of the three scenarios [5].

Environments	Average disturbance ratio (R)	Average impulse rate (r_{imp})	total number of impulses
heavily disturbed	0.327 %	$51.1\,s^{-1}$	1,020,409
medium disturbed	0.00632 %	$1.04\,s^{-1}$	20,730
weakly disturbed	0.00135 %	$0.122\,s^{-1}$	2,440

In order to investigate time behavior of impulsive noise, a series of measurements was conducted over a time span of 89 hours [5]. Three typical environments were distinguished, namely the "heavily disturbed" environment, the "medium disturbed" environment and the "weakly disturbed" environment. The first environment corresponds to the impulsive noise characteristics observed in a transformer substation in industrial areas during night time. The measurements of the second environment were recorded in a transformer substation in a residential area with detached and terraced houses. The last environment was recorded during nighttime in an apartment inside large buildings. The average impulse rate and disturbance ratio measured in these scenarios are provided in Table 2.7 [5]. It can be noted from the table that although the impulse rate is quite high, the disturbance ratio is below 1% in all scenarios (largely below 1% in medium and weakly disturbed environments). This means that, even in the heavily disturbed environment, more than 99% of the time is not affected by the impulse events, and could therefore be used for error-free communication [5]. Also, it was found that no periodic impulses were present at all for the weakly and medium disturbed scenarios [5]. Whereas more than 99% of the measured impulses in the heavily disturbed environment were periodic with deterministic inter-arrival time, which actually corresponds to the time duration of the network mains cycle (20 ms in Europe). In the three scenarios, the asynchronous impulsive noise appeared as statistically independent impulses with exponentially distributed inter-arrival times. In addition, it turned out that the two other noise parameters, i.e. the impulse power (or amplitude A_k) and the impulse duration $t_{w,k}$, exhibit an exponential distribution.

Burst events have been also studied in [5]. In general, burst event can be characterized by a succession of impulses, very close in time compared to the average inter-arrival time. In [5], a burst is defined as a train of at least three impulses where the maximum time span between two successive impulses is lower than 4 milliseconds. The disturbance ratio for burst events was found to be greater than 30% for more than 50% of the events, and even above 50% for more than 10%. In addition, burst events were found to be longer than $1\,ms$ and can reach values of more than $10\,ms$. Note that high-speed data transmissions over PLC channels is almost impossible during burst occurrence. However, the typical rate of impulsive bursts was

found to be in the range $0.01\,s^{-1}$ to $0.1\,s^{-1}$, which is very small compared to the values of the average impulse rate reported in Table 2.7. Thus, impulsive bursts are rare events.

Markovian-Based Noise Models The statistical distribution of the impulsive noise parameters, namely the impulse amplitude, impulse width, and interarrival time, established through the measurement campaign in [5], allowed to describe the asynchronous impulsive noise in a realistic way. Zimmermann and Dostert [5] have further derived, based on the results of the measurement campaign, a mathematical model of the time behavior of random impulsive noise by utilizing a partitioned Markov chain. Following Zimmerman's noise model, several Markovian-based BG and Middleton noise models have been proposed [83,84]. In fact, the advantages of such modeling approach are twofold: on the one hand, it can provide a generic and tractable PDF expression, while on the other hand it takes into account the impulsive noise memory [84]. Below, we briefly describe the Markov chains and the noise model proposed by Zimmermann and Dostert in [5].

Markov chains actually enable to describe random processes whose future behavior only depend on the present state or a limited period in the past. Figure 2.9 visualizes a simple two-states Markov chain by means of a state graph. The circles represent the states and the weighted arcs represent the transition probabilities $p_{i,j}$ from state i to state j $(i, j = 1, 2, ..., n)$. The process can remain in the state it is in, and this occurs with probability $p_{i,i}$. All statistic properties of a Markov chain are described by its transition probability matrix:

$$P = \begin{bmatrix} p_{1,1} & p_{1,2} & \cdots & p_{1,n} \\ p_{2,1} & p_{2,2} & \ddots & \vdots \\ \vdots & \ddots & \ddots & p_{n-1,n} \\ p_{n,1} & \cdots & p_{n,n-1} & p_{n,n} \end{bmatrix}. \tag{2.40}$$

In [5], Zimmermann et al. proposed to use the partitioned Markov chains, a special form of the Markov chain, to model impulsive noise over PLC. The n states $z_i\,(i = 1, 2, .., n)$ that represent the noise states are partitioned into two groups $A\,(i = 1, 2, ..., v)$ and $B\,(i = v + 1, v + 2, ..., n)$. Group A represents the states where there is no impulsive noise, while group B represents the case where the impulse occurs. The output function is given by

$$\Phi(k) = \Phi\left(z(k) = z_i\right) = \begin{cases} 0 & i \in A \\ 1 & i \in B \end{cases}, \tag{2.41}$$

where k represents the discrete time instants $(k = 0, 1, ..)$. Note that the well-known Gilbert-Elliot model is a particular case of the proposed partitioned Markov chain model with $n = 2$,

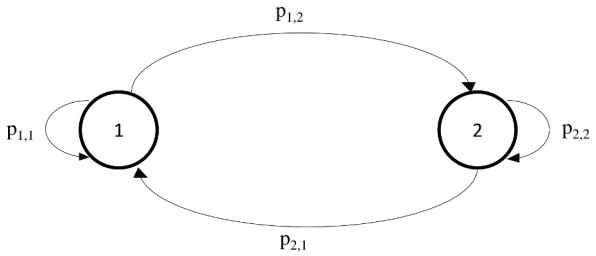

FIGURE 2.9: A two-states Markov chain.

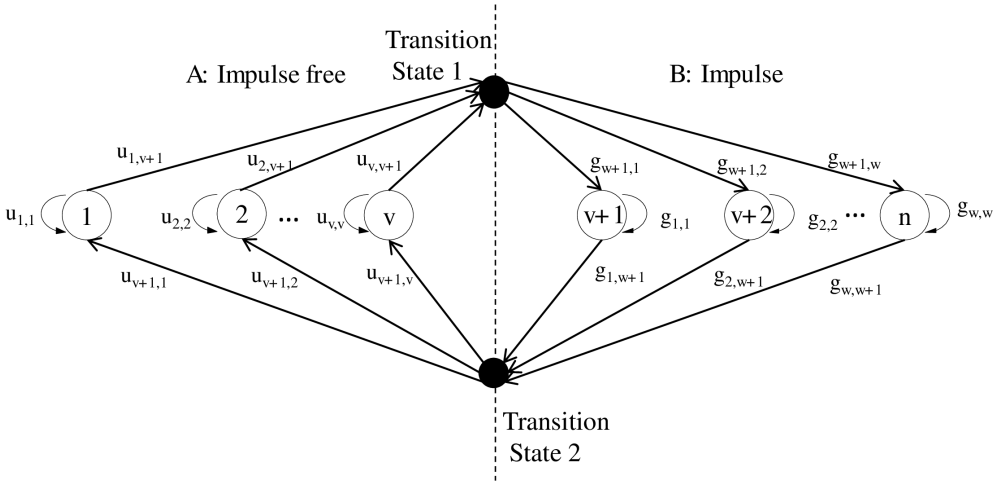

FIGURE 2.10: Partitioned Markov chain model.

$w = 1$ and $v = 1$. The proposed partitioned Markov chain is depicted in Figure 2.10. The transition probability matrices are therefore given by:

$$U = \begin{bmatrix} u_{1,1} & 0 & \cdots & 0 & u_{1,v+1} \\ 0 & u_{2,2} & \ddots & \vdots & u_{2,v+1} \\ \vdots & \ddots & \ddots & 0 & \vdots \\ 0 & \cdots & 0 & u_{v,v} & u_{v,v+1} \\ u_{v+1,v} & u_{v+1,2} & \cdots & u_{v+1,v} & 0 \end{bmatrix}, \tag{2.42}$$

$$G = \begin{bmatrix} g_{1,1} & 0 & \cdots & 0 & g_{1,w+1} \\ 0 & g_{2,2} & \ddots & \vdots & g_{2,w+1} \\ \vdots & \ddots & \ddots & 0 & \vdots \\ 0 & \cdots & 0 & g_{w,w} & g_{w,w+1} \\ g_{w+1,w} & g_{w+1,2} & \cdots & g_{w+1,w} & 0 \end{bmatrix}. \tag{2.43}$$

The elements of U and G can be derived from the measurements, by means of curve fitting methods as [5].

2.4 Conclusion

In this chapter, we have addressed the issues of PLC CTF and noise characterization and modeling. Below, each of these issues will be summarized separately.

PLC CTF Characterization and Modeling

Due to various signal reflections in PLC networks and to cable losses, the SISO-PLC link was described as a multipath channel with frequency-selective fading. Therefore, we presented a commonly accepted multipath channel model, following a formalism first proposed by Zimmerman and later extended statistically by Tonello. In addition, we described the channel model proposed by France Télécom, where the measured channels were interestingly classified into nine classes. The random channel generator proposed by Tonello, which was applied to the set of nine channel classes proposed by France Télécom, was also presented.

Next, we turned to MIMO-PLC channels, where different SISO-based models were described. Specifically, two different approaches were investigated. In order to reflect the correlation observed in experimental measurements, the first approach is based on assigning a random phase shift to each defined path of SISO CIR models (e.g., OPERA model) or SISO CTF models (e.g., Zimmerman-statistically-extended model). The second approach is based on modeling the eigenvalues of the spatial correlation matrices, following the Kronecker model which is well known in MIMO radio systems. Finally, we highlighted the importance of devising novel MIMO models based on the European MIMO PLC field measurements.

In this thesis, we apply the formalism of introducing a random phase shift to the Tonello's random channel generator and propose a MIMO random channel generator for broadband indoor PLC [85] (Chapter 3). We aim at reproducing the spatial correlation of the European MIMO PLC field measurements.

PLC Noise Characterization and Modeling

The interference scenario, which can be separated into five classes, was also characterized in this chapter. The asynchronous impulsive noise was presented as the most detrimental noise term among the five noise classes since its exhibits the highest PSD and may thus lead to significant performance degradation. Hence, we described some of literature models of the asynchronous impulsive noise. Notably, we focused on the noise characterization and modeling approaches proposed by Zimerrmann and Dostert [5] since they well represent the impulsive noise observed over PLC channels.

In this thesis and more specifically Chapter 4, the statistical analyses of the impulsive noise characteristics obtained by Zimerrmann and Dostert are taken into account. We consider impulsive noise of both moderately and weakly disturbed environments, where no periodic impulses were found at all. In other words, we only consider asynchronous impulsive noise, which is of major importance compared to periodic impulsive noise. Therefore, the impulsive noise is modeled through the three exponentially distributed time-domain parameters, namely the impulse power (or amplitude), impulse width and inter-arrival time. Thus, the impulse amplitudes can be modeled using Gaussian distribution. Concerning the background noise, the colored Gaussian model for the PSD proposed by OMEGA project is considered in this study. First, we examine the influence of the impulsive noise parameters on the BER performance by using the pulse train noise model. Next, we propose an information theory-based approach in order to ensure maximum data transmission rate in OFDM communication systems affected by impulsive noise.

CHAPTER 3

A MIMO Random Channel Generator for Indoor Broadband PLC

3.1 Introduction

Although power-lines have not been designed for data communication purposes, PLC has become nowadays a prime mode in this sense exploiting the already existing electrical power distribution grid as transmission medium. Over the past few years, many investigations have been undertaken relating to the applicability of MIMO techniques in PLC, utilizing the three-wire installations, and large-scale measurement results on MIMO power-line channel have become available. MIMO has proved to be effective in increasing the capacity by approximately a factor of two in comparison with SISO PLC systems [35]. Consequently, the ITU has published a MIMO transceiver extension (G.9963) to their G.hn standard family. Simultaneously, the HomePlug Alliance have introduced MIMO signal processing within the HomePlug AV2 specification [18].

An accurate description of MIMO channels for PLC network topologies is of great interest and importance in the development and testing of digital communication algorithms. However, the considerable variability of PLC networks makes this task quite difficult. In this regard, a random channel generator for a SISO configuration has been presented in the literature. In this chapter, based on the aforementioned SISO configuration, we propose a MIMO random channel generator that targets the European MIMO PLC field measurements.

3.2 Literature Overview and Proposal

The goal of this section is to provide a brief overview of the literature channel models, discussed in Chapter 2, in order to introduce our proposed MIMO channel model.

Much effort has been devoted to modeling SISO-PLC channels. Different deterministic models have been published in the literature. A parametric model for the channel frequency response based on physical effects, such as multi-path signal propagation and cable losses is presented in [40]. In [4], a deterministic complex transfer function generator, based on a large-scale measurement campaign undertaken in [24], was provided over an extended bandwidth up to 100 MHz. Interestingly, the channels were divided into nine classes, and an average magnitude and phase model is proposed for each class. On the other hand, different stochastic models have been also proposed. In fact, due to the random nature of power-line load impedances (various electrical appliances in a home), and link topologies, PLC channels give rise to a stochastic aspect which requires to be well characterized.

Several attempts have been made to characterize statistically the power-line channels [86–90]. In [55], a statistical extension of the parameters from the model presented in the [40] was performed. This work has been continued in [3] to represent the channel frequency responses of the nine channel classes from [4]. The model in [3] has permitted a closed-form description of both the mean path loss profile and the statistical correlation function of the channel frequency response to the nine classes. A full random channel generator has been obtained by merging all the classes according to a certain class occurrence probability to reflect the entire heterogeneity of in-home PLC networks [3].

Several SISO-based MIMO-PLC channel models have been proposed. In [36], a MIMO-PLC channel generator was proposed based on the SISO-PLC channels of the OPERA project [65]. To obtain the spatial channels, the impulse responses of a MIMO channel were generated in such a way that they differed from each other by the phase value of each tap. The same idea of introducing a phase factor was adopted in [63]. In this model, the phase-neutral link was illustrated as a multipath channel with frequency-variable attenuation, according to the formalism proposed in [55]. The full channel matrix was obtained by selecting a suitable path phase for each channel matrix tap.

These approaches are good attempts at capturing the correlation of MIMO-PLC channels. However, they are insufficient to provide an *a priori* full power-line channel generator that describes the wide variety of PLC channels. An *a priori* approach allows PLC channels to be characterized without taking actual measurements. This provides a model that can be used to draw general conclusions and has practical value for designing and testing PLC systems. The SISO random channel generator proposed in [3] can be considered as a good attempt in

this sense.

In this chapter, we propose a random channel generator for MIMO-PLC channels. We use the same formalism as described in [36] and [63] in order to extend the random channel generator presented in [3] to the MIMO case. We consider that a MIMO-PLC channel can be defined as the superposition of correlated SISO channels, so we attempt to describe the MIMO channel using the nine classes obtained with the SISO configuration. An additional parameter, related to the correlation factor, has to be taken into account. This parameter is a random phase that allows the path phase of the multipath SISO model to be changed. In detail, we consider a 2×2 MIMO-PLC system. Four spatial paths are defined for each class and the spatial correlation is introduced by changing the path phase. The MIMO classes are then merged, similarly to [3], according to the class occurrence probabilities presented in [4], to obtain the full variety of MIMO-PLC channels. An offset range of path phases is then chosen for each class in order to reproduce the spatial correlation of the European MIMO-PLC field measurements obtained in [6].

The remainder of this chapter is organized as follows: The proposed MIMO channel model is presented in Section 3.3. The results and the validation of the model are presented in Section 3.4. Finally, Section 3.5 concludes the chapter.

3.3 MIMO-PLC Random Channel Generator

First, we recall the SISO-PLC random channel model on which our work is based, which has been described in Section 2.2.2. Then, the extension to MIMO-PLC channel model is proposed.

3.3.1 SISO PLC Channel Model

An interesting approach of modeling SISO-PLC channels is addressed in [40]. The model presented a parametric function describing the channel frequency response based on the physics of signal propagation, namely multipath propagation with frequency-selective fading and cable losses. The parameters of the model can be obtained from well-known geometry network measurements. A statistical extension of the model parameters has been proposed in [3], where the CTF model defined in the frequency band $2 - 100$ MHz is denoted by:

$$h(f) = A \sum_{i=1}^{N_p} (g_i + c_i f^{K2}) e^{-(a_0 + a_1 f^K)\ell_i} e^{-j2\pi f \ell_i / \nu}. \tag{3.1}$$

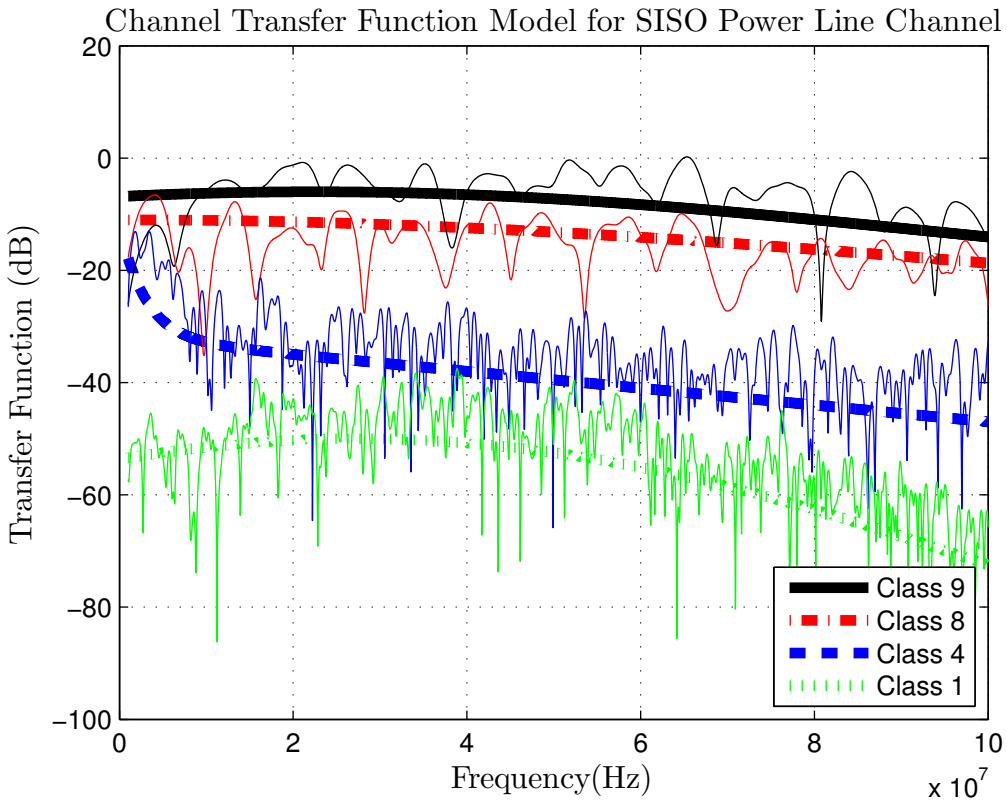

FIGURE 3.1: Channel transfer function and target average channel attenuation of classes 9, 8, 4 and 1.

A, a_0, a_1, ν, K and $K2$ are constant parameters and can be obtained by fitting the model to channel measurements; a_0, a_1 and K describe the characteristics of the cables; ν is the phase velocity of the wave inside power-line cables and is equal to $c/\sqrt{\varepsilon_r}$, where c is the speed of light in vacuum and ε_r is the dielectric constant of the insulating material. The parameters g_i, c_i, ℓ_i, and N_p are random variables [3]; g_i and c_i are the path gain coefficients resulting from the product of the reflection and transmission coefficients, they are assumed to be lognormally distributed random variables multiplied by random sign flips; ℓ_i is the length of the i-th path and is modeled as a uniformly distributed random variable in $[0,L]$ (L is constant); N_p is the number of paths and is modeled as a Poisson random variable with mean ΛL and $\Lambda = 0.2$.

The model was fitted to the results of the measurement campaign performed in [4, 24], where the channels were divided into nine classes according to their capacities. The model enabled a closed-form description of both the mean path loss profile and the average coherence bandwidth for all the classes [3]. For each class, all the parameters, the average path profile, the coherence bandwidth and the delay spread were provided. An example of CTFs generated

according to this model [3] and the target average channel attenuation [4] of classes 9, 8, 4 and 1 are depicted in Figure 3.1. The differences between the classes in terms of the average channel gain and the coherence bandwidth can be observed, especially between same-circuit classes (i.e., classes 9 and 8) and different-circuit ones (i.e., classes 4 and 1).

Finally, a random channel generator has been proposed by merging all the channel classes according to the class occurrence probability described in [4] in order to reflect the entire heterogeneity of in-home PLC networks.

3.3.2 Extension to a MIMO PLC Channel Model

Several MIMO CTF measurements have been presented in the literature [63] [6]. Consequently, it can be seen that a MIMO channel is the superposition of correlated SISO channels. Thus, we attempt to describe a MIMO channel using the same nine classes obtained with a SISO configuration. We consider that a SISO channel class, characterized by a certain average path loss profile and a certain average coherence bandwidth, can be extended to a MIMO channel class with similar characteristics. An additional parameter, related to the correlation between the spatial channels of each class, is taken into consideration.

For the sake of simplicity, we consider a 2×2 MIMO configuration in this study. $(\cdot)^C$ refers to the channel class C, $C = \{1, 2, .., 9\}$. The class C SISO CTF is denoted $h^C(f)$, where $h^C(f)$ is obtained from Eq. (3.1) by inserting the values of the parameters corresponding to the class C parameters defined in [3] (see Section 2.2.2). Once $h^C(f)$ is modeled, the four spatial paths of the 2×2 MIMO matrix of the same class has to be defined. The class C MIMO channel matrix, denoted as $H^C(f)$, is given by:

$$H^C(f) = \begin{pmatrix} h_{11}^C(f) & h_{12}^C(f) \\ h_{21}^C(f) & h_{22}^C(f) \end{pmatrix}, \tag{3.2}$$

where $h_{nm}^C(f)$ is the complex channel transfer coefficient from the m^{th} transmitter to the n^{th} receiver of channel class C at frequency f. The channel coefficient $h_{nm}^C(f)$ is given by:

$$h_{nm}^C(f) = A_{nm}^C \sum_{i=1}^{N_p} \left(g_i + c_i f^{K_2^C}\right) e^{-\left(a_0^C + a_1^C f^{K^C}\right)\ell_i} e^{-j2\pi f \ell_i/\nu} e^{-j\varphi_i^C}. \tag{3.3}$$

$h_{nm}^C(f)$ differs from $h^C(f)$ by the last exponential term, where φ_i^C is a random phase which represents the additional parameter. φ_i^C is randomly selected according to a uniform distribution between $-\Delta^C\varphi/2$ and $+\Delta^C\varphi/2$:

$$\varphi_i^C \in U\left[-\frac{\Delta^C\varphi}{2}, +\frac{\Delta^C\varphi}{2}\right], \tag{3.4}$$

where $\Delta^C\varphi$ is an offset range of path phases which specifies the spatial correlation of the channel class C. This allows the path phase between class C MIMO taps to be changed resulting in different spatial correlation scenarios depending on the value of $\Delta^C\varphi$. If $\Delta^C\varphi = 2\pi$ class C MIMO channels have a minimum spatial correlation, whereas if $\Delta^C\varphi = 0$ MIMO channels are totally correlated. As $\Delta^C\varphi$ increases from 0 to 2π, MIMO channels given in Eq. (3.2) show lower spatial correlation. $\Delta^C\varphi$ are chosen according to a strategy described in the next section. To reflect the channel measurements performed in [63], where it was found that the co-channels were slightly stronger than the cross-channels in the same-circuit case (i.e., for classes 8 and 9), the parameter A defined in Eq. (3.1) for the cross-channels is reduced by a factor of 3 dB in relation to parameter A for co-channels in the same circuit case. Therefore, A_{nm}^C is defined as:

$$A_{nm}^C = \begin{cases} A^C & (n = m \text{ and } C = 8, 9) \\ A^C \Delta A & \text{otherwise ,} \end{cases} \tag{3.5}$$

with:

$$\Delta A = 0.5. \tag{3.6}$$

3.3.3 Strategy for Choosing an Offset Range for Each Channel Class

We propose to define for each channel class C, characterized by a certain average path loss profile and average coherence bandwidth, a certain spatial correlation specified by the offset range $\Delta^C\varphi$ in order to capture the spatial correlation of the European MIMO PLC field measurements reported in [6] (see Section 1.5.2). We generate 500 channel realizations of the MIMO channel matrix defined in Eq. (3.2) according to the class occurrence probability reported in Table 3.1 [4] (to obtain the full variety of power-line channels) with initial values of $\Delta^C\varphi$, $C = 1, .., 9$. We calculate the spatial correlation coefficient κ_{dB} defined in Section 1.5.2 Eq. (1.9) at each frequency f for the 500 channel realizations generated, where f varies from 1.001 MHz to 100 MHz with a frequency spacing $\Delta f = 24.414$ kHz. Let X be the vector containing the resulting 2,028,000 values of κ_{dB}. For each channel class C, the value of the offset range $\Delta^C\varphi$ is further varied from $V_I^C\varphi$ to $V_F^C\varphi$ with a $step = 0.1$, where $V_I^C\varphi$ and $V_F^C\varphi$ are the initial and final values of $\Delta^C\varphi$, respectively. Let $\Delta\varphi_{Set}$ be the set defined as follows:

TABLE 3.1: Offset ranges $\Delta^C\varphi$ of the proposed MIMO-PLC model for all C classes

C classes	Class occurrence probability %	$\Delta^C\varphi$
$Class\ 1$	3.49	0.1
$Class\ 2$	16.78	0.5
$Class\ 3$	18.18	1.3
$Class\ 4$	11.88	1.6
$Class\ 5$	11.88	1.3
$Class\ 6$	12.58	1.4
$Class\ 7$	9.79	3.1
$Class\ 8$	7.69	3.1
$Class\ 9$	7.69	3.1

$$\Delta\varphi_{Set} = \left\{\Delta^1\varphi, \Delta^2\varphi, .., \Delta^9\varphi\right\}, \tag{3.7}$$

where

$$\Delta^C\varphi = \left\{V_I^C, ..., V_F^C\right\}, \quad C = \{1, 2, .., 9\}. \tag{3.8}$$

For each possible combination of $\Delta\varphi_{Set}$, we generate 500 channel realizations, compute the vector X and compare its CDF with the known CDF obtained from the European measurements. Let $\Delta^C\varphi_{Vector}$ be the vector containing all the values of $\Delta^C\varphi$ (from $V_I^C\varphi$ to $V_F^C\varphi$) and L^C be its length:

$$L^C = \frac{V_F^C\varphi - V_I^C\varphi}{0.1} + 1. \tag{3.9}$$

The strategy used for choosing $\Delta\varphi_{Set}$ is based on computing the well-known Kolmogorov-Smirnov (KS) distance. The best $\Delta\varphi_{set}$ is the one which minimizes the KS distance between the empirical CDF from the channel generator and the known CDF obtained from the European measurements. The strategy used can be summarized by the following pseudo code.

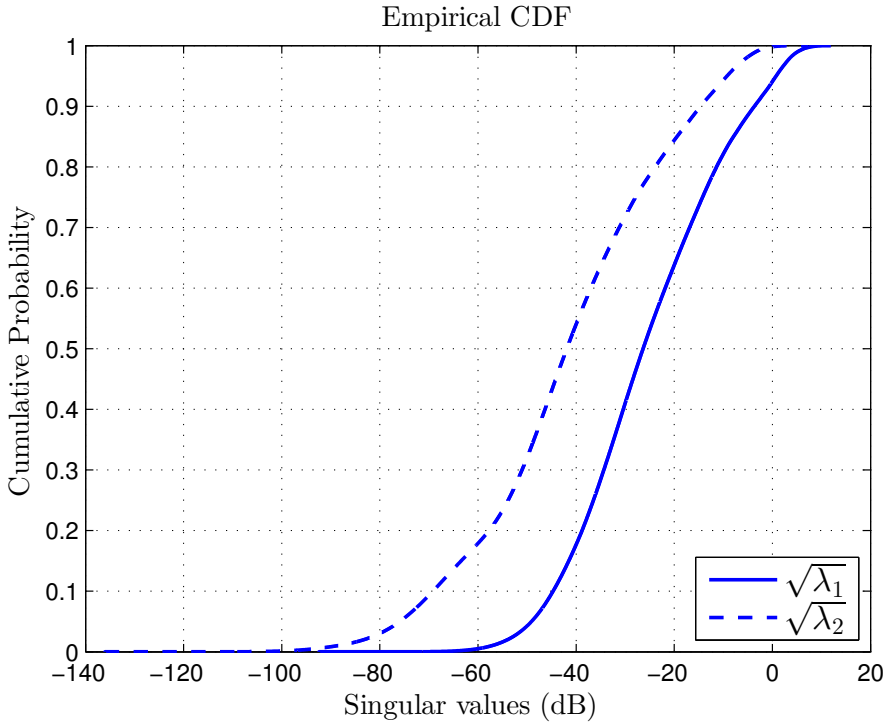

FIGURE 3.2: Singular values of the 2×2 MIMO random channel generator.

Initialization: $\Delta^C\varphi \leftarrow V_I^C\varphi$, C={1,2,..,9}

for i^C= 1 to L^C, C={1,2,..,9} **do**

$\Delta\varphi_{Set} \leftarrow \Delta^C\varphi$, C={1,2,..,9}

Compute X

$D_{max} \leftarrow max|CDF_{Model}(X) - CDF_{EuropMeasure}(X)|$

end

choose $\Delta\varphi_{Set}$ corresponding to distance (d) $= min(D_{max})$

For each $\Delta\varphi_{Set}$, the CDF of X is compared with the CDF from the European measurements [6] using sufficient number of points, and the maximum distance between the two CDF plots is investigated. Finally, the $\Delta\varphi_{Set}$ with $d = min(D_{max})$ is chosen. We note that the CDF plot of the European measurements is redrawn using high resolution software. The result of the best $\Delta\varphi_{set}$ is reported in Table 3.1, where the obtained $d = min(D_{max})$ was 0.0052.

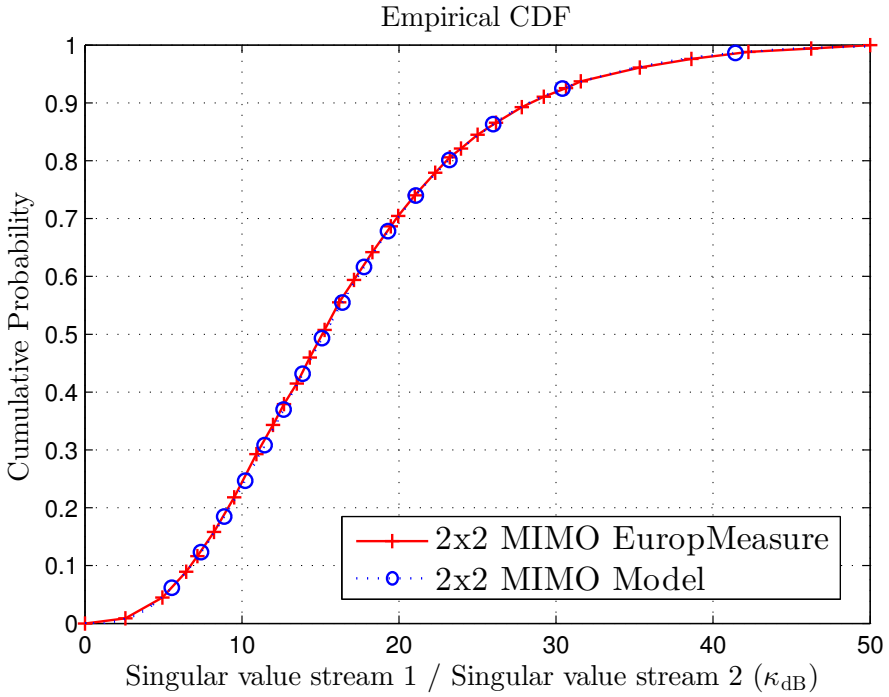

FIGURE 3.3: Fitting of the spatial correlation of the model with the spatial correlation of the European measurements for 2×2 MIMO configuration.

3.4 Results and Validation of the Model

In this section, we report simulation results of 1000 channel realizations generated using the MIMO random channel generator. $\Delta^C\varphi$ and the class occurrence probability are chosen from Table 3.1. The value of the spatial correlation coefficient κ_{dB} (defined in Eq. (1.9)) is calculated at each frequency f for all the channel realizations generated.

3.4.1 Spatial Correlation of the Model

As mentioned previously, the singular values are good parameters for investigating the spatial correlation of a MIMO communication system. They also provide information on channel attenuation as they are the channel gains for the logical streams. Figure 3.2 shows the CDF of the singular values of the MIMO channel generator. The solid line represents the first logical stream and the dashed line represents the second logical stream. The results show that, in comparison with the European channel measurements in the case of a 2×2 MIMO configuration [6], some channels (within the European field measurements) have higher attenuation than class 1 channels (the most attenuated channel class).

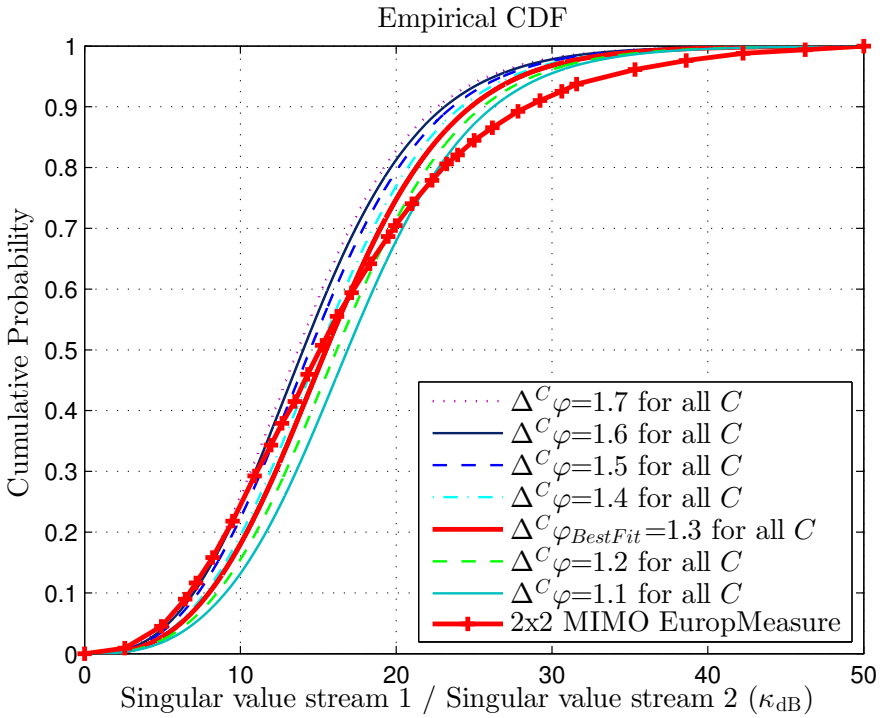

FIGURE 3.4: Best fit for the spatial correlation of the model with the target measurements when considering a constant $\Delta^C\varphi$ for all C classes.

Figure 3.3 shows the CDF of the spatial correlation ratio κ_{dB} of the proposed MIMO channel generator and the ratio obtained with the European MIMO PLC field measurements [6]. The fit of the two curves is excellent (the $\Delta^C\varphi$ values were chosen for this purpose). The measurements show that a few channels have very high spatial correlations [6]. The model represents these channels in class 1, where $\Delta^1\varphi = 0.1$ and the probability of occurrence is 0.0349 (low probability of occurrence).

To verify the proposed $\Delta^C\varphi$ values presented in Table 3.1, a constant $\Delta^C\varphi$ is assumed for all the classes and the case that fit the European spatial correlation measurements best is sought. Figure 3.4 shows the CDF of the κ_{dB} ratio taking different $\Delta^C\varphi$ values from 1.7 (the upper curve) to 1.1 into consideration. The best fit is obtained for $\Delta^C\varphi = 1.3$ for all C and is chosen on the basis of the KS distance between the empirical CDF and the reference CDF. The figure shows that by considering a constant $\Delta^C\varphi$ for all C classes, i.e., same spatial correlation for all classes, the channel generator cannot correctly reproduce the target spatial correlation. The best fit is still considerably different from the target European measurements. However, choosing $\Delta^C\varphi$ from the set reported in Table 3.1 enables the MIMO random channel generator to accurately represent the target spatial correlation (as shown in Figure 3.3).

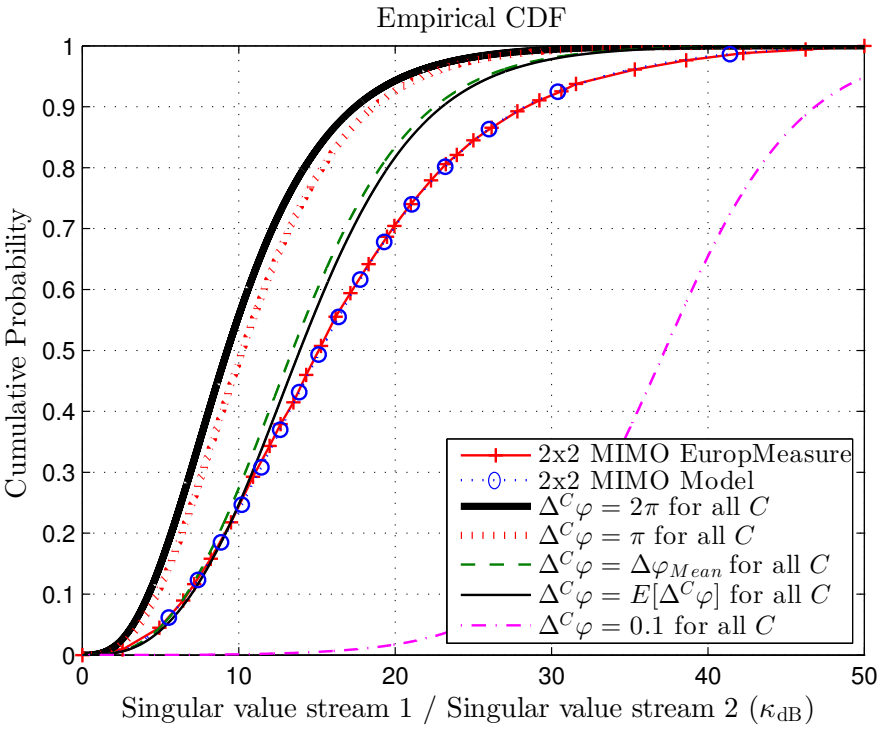

FIGURE 3.5: spatial correlation of the model with different cases of interest.

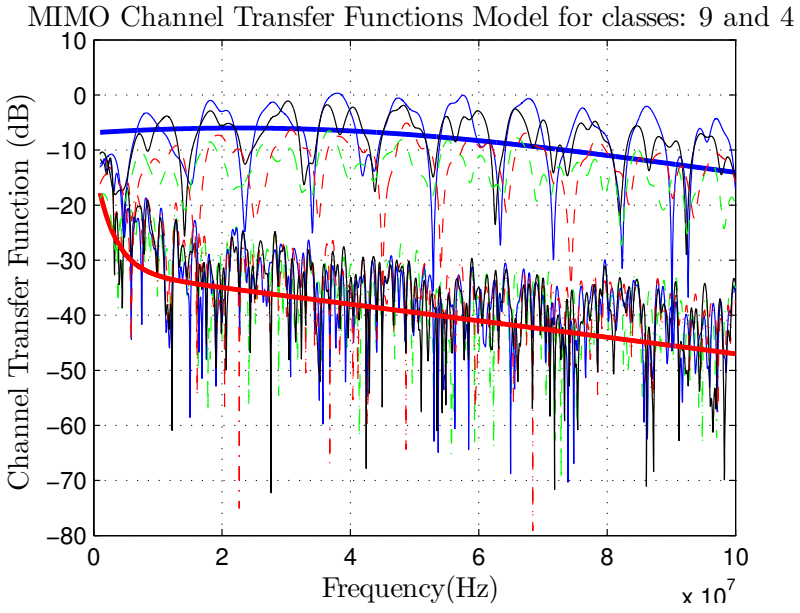

FIGURE 3.6: MIMO channel transfer function model for classes 9 and 4.

For comparison, we plot the spatial correlation of the proposed MIMO random channel generator, i.e., with the $\Delta^C\varphi$ set reported in Table 3.1, with other cases of interest where

the values of $\Delta^C\varphi$ are fixed for all the C classes. The chosen values of $\Delta^C\varphi$ are: 2π, π, 0.1, $\Delta^C\varphi_{Mean}$ and $E[\Delta^C\varphi]$. A value of 2π for all C represents the minimum spatial correlation that can be obtained by the random channel generator. The values π and 0.1 correspond to the offset ranges assigned to classes 9 and 1, respectively. $\Delta^C\varphi_{Mean}$ and $E[\Delta^C\varphi]$ are respectively the arithmetic mean and the expected value of $\Delta^C\varphi$ reported in Table 3.1. The results are depicted in Figure 3.5. It is clear that by considering a constant $\Delta^C\varphi$ value of 0.1 and 2π for all C classes, MIMO-PLC channels present very high and very low correlations, respectively.

3.4.2 MIMO Channel Transfer Function Model

Figure 3.6 shows the CTF of the MIMO-PLC channel generated for classes 9 and 4. The upper group of curves corresponds to class 9 MIMO channels, and the lower group corresponds to class 4 MIMO channels. The solid lines of both channel classes represent the co-channels, and the dashed lines represent the cross-channels. The two bold lines correspond to the average channel attenuation of the channel classes 9 and 4. As shown in Figure 3.6, the co-channels are slightly stronger than the cross-channels for class 9 MIMO channels (same electrical circuit), whereas for class 4 MIMO channels (different electrical circuit) co-channels and cross-channels cannot be distinguished.

3.5 Conclusion

In this chapter, we presented a MIMO random channel generator for indoor PLC channels based on a SISO configuration presented in the literature. First, we described the SISO random channel generator, for which the proposed method was applied to a set of nine channel classes. For each class, the model enabled a closed-form description of both the average path loss profile and the average coherence bandwidth of the CTF. We highlighted the importance of such a method as well as the nine channel classes. Then, we proposed an extension to a MIMO system. We considered that a MIMO channel can be defined as the superposition of correlated SISO channels, so we then attempted to describe the MIMO channel starting from a SISO channel. We considered the same measurement campaign where the channels were divided into nine classes and we aimed to represent the spatial correlation of the European MIMO PLC field measurements. An additional parameter, related to the spatial correlation factor, had to be taken into account. In practice, we considered a 2×2 MIMO system. So, for each class we defined its corresponding MIMO class by introducing its spatial correlation. We have shown that when a specific spatial correlation is chosen for each class, the target spatial correlation can be accurately reproduced by the channel generator.

Finally, it was shown that the proposed MIMO random channel generator represents the wide variation of MIMO-PLC channels. This work will enable the development and testing of digital communications algorithms.

CHAPTER 4

An Outage Capacity Approach for OFDM Systems Affected by Impulsive Noise

4.1 Introduction

Despite the main advantages inherent in in-home broadband PLC technology, it faces a number of serious challenges related to the harsh nature of the power-line medium. Some of these challenges are the various interference sources (such as impulsive noise), the multipath propagation with frequency selective fading and the channel attenuation. To overcome the multipath effect and channel attenuation, much effort has been devoted to characterizing and modeling PLC CTFs [3, 40, 85].

Impulsive noise is known to be a physical phenomenon that drastically affects the performance of indoor broadband PLC systems. It is introduced in the literature as a catastrophic event that may cause bit or burst errors. As an illustration of the impact of impulsive noise in OFDM PLC systems, we first examine the influence of its characteristics on the BER performance and provide an overview of the strategies for countering its effect. Next, we propose an outage capacity approach in order to optimize the average data rate in OFDM systems affected by impulsive noise. To this end, we study the channel capacity of the system by adding a noise margin to the transmitted symbols. The system declares an outage if the energy of the impulsive noise contained in an OFDM symbol exceeds the added noise margin. The outage capacity is investigated by deriving both the outage probability and

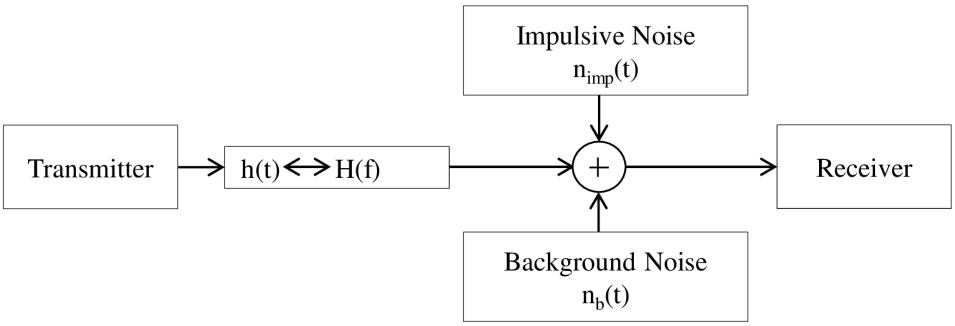

FIGURE 4.1: In-home power-line channel model.

channel capacity in terms of the noise margin. Then, based on the obtained outage capacity, we propose an approach that maximizes the average data rate of the system. As a particular case, we consider the characteristics of impulsive noise specific to indoor broadband PLC.

4.2 Impulsive Noise in OFDM PLC: Illustration of its Detrimental Effect

Impulsive noise is usually described in the literature as a process characterized by a train of pulses whose amplitude, duration and arrival time are random. Different statistically-based approaches have been proposed for modeling the impulsive noise. Some of them are the statistical amplitude noise models, such as Bernoulli-Gaussian (BG) [91] and Middleton class A [75] noise models. These models provide a closed-form and simple PDF expression which is needed in designing optimum receivers of low complexity. However, they do not represent the time correlation of the impulses (i.e., impulses durations) observed over PLC channels, as they assume independent impulse emission. This section first briefly shows the impact of impulsive noise on the BER performance of OFDM PLC systems using the pulse train noise model described in Section 2.3.2. We study the influence of the impulsive noise parameters, namely the impulse amplitude, impulse width and interarrival time on the system, based on the noise characterization made in [5]. Then an overview on the impulsive noise countering strategies is provided.

4.2.1 Impact of Impulsive Noise Parameters on BER Performance

Here we consider the system model depicted in Figure 4.1. The statistical CTF model proposed by Tonello in [3], which is detailed in Section 2.2.2, is considered where a CTF $H(f)$ is set from Eq. (2.10). The chosen values of the path-depend parameters are presented in Table 4.1; N_p, K, K_2, ν and A are 5, 2.21, 0.34, $\frac{2c}{3}$ and $2.4 \times 10^{-5.3}$, respectively. The

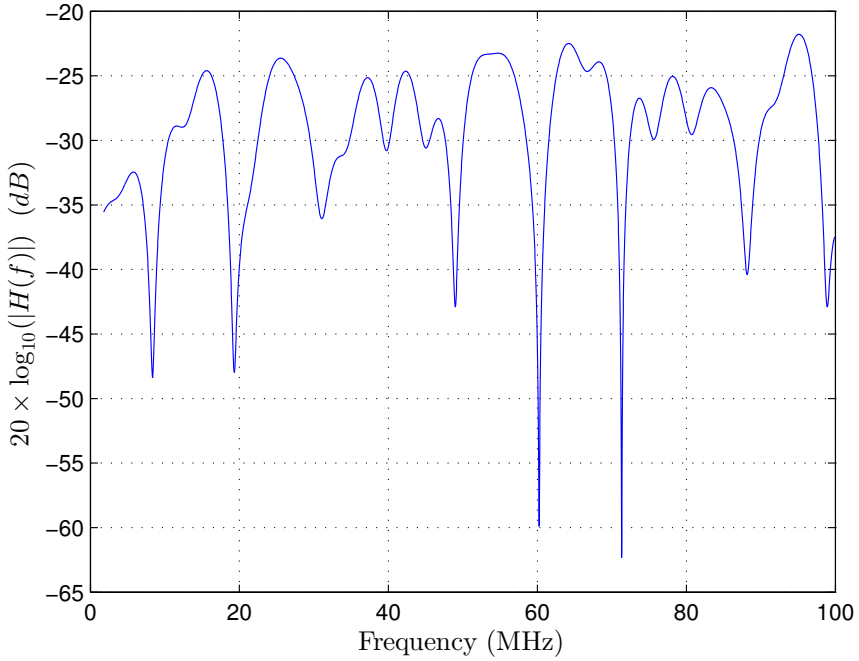

FIGURE 4.2: Simulated PLC channel transfer function.

TABLE 4.1: Parameters for $H(f)$

i	g_i	c_i	ℓ_i
1	-0.14	0.997	5
2	0.61	-0.998	12
3	-6.61	0.998	30
4	-0.38	-0.991	35
5	-1.65	-1.001	50

magnitude of $H(f)$ in dB scale in the frequency band $1.8 - 100$ MHz is shown in Figure 4.2.

The general expression of the considered noise model, expressed as the sum of the background noise and impulsive noise, can be derived from the pulse train noise model proposed in [5] (see Section 2.3.2) as follows:

$$n(t) = \sigma_{_G} \cdot n_{_{G_1}}(t) + \sum_{k=1}^{N_I} \frac{\sigma_{_{I,k}}}{\sigma_{_G}} \text{imp}\left(\frac{t - t_{_{A,k}}}{t_{_{w,k}}}\right) \cdot n_{_{G_2}}(t), \tag{4.1}$$

where imp(t) is the impulse function with unit amplitude and unit width; $n_{_{G_1}}(t)$ and $n_{_{G_2}}(t)$ are two zero-mean Gaussian realizations with variance equal to one; N_I is the number of impulses present over the transmission time; $\sigma_{_G}$ and $\sigma_{_I}$ are Gaussian and impulsive noise amplitudes, respectively; $A_{_k} = \frac{\sigma_{_{I,k}}}{\sigma_{_G}}$, $t_{_{A,k}}$ and $t_{_{w,k}}$ are impulse amplitude, impulse arrival

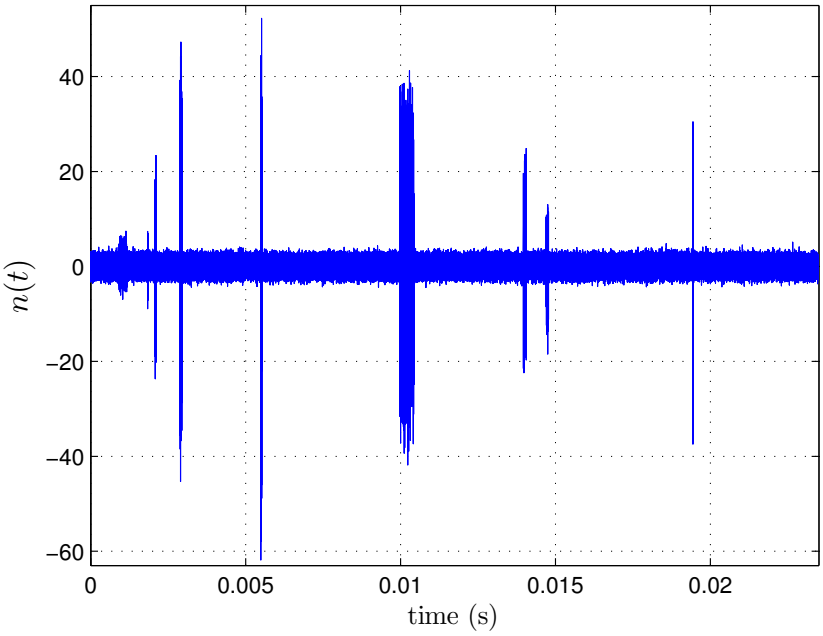

FIGURE 4.3: Impulsive noise model with $\lambda = 0.005\ s$, $\Gamma = 100$ and $W = 100\ \mu s$.

time and impulse time width, respectively. The three random parameters A_k^2, $t_{w,k}$ and the interarrival time $t_{IA,k}$ $(t_{IA,k} = t_{A,k+1} - t_{A,k})$ can be statistically modeled using an exponential distribution [5, 92]. Consequently, for a given σ_G^2, the noise model can be generated through the three mean parameters of the exponential distributions. The mean parameters of A_k^2, $t_{IA,k}$ and $t_{w,k}$ are denoted by Γ, λ and W, respectively (we note here that the parameters Γ and λ are analogous to μ and ψ of BG noise model, presented in Section 2.3.2, respectively). An example of the considered noise model for practical values of $\lambda = 0.005\ s$, $\Gamma = 100$ and $W = 100\ \mu s$ over a time duration of 500 OFDM symbols is presented in Figure 4.3. Compared to the considered OFDM symbol duration of $40.96\,\mu s$, it can be noted that an impulse may affect one or several consecutive symbols, and many symbols may not be affected by impulsive noise. In fact, all of the possible cases regarding the occurrence of an impulse during the transmission of a symbol (or a block) can be reflected by the considered model, which makes it the best to describe asynchronous impulsive noise over PLC channels.

For the sake of simplicity, we assume ideal synchronization and use the binary phase-shift keying modulation scheme in simulations. The OFDM modulator block is implemented using $N = 1024$ point Inverse Fast Fourier Transform (IFFT) in the frequency band 1.8-10 MHz with subcarrier spacing of 24.414 kHz, in respect to the subcarrier spacing specified in Home-Plug Alliance [18]. Note that choosing higher transmission frequency bans and higher order modulation schemes would result in similar conclusions in our case. The chosen sampling frequency is 24.999936 MHz. After IFFT, a 150 (6 μs in time) length cyclic prefix is added

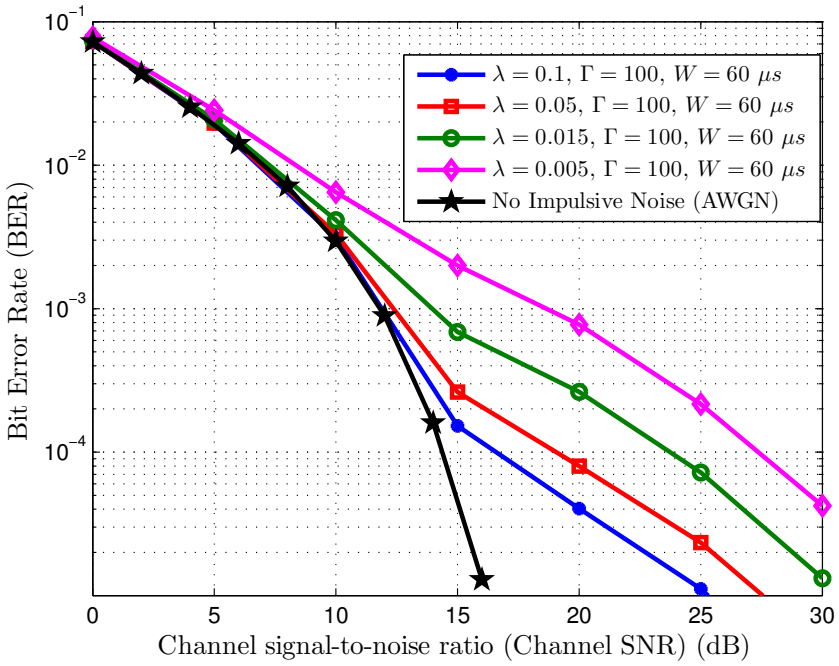

FIGURE 4.4: BER performance for different values of λ and for $\Gamma = 100$ and $W = 60\ \mu s$.

at the beginning of the OFDM symbol. The length of the extended OFDM symbol is 1174 samples (46.96 μs in time). The noise $n(t)$ is generated over a transmission time of 10^6 OFDM symbols. During a symbol transmission, the amount of the noise already generated from $n(t)$ is then added to the symbol. The results are reported as a function of the SNR.

The impulsive noise is characterized by a high PSD that can reach values of more than 50 dB above the background noise [5]. Consequently, three different values of Γ are set in this study, which are 10, 100, and 1000. Practical values of λ and W in PLC are 0.015 s and 60 μs, respectively [5]. Three other values of λ of 0.005, 0.05 and 0.1 are also taken into account in order to examine heavier and milder impulsive noise conditions. Another value of W of 1 μs is chosen to check the effect of the impulse width characteristic parameter on the system's performance.

The λ parameter, which is the mean interarrival time between impulses, can be considered as the most important characteristic parameter. It gives information about how much the system is affected by impulsive noise. Figure 4.4 shows its influence on the BER performance for $\Gamma = 100$ and $W = 60\ \mu s$. The lower the value of λ the more dense the impulses in the system, the more errors produced. This can explain the obtained results where it can be noted that λ has a significant influence on the BER performance.

In Figure 4.5, the system's performance is illustrated for $\lambda = 0.015\ s$ and for two different

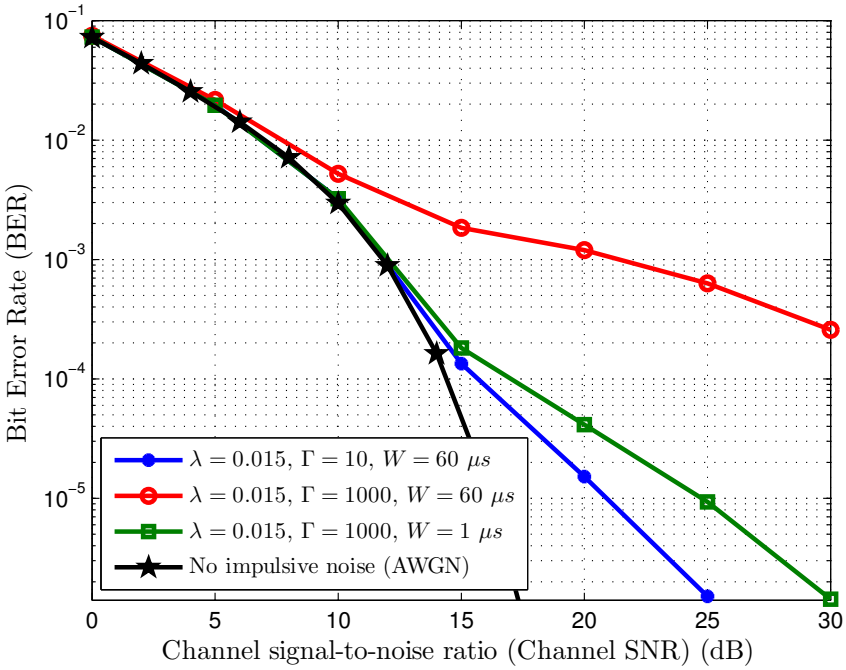

FIGURE 4.5: BER performance for two different values of each of Γ and W while keeping the other parameters constant.

values of each of Γ and W, while keeping the other parameter constant. This allows us to examine the influence of the two parameters Γ and W on the system. The Γ parameter represents the mean power ratio of the impulsive noise to the background noise. Thus, the higher the Γ, the more error produced in the system. This can explain the significant difference between the two resultant BERs for $\Gamma = 10$ and $\Gamma = 1000$ with $W = 60\ \mu s$.

The W parameter represents the mean time width of the impulses. Obviously, the higher the value of W the more signal samples affected by the impulses, the more errors produced. An impulse may affect one or more OFDM symbols resulting in burst errors in data transmission. By comparing the two resultant BERs for $W = 60\ \mu s$ and $W = 1\ \mu s$ with $\Gamma = 1000$, it can be noted that the W parameter can significantly change the system's performance. At high SNR, a value of W of 1 μs can affect significantly the system's performance (see Figure 4.5).

For the reason of comparison, we apply the popular BG noise model to the PLC channel. The BG model is characterized by two parameters, ψ and μ, as described is Section 2.3.2. We checked the effect of the ψ parameter by setting two values of 0.1 and 0.01, while keeping $\mu = 10$. We also checked the effect of the μ parameter by setting two values of 10 and 1000 with $\psi = 0.1$, the results are depicted in Figure 4.6. The ψ and μ parameters are analogous to λ and Γ parameters, respectively. It can be noted from Figure 4.6 that they have a significant

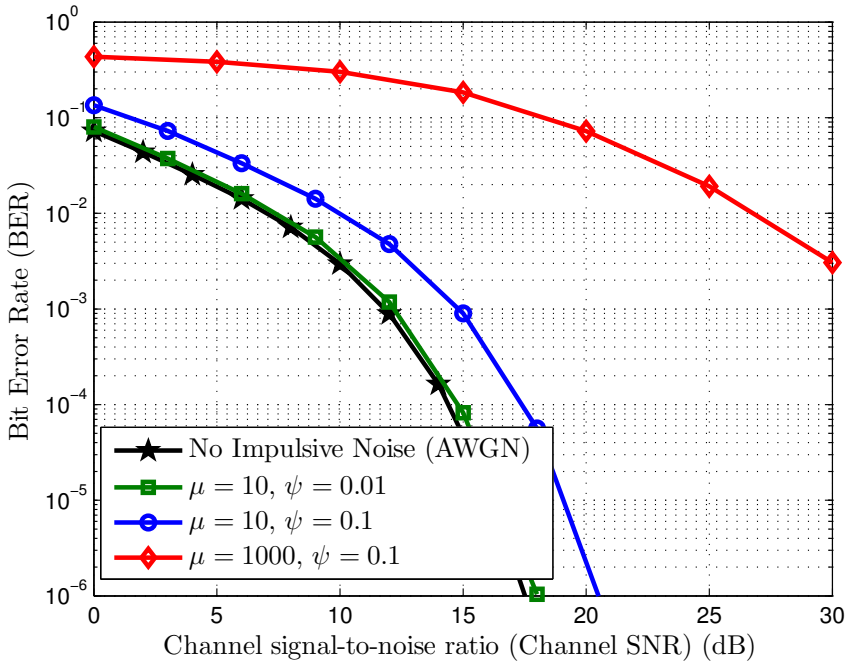

FIGURE 4.6: BER performance using BG noise model with different values of model's parameters.

influence on the system's performance.

By comparing Figure 4.6 with Figures 4.4 and 4.5, it can be noticed that the resultant BERs using the two noise models follow a different trend. The OFDM performance curves, using the BG model, have the same shape as the BER obtained with AWGN, but with higher power. However, it is not the case, when the considered model is used. This can be attributed to the fact that the characteristic parameters of the two models are different. The ψ parameter represents the probability of the occurrence of the impulses within the symbol duration. The effect of these impulses is spread over N subcarriers resulting in BER performance that follows the same trend with AWGN performance. On the other hand, by using the considered pulse train noise model, one impulse may affect one or several OFDM symbols, and many symbols may not be affected by impulsive noise at all.

4.2.2 Impulsive Noise Mitigation Methods

As can be seen from the previous section, and as is to be expected, the impulsive noise largely affects PLC systems. Many studies have addressed the problem of providing reliable communication in the presence of impulsive noise. Many alternative techniques, which can be broadly divided into three categories, have been developed to deal with its detrimental

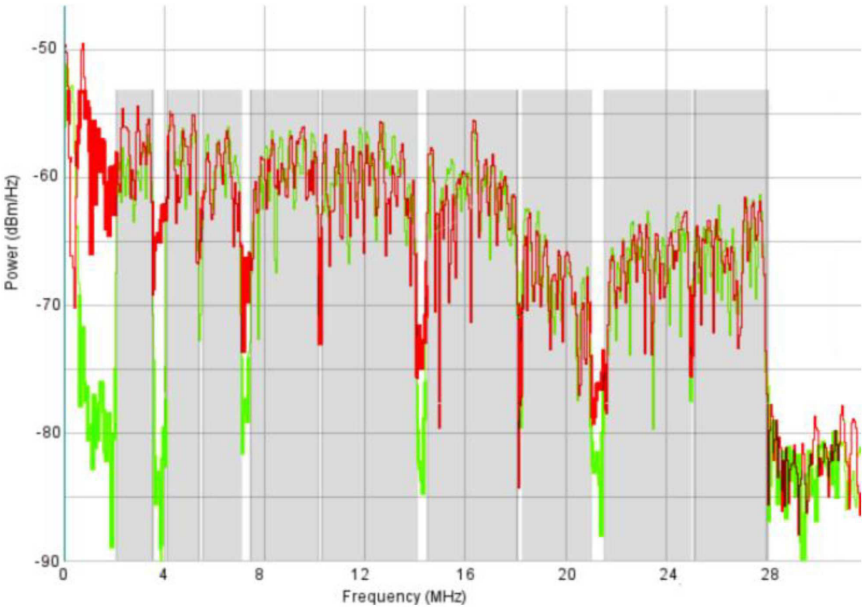

FIGURE 4.7: HomePlug AV signal spectrum during the presence and absence of an impulse [99].

effects [54]. The first category is referred to as channel coding-based solutions, which consist in applying Forward Error Correction (FEC) codes, such as turbo codes and low density parity check codes, to an impulsive environment [93–95]. The main idea behind the concept of FEC codes is to add at the transmitter side some redundant bits derived from the useful ones in order to allow the receiver to detect as much as possible the errors encountered during the transmission. The second family of impulsive noise mitigation techniques concerns the modulation scheme. It is shown that multi-carrier modulation (or OFDM modulation) is more robust against impulsive noise compared with single-carrier modulation due to the spreading effect of the Discrete Fourier Transform (DFT) operation at the receiver [81]. A symbol in a single-carrier system can be completely masked by an impulse, while in an OFDM system the energy of each impulse is spread over all the subcarriers in that symbol. The last family consists of signal processing-based solutions. The nonlinearity technique is a widely-used method which includes clipping and/or blanking non-linearities [82, 96–98].

Signal processing techniques based on impulsive noise detection and estimation have to be proposed to mitigate the effect of impulsive noise. In [100], three algorithms were proposed to detect impulsive noise. An impulse was detected in the time domain (based on a time domain monitoring of the amplitude level), in the frequency domain (based on a frequency domain monitoring of each of the received symbol subcarriers to see if it is apart from the maximum constellation envelop), or by combining the time and frequency domain analysis

(based on a mean-square-error monitoring). In [101], authors proposed to use pilots to detect impulses. In [101, 102], adaptive and iterative impulsive noise suppression algorithms were proposed. Recently, an approach for impulsive noise estimation and removal has been proposed, based on the exploitation of the unused/null subcarriers in order to obtain a signal-free subspace onto which the impulsive noise can be projected [103]. The same idea was adopted in [99], which proposed to measure the power on the masked/null carriers to detect the presence of impulsive noise. Figure 4.7 shows an HomePlug AV signal spectrum during normal transmission (green) and during the presence of an impulse (red), where carriers used for transmission are hidden by gray mask [99]. It can be noticed that in the presence of an impulse the noise power on the masked carriers increases remarkably.

4.3 Motivations and Proposal

The impact of impulsive noise on the performance of communication systems constitutes a major problem that must be overcome. As illustrated in the previous section, several techniques have been proposed to mitigate the detrimental effect of impulsive noise, and significant improvements in the BER performance have been achieved [82, 93, 103–108]. For example, works in [103,107] have exploited the sparsity of the impulsive noise in the time domain and made use of the null subcarriers in OFDM transmission to combat impulsive noise. However, if the impulses widths are of the same order as the width of a signal-processing frame, impulsive noise mitigation methods cannot be successful and a single impulse might result in the erasure of one or even several consecutive OFDM symbols. This results in a significant degradation of the data rate performance and thus the channel capacity. This chapter aims at investigating the maximum achievable data rate in OFDM communication systems affected by impulsive noise, based on the principle of outage capacity.

Some works have been devoted to the channel capacity of communication systems affected by impulsive noise. In [109] and [110], the capacity of BG noise channel in Rayleigh fading was investigated through its tight lower and upper bounds, and a capacity analysis for broadband frequency-selective BG noise channels was reported in [111]. In [112], the ergodic capacity for broadband PLC in the presence of impulsive noise was investigated by considering two coding schemes, namely the erasure and the full decoding schemes.

In the rest of this chapter, we present an information theory-based approach in order to ensure maximum data transmission rate in OFDM communication systems affected by impulsive noise. The impulsive noise is modeled through the three exponentially distributed time-domain parameters, namely the impulse power (or amplitude), impulse width and inter-arrival time (see Section 2.4). In other words, we consider a Poisson-Gaussian impulsive noise

model [5, 80]. The temporal aspect of impulsive noise is taken into consideration in order to study the overlap between an impulse of noise and an OFDM symbol. Examining the time aspect excludes the direct use of the amplitude PDF of noise (note that the considered noise model leads to the PDF of Middleton class A noise model). By adding a noise margin to the transmitted symbols, we study the outage capacity of the system. To this end, we first find the channel capacity as a function of the noise margin. Note that we consider that the CTF is stationary and both the background noise and impulsive noise are colored noises. We then find the outage probability defined as the probability that the energy of the impulsive noise contained in an OFDM symbol exceeds the noise margin (the study of outage probability is provided in Appendix A). Based on the two aforementioned findings, we investigate the outage capacity of the system. Next, based on the obtained outage capacity, we propose an approach that enables the required optimal outage probability (or noise margin) to be determined to maximize the average data rate. As a particular case, we present the results of high-speed transmission over indoor broadband PLC channels in the presence of impulsive noise.

4.4 Outage Capacity Approach

The most common channel model assumed in communication theory is the AWGN in which transmitted signals are only distorted by a linear addition of white noise with a constant spectral density and a Gaussian distribution of amplitude. Although the channel in reality is more complex, characterized by fading, frequency selectivity, interference or nonlinearity, this model is important for gaining insight into the basic behavior of a system without considering these characteristics and is very efficient when simulating background noise. According to Shannon's theory [25], the theoretical limit of the data rate over AWGN channel can be specified. The capacity of the AWGN channel with received SNR γ, denoted as C, is given by:

$$C = \log_2(1 + \gamma) \quad \text{bits/s/Hz}, \tag{4.2}$$

with

$$\gamma = |h|^2 \cdot \gamma_0, \tag{4.3}$$

where $|h|^2$ is the channel gain and γ_0 is the power ratio of the transmitted signal to the noise. This capacity result can be applied as well to analyze the limits of communication over fading and frequency-selective channels.

In many cases, communication channels vary slowly compared with the symbol rate. For

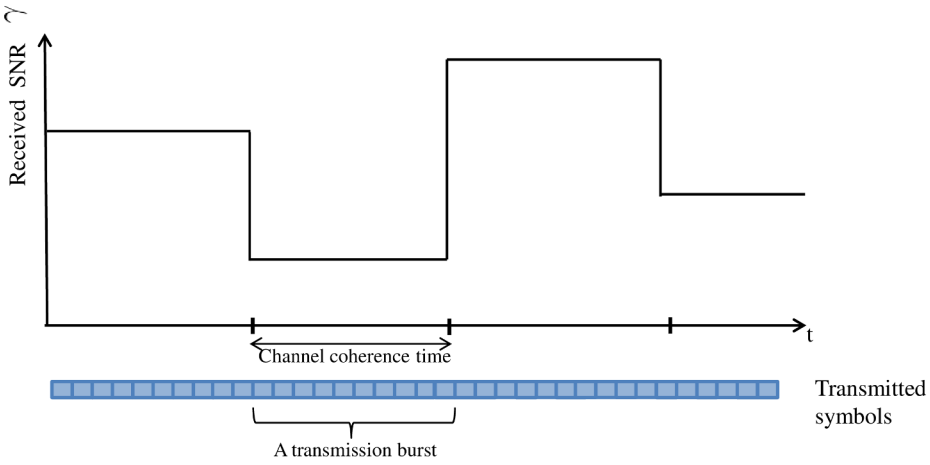

FIGURE 4.8: Typical representation of a slow fading channel.

example, in typical wireless channels, the coherence time is of order of hundreds of symbols. This represents the slow fading or quasi-static scenario where the coherence time is greater than the latency requirement. The instantaneous SNR in this case is constant over a large number of transmitted symbols (a transmission burst) and then changes to a new value depending on the fading distribution [113] (see Figure 4.8). So, during a transmission burst over a channel realization h, the communication channel can be considered as an AWGN one with received SNR γ. The maximum rate of information that can be reliably transmitted over this channel is thus $\log_2(1+|h|^2\gamma_0)$ bits/s/Hz, which depends on the random channel gain $|h|^2$, which is unknown to the transmitter. If the transmitter encodes data at rate R bits/s/Hz in which the channel capacity $\log_2(1+|h|^2\gamma_0) < R$, for a deep fade channel realization h, then the bits received within that transmission burst cannot be decoded correctly with probability approaching one. In this case, the system is said to be in outage and the outage probability is given as:

$$p_{out}(R) = \text{prob}\left\{\log_2(1+\gamma) < R\right\}, \tag{4.4}$$

where prob$\{\cdot\}$ refers to probability. Or equivalently, the system is in outage if the received SNR γ is below a certain minimum received SNR γ_o. Thus the outage probability can also be given as:

$$p_{out} = \text{prob}\{\gamma < \gamma_o\}. \tag{4.5}$$

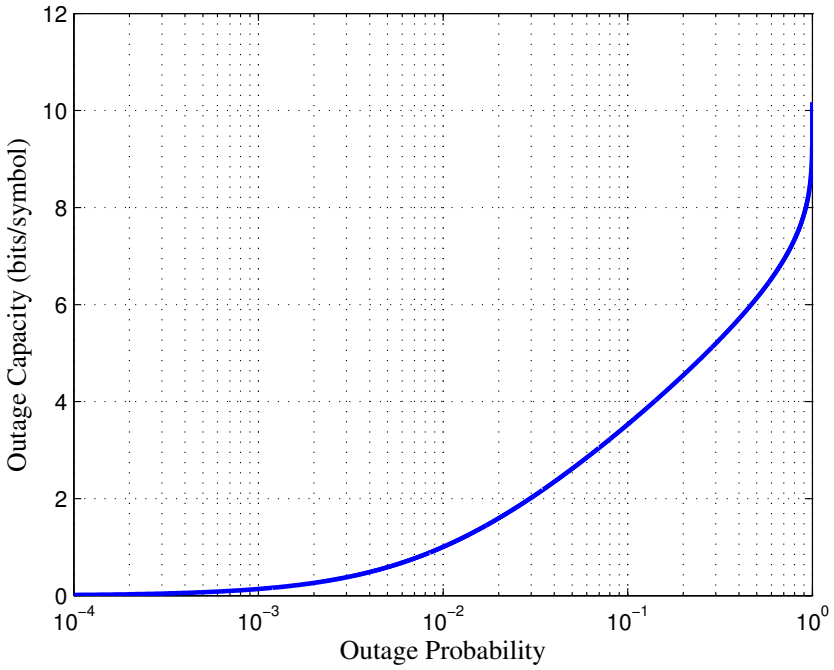

FIGURE 4.9: Outage capacity versus outage probability for a Rayleigh fading channel.

Since the transmitter does not know the instantaneous channel state information, it transmits using a constant data rate equal to C_{out}:

$$C_{out} = \log_2(1 + \gamma_o) \quad \text{bits/s/Hz}, \tag{4.6}$$

which is correctly decoded with probability $1 - p_{out}$. Hence the average data rate correctly received over many transmission bursts can be defined as:

$$R_{out} = (1 - p_{out}) \log_2(1 + \gamma_o) \quad \text{bits/s/Hz}. \tag{4.7}$$

The value of γ_o is a design parameter which is based on the acceptable outage probability.

Outage capacity is characterized by a plot of capacity versus outage probability. For example, for a Rayleigh fading channel (γ is modeled using an exponential distribution), the outage capacity versus the outage probability can be obtained by deriving the later as follows:

$$p_{out} = \text{prob}\{\gamma < \gamma_o\} = F_\gamma(\gamma_o) = 1 - e^{-\frac{\gamma_o}{\bar{\gamma}}}, \tag{4.8}$$

where F is the CDF and γ is an exponentially distributed random variable with a mean $\bar{\gamma}$. The outage capacity can thus be given as:

$$C_{out} = \log_2(1 + \gamma_o) = \log_2[1 - \bar{\gamma}\ \log(1 - p_{out})]. \tag{4.9}$$

Figure 4.9 plots the outage capacity versus the outage probability with $\bar{\gamma} = 20$ dB. It can be noticed that the capacity approaches zero for small outage probabilities, due to the precondition for successfully decoding of the transmitted bits under severe fading, and increases significantly as outage probability increases. It should be noted, however, that the probability of incorrect data reception is higher for these high capacity values. The average rate R_{out} correctly received can be optimized by finding the optimal p_{out} (or γ_o) that maximizes C_{out}.

4.5 Schematic Representation of the Proposed Approach

Typically, outage capacity is applied to quasi-static or slow varying channels, where the instantaneous SNR can be assumed constant over a transmission burst and then changes to a new value based on the fading distribution. The channel gain $|h|^2$ in this case is random but remains constant over a given transmission burst. As mentioned in the previous section, the system is said to be in outage if the transmitter encodes data at a rate of R bits/s/Hz that is greater than channel capacity $\log_2(1 + |h|^2\gamma_0)$. The outage probability can thus be written as:

$$\begin{aligned} p_{out}(R) =& \text{prob}\left\{\log_2(1 + |h|^2\gamma_0) < R\right\} \\ =& \text{prob}\left\{|h^2| < \frac{2^R - 1}{\gamma_0}\right\}, \\ =& \text{prob}\left\{|h|^2 < |h_o|^2\right\}, \end{aligned} \tag{4.10}$$

where $|h_o|^2$ represents a channel-gain threshold below which the received symbols cannot be successfully decoded (see Figure 4.10 (top graph)).

In what follows, we propose an original outage capacity approach for communication systems affected by impulsive noise based on an analogy with slow fading channels. We suppose that the temporal variation of the channel characteristics is now due to the impact of impulsive noise on the transmitted symbols, rather than the variation of the CTF due to fading. In the presence of impulsive noise, the overall noise of the system can be considered as a combined sum of the background noise and the impulsive noise. The total noise power ψ

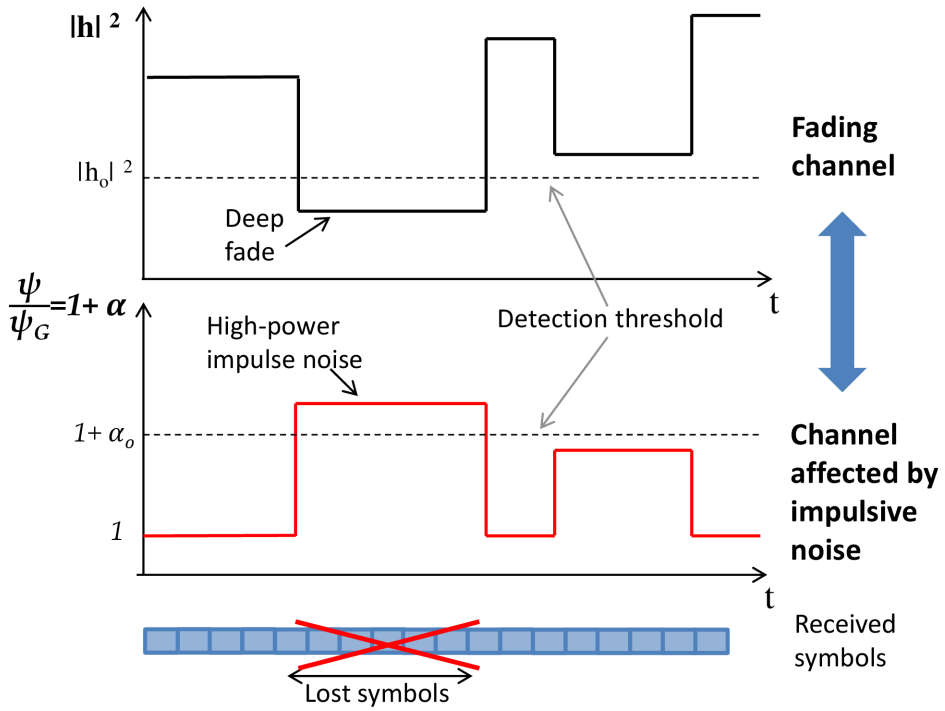

FIGURE 4.10: Schematic representations of a fading channel (top graph) and a channel affected by impulsive noise (bottom graph) and an analogy proposed between them.

can thus be expressed as $\psi = \psi_G + \psi_I$, where ψ_G is the background (Gaussian) noise power and ψ_I is the impulsive noise power. The impulsive noise power can be defined in terms of the background noise power as $\psi_I = \alpha\psi_G$, where α is the noise power ratio ($\alpha = \frac{\psi_I}{\psi_G}$). Herein, we draw an analogy between the parameter α and the channel gain $|h|^2$ of slow fading channels. Figure 4.10 depicts the analogy of a channel affected by impulsive noise (bottom graph), where ψ is normalized by ψ_G, with a fading channel gain $|h|^2$ (top graph). The maximum rate of reliable communication supported by this channel can thus be obtained by:

$$C = \log_2\left(1 + \frac{\gamma_G}{1+\alpha}\right) \quad \text{bits/s/Hz}, \tag{4.11}$$

which depends on the parameter α; γ_G represents the SNR at the receiver in the presence of only background noise. For a high power impulse noise, if the transmitter encodes data at a rate of R bits/s/Hz that is greater than the channel capacity $\log_2\left(1 + \frac{\gamma_G}{1+\alpha}\right)$, then the system declares an outage and the outage probability is given by:

$$\begin{aligned} p_{out}(R) =& \text{prob}\left\{\log_2\left(1+\frac{\gamma_G}{1+\alpha}\right) < R\right\} \\ =& \text{prob}\left\{\alpha > \frac{\gamma_G}{2^R-1} - 1\right\} \\ =& \text{prob}\left\{\alpha > \alpha_o\right\}, \end{aligned} \tag{4.12}$$

where α_o represents a power-ratio threshold or a noise margin above which the received symbols cannot be successfully decoded.

Here, we propose to provide the transmitted symbols with a noise margin (α_o) or a detection threshold in order to study the outage capacity. The received symbols with a total normalized noise power $\frac{\psi}{\psi_G}$ that exceeds the detection threshold $(1+\alpha_o)$ are lost while the others are successfully decoded (see Figure 4.10). We further search for the optimal α_o that maximizes the average data transmission rate.

4.6 Proposed Outage Capacity Approach for OFDM Systems

In this section, first, the channel capacity of OFDM systems in the presence of only background noise is given. Then, we investigate the channel capacity in the presence of impulsive noise. Next, the outage capacity for OFDM systems affected by impulsive noise is investigated. And finally, the outage capacity for PLC is provided.

4.6.1 Channel Capacity in the Presence of Only Background Noise

The overall bandwidth of a frequency-selective channel can be divided into a sufficiently high number of flat independent subbands. Hence, the total capacity of the overall channel, which is subject to the constraint of the total transmit power, can be given by:

$$C = \max_{\{p_k\}} \left\{ \sum_{k=1}^{N} \log_2\left(1+\frac{p_k}{\eta_k}\right) \right\}, \tag{4.13}$$

where

- k is the subchannel (or subband) index;
- p_k is the emitted power on subchannel k;
- N is the total number of subchannels;

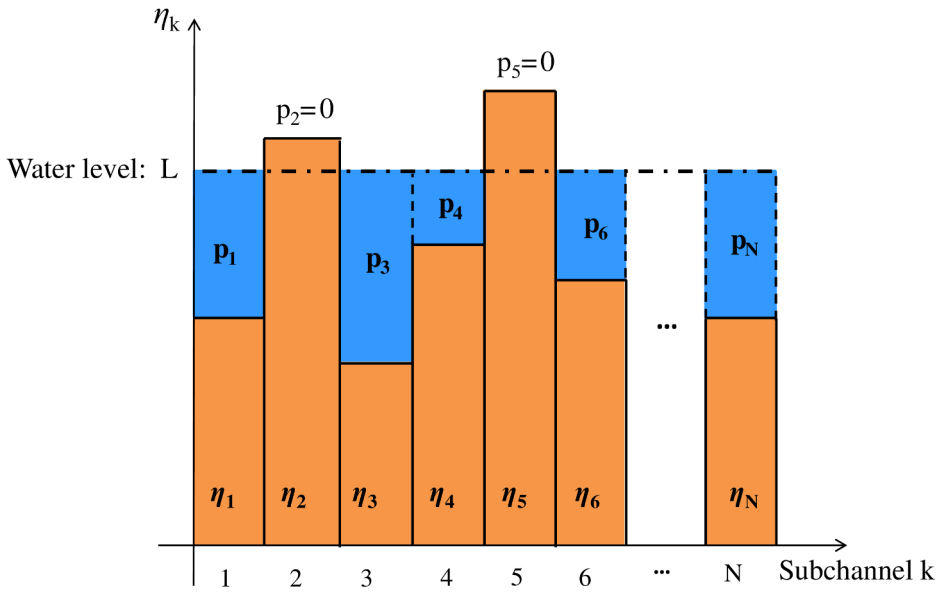

FIGURE 4.11: Water-filling power allocation.

- η_k is the subchannel input equivalent noise,
  $\eta_k = \frac{\psi_k}{|H_k|^2}$; we use the same notation as in [114];
- ψ_k is the subchannel noise power and
- $|H_k|^2$ is the subchannel gain.

It is well known that the optimal transmission power distribution in subchannels is achieved using the water-filling algorithm. This optimal distribution can be schematized as in Figure 4.11. The water level L represents the optimization parameter. This level is reached when all the available water (i.e., the total power) is poured into all the subchannels. Given the total transmission power P_{tot}, the optimal transmission power distribution of p_k can be written as:

$$p_k = \begin{cases} 0 & , \quad \eta_k \geq L \\ L - \eta_k & , \quad \eta_k \leq L \end{cases} \tag{4.14}$$

with:

$$L = \frac{1}{N_u} \left(P_{tot} + \sum_{k \in S_u} \eta_k \right) \tag{4.15}$$

and

$$P_{tot} = \sum_{k \in S_u} p_k, \tag{4.16}$$

where S_u is the set of indices of the useful subchannels (in Figure 4.11 $S_u = \{1, 3, 4, 6, .., N\}$) and N_u is the number of useful subchannels. Using the optimal transmission power allocation, Eq. (4.13) becomes:

$$C = \sum_{k \in S_u} \log_2 \left(\frac{L}{\eta_k} \right). \tag{4.17}$$

4.6.2 Channel Capacity in the Presence of Impulsive Noise

As mentioned previously, the impulsive noise is modeled through the three exponentially distributed time-domain parameters [5], namely the impulse power, impulse width and inter-arrival time. That is, the impulses amplitudes are modeled using Gaussian distribution. It can also be assumed that in OFDM systems with large number of subcarriers, the impulsive noise at the output of DFT becomes Gaussian [115], thanks to the central limit theorem. Regarding the background noise, we consider the colored Gaussian model for the PSD over an extended bandwidth up to 100 MHz proposed in [24]. In the presence of impulsive noise, the subchannel input equivalent noise $\eta_k^{'}$ is given by:

$$\eta_k^{'} = \eta_{G_k} + \eta_{I_k}, \tag{4.18}$$

where η_{G_k} and η_{I_k} are the subchannel input equivalent noise for the background and impulsive noises, respectively. The channel capacity can be defined as a function of the noise power ratio α defined in Section 4.5. Hence the instantaneous capacity for OFDM systems affected by impulsive noise is given by:

$$C^{'} = \sum_{k \in S_u^{'}(\alpha)} \log_2 \left(\frac{L^{'}(\alpha)}{\eta_{G_k} + \eta_{I_k}(\alpha)} \right), \tag{4.19}$$

where $(\cdot)^{'}$ refers to the case where impulsive noise is present. As indicated in Eq. (4.19), the parameters $S_u^{'}$, $L^{'}$ and η_{I_k} are a function of α, which is given by:

$$\alpha = \frac{\sum\limits_{k=1}^{N} \psi_{I_k}}{\sum\limits_{k=1}^{N} \psi_{G_k}} = \frac{\sum\limits_{k=1}^{N} \psi_{I_k}}{\psi_G}, \tag{4.20}$$

where ψ_{I_k} and ψ_{G_k} are the subchannel impulsive noise power and subchannel background noise power, respectively.

4.6.3 Proposed Outage Capacity Approach

In order to study the outage capacity of the system, we provide the transmitted symbols with a certain α_o noise margin (α_o is a particular value of α). The system transmits using a data rate $C_o^{'}$, defined as:

$$C_o^{'} = \sum_{k \in S_u^{'}(\alpha_o)} \log_2 \left(\frac{L^{'}(\alpha_o)}{\eta_{G_k} + \eta_{I_k}(\alpha_o)} \right). \tag{4.21}$$

The system declares an outage if the data rate $C_o^{'}$ is higher than the instantaneous channel capacity $C^{'}$ defined in Eq. (4.19). First, we find the data rate $C_o^{'}$ as a function of the noise margin α_o from Eq. (4.21). Then, we find the outage probability as a function of α_o, which can be written as follows:

$$\begin{aligned} p_{out} =& \text{prob}\left\{C_o^{'} > C^{'}\right\} \\ =& \text{prob}\left\{\alpha > \alpha_o\right\} \\ =& \varepsilon. \end{aligned} \tag{4.22}$$

The outage probability is the probability that the energy of the impulsive noise contained in an OFDM symbol exceeds the noise margin. Equivalently, we define ε as the probability that a symbol is lost, given that it is affected by impulsive noise. A detailed study of the impact of impulsive noise on a transmitted symbol is presented in Appendix A where ε is obtained. We show that ε depends on three parameters and is given by:

$$\varepsilon(\tau, \mu, \alpha_o) = \int_{\frac{\alpha_o}{\mu}}^{\infty} e^{-(\frac{\alpha_o}{\tau\mu y} + y)} \, \mathrm{d}y - \frac{2\alpha_o e^{\frac{1}{\tau}}}{\tau\mu} \int_{\frac{\alpha_o}{\mu}}^{\infty} \frac{\mathrm{E}_1\left(\frac{1}{\tau}(1 + \frac{\alpha_o}{\mu y})\right) e^{-y}}{y} \, \mathrm{d}y, \tag{4.23}$$

where τ is the ratio of the average impulsive noise time width t_{w_0} to the OFDM symbol duration T_S

$$\tau = \frac{t_{w_0}}{T_s}, \tag{4.24}$$

μ is the ratio of the average impulsive noise power ψ_{I_0} to the background noise power ψ_G

$$\mu = \frac{\psi_{I_0}}{\psi_G}, \tag{4.25}$$

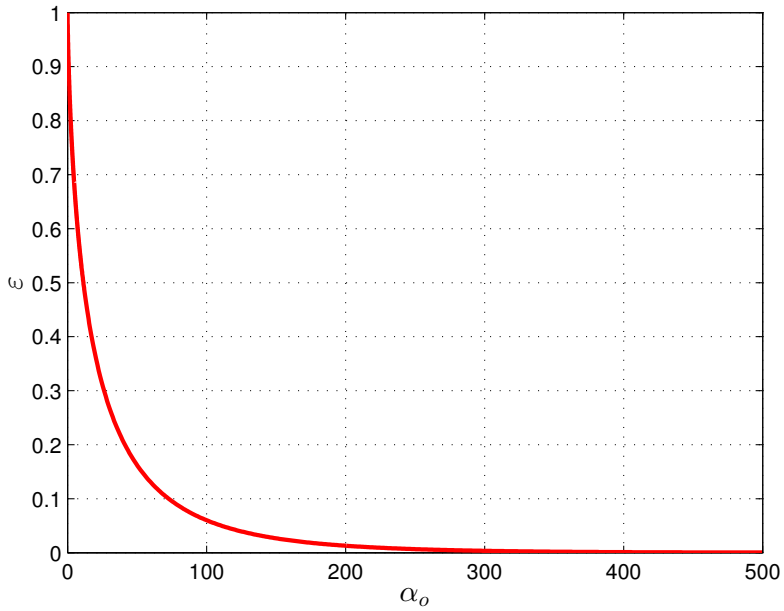

FIGURE 4.12: The outage probability ε versus the noise margin α_o.

and E_1 is the exponential integral function and can be defined for positive real x by:

$$\mathrm{E}_1(x) = \int_x^{\infty} \frac{e^{-u}}{u}\,\mathrm{d}u. \tag{4.26}$$

The values of the parameters μ and τ can be deduced from noise measurements. For a given τ, μ and α_o, the integral presented in Eq. (4.23) can be approximated numerically. Figure 4.12 plots the outage probability ε versus the noise margin α_o for practical values of $\tau = 0.5$ and $\mu = 100$ in PLC (as an example). As expected, symbols affected by impulsive noise provided with a zero noise margin (i.e. $\alpha_o = 0$) are incorrectly decoded with probability equal to one (i.e., $\varepsilon = 1$). We can also notice that providing these symbols with a very large noise margin α_o (compared to the value of μ) cause them to be correctly decoded with probability equal to one (i.e., $\varepsilon = 0$).

Finally, for given values of τ and μ, the outage capacity, C_ε, can be investigated using equations (4.21) and (4.23). For any given value of the noise margin α_o, the corresponding channel capacity from Eq. (4.21) and the outage probability from Eq. (4.23) can be associated and thus the outage capacity can be obtained.

The numerical evaluation of ε is not simple due to the nature of the function that is to be integrated (integrand) and the upper limit of the integral (infinity). For this reason, a precise numerical approximation of ε is proposed in Appendix B.

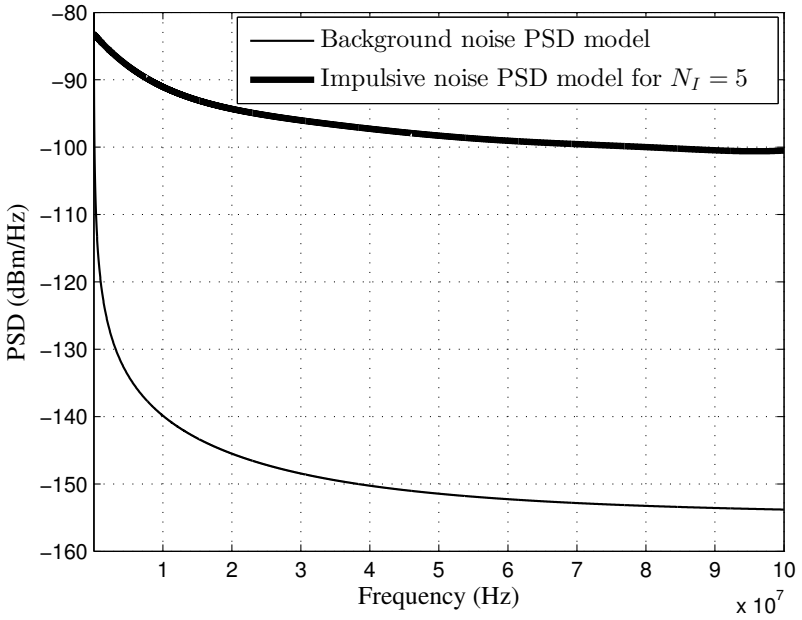

FIGURE 4.13: Models for the PSD of the impulsive noise and the background noise.

4.6.4 Proposed Outage Capacity Approach for PLC

As mentioned previously, the PSD model for the background noise proposed by OMEGA project in [24] over an extended bandwidth up to 100 MHz is considered in this study. Regarding the impulsive noise, the model for its PSD covering a frequency band up to 100 MHz, which is proposed in [112] by assuming N_I independent sources of white noise that propagate through N_I distinct channels described by the CTF model proposed in [40], is considered. The two PSD models are depicted in Figure 4.13, where a proportion between the two plots can be noticed. Based on the proportionality noticed between the two noise models, $\eta_k^{'}$ in Eq. (4.18) becomes:

$$\eta_k^{'} = \eta_{G_k}(1+\alpha) \tag{4.27}$$

for all the subchannels k. Hence, the capacity limit defined in Eq. (4.19) can be written as:

$$C^{'} = \sum_{k \in S_u^{'}} \log_2 \left(\frac{L^{'}}{\eta_{G_k}\,(1+\alpha)} \right). \tag{4.28}$$

In this case, the system transmit using a data rate $C_o^{'}$ defined as:

$$C_o^{'} = \sum_{k \in S_u^{'}} \log_2 \left(\frac{L^{'}}{\eta_{G_k}(1+\alpha_o)} \right) \text{bits/symbol.} \tag{4.29}$$

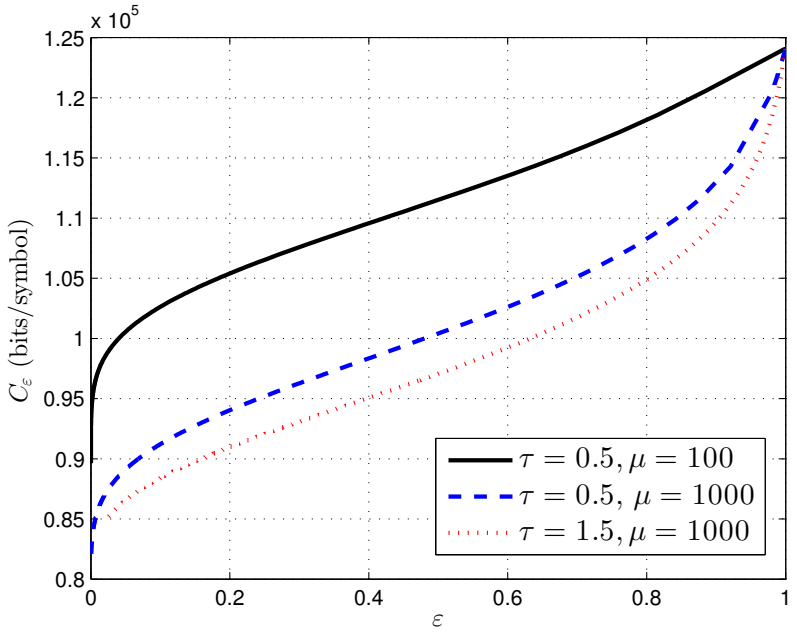

FIGURE 4.14: The outage capacity C_ε for three practical values of τ and μ for PLC channels.

Similar to what described in the previous section, we investigate the outage capacity based on the equations Eq. (4.29) and Eq. (4.23) as follows. For any given value of α_o, the corresponding data rate from Eq. (4.29) and the outage probability from Eq. (4.23) can be associated and thus the outage capacity can be obtained. Figure 4.14 plots the outage capacity C_ε for three practical values of the noise parameters τ and μ for PLC channels, based on the measurements in [5]. According to this study, the PSD of the asynchronous impulsive noise can reach values of more than 50 dB above the background noise. t_{w_0} for moderately and weakly disturbed environment are 60.7 μs and 110.7 μs, respectively [5]. The time duration of the OFDM symbol specified in the HomePlug Alliance is taken into account in this thesis; $T_S = 40.96\ \mu s$. We consider the channel model for class nine (the best channel class) presented in [3] in the frequency band $1.8 - 86.13$ MHz with a total transmit power $P_{tot} = 0.28\ W$. It can be noted from Figure 4.14 that the impulsive noise parameters τ and μ have a significant impact on the outage capacity C_ε.

Based on Eq. (4.28), we propose an algorithm for computing the capacity of PLC channels. The proposed algorithm, which is given in Appendix C, can serve as a basis for a low complexity bit-loading algorithm for broadband PLC.

4.7 Proposed Approach for Optimizing the Average Data Rate

In this section, we seek to optimize the average data rate that can be transmitted in OFDM systems affected by impulsive noise, based on the obtained outage capacity. A new parameter needs to be defined, which is the probability that a symbol is affected by impulsive noise, denoted by P_A. Our scheme transmits using a data rate C_ε that is successfully decoded with probability $1 - P_{lost}$, where P_{lost} is the probability of loosing a transmitted data symbol:

$$P_{lost} = P_A \cdot \varepsilon. \tag{4.30}$$

Hence, the average data rate of the system can be given as follows:

$$R_\varepsilon = (1 - P_A \cdot \varepsilon)\, C_\varepsilon. \tag{4.31}$$

Taking into account the exponential distribution of the interarrival times of the impulses, P_A can be calculated from:

$$P_A = 1 - \left[(1 - \lambda t_{w_0}) e^{-\lambda T_S}\right], \tag{4.32}$$

where λ is the impulse rate. In order to ensure maximum data transmission rate, we search for the optimal outage probability ε required to maximize the average data rate of the system R_ε. To do so, we investigate the sign of its derivative, which is given by:

$$\frac{\mathrm{d}R_\varepsilon}{\mathrm{d}\varepsilon} = C_\varepsilon(1 - P_A\varepsilon)\left[\frac{\frac{\mathrm{d}C_\varepsilon}{\mathrm{d}\varepsilon}}{C_\varepsilon} - \frac{P_A}{1 - P_A\varepsilon}\right]. \tag{4.33}$$

The derivative is negative, positive or zero depending on the two curves:

$$y_1 = \frac{C_\varepsilon}{\frac{\mathrm{d}C_\varepsilon}{\mathrm{d}\varepsilon}} \tag{4.34}$$

and

$$y_2 = \frac{1}{P_A} - \varepsilon \tag{4.35}$$

(y_2 is a straight line which depends on P_A; y_1 is a curve independent of this parameter). y_1 and y_2 are plotted in Figure 4.15 for $\tau = 1.5$, $\mu = 1000$ and three different values of P_A. If $y_2 > y_1$, the derivative in Eq. (4.33) is positive; if $y_2 < y_1$, the derivative is negative; and

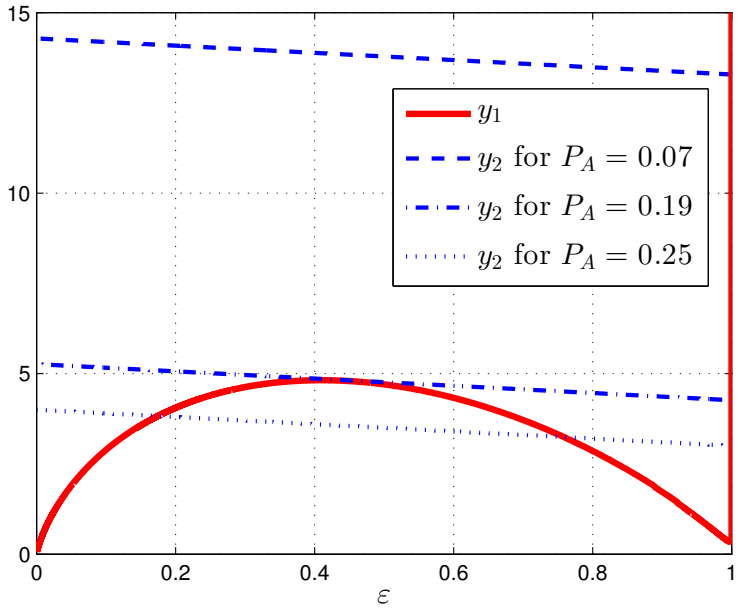

FIGURE 4.15: Analysis results for a PLC channel where $\tau = 1.5$ and $\mu = 1000$ using three different values of P_A.

finally, if $y_2 = y_1$, the derivative is zero and thus the curve of the average rate R_ε reaches a maximum value (a local or global maximum). Note, however, that in Figure 4.15 the point at which the straight line y_2 is tangent to the curve y_1 (for $P_{A_{th}} = 0.19$) is neither a maximum nor a minimum (it is a point of inflection) because the sign of the derivative does not change around the point of intersection. One can notice from Figure 4.15 that the limit of y_1 tends to infinity as ε tends to 1. In appendix D, we present a detailed study of the function y_1 and demonstrate its limit as ε tends to 1. Thus, in the example presented in the figure, all the y_2 curves intersect with y_1 at ε very close to one.

In the large majority of cases for PLC channels, the shape of y_1 was similar to the one in Figure 4.15. An important parameter, $P_{A_{th}}$, which is P_A for which the straight line is tangent to the curve, need to be investigated (in the example presented in Figure 4.15, $P_{A_{th}} = 0.19$). For given values of τ and μ, this parameter represents a limit that separates two cases; the case where there is only one maximum at ε very close to one ($P_A < P_{A_{th}}$) and the other case where there are maxima ($P_A > P_{A_{th}}$). Table 4.2 shows $P_{A_{th}}$ for different values of τ and μ where it can be noted that they are quite large. Practical values of P_A for PLC channels are much lower than $P_{A_{th}}$ for all the practical values of τ and μ. For example, values of P_A for asynchronous impulsive noise deduced from [5] could be one percent (and even lower). This means that the optimal ε that maximizes R_ε is found at ε very close to one. Table 4.3 presents a comparison between the data rate at this point $R_{\varepsilon_{max}}$ and R_{ε_1} for $\varepsilon = 1$ by computing the

TABLE 4.2: $P_{A_{th}}$ for different values of τ and μ for PLC channels.

$10\log_{10}(\tau)$ \ $10\log_{10}(\mu)$	20	30	40
-10	0.149	0.177	0.198
-5	0.154	0.182	0.209
0	0.166	0.189	0.215
5	0.161	0.182	0.207
10	0.146	0.164	0.187
15	0.135	0.152	0.173
20	0.129	0.146	0.166

TABLE 4.3: F_R factor for different values of τ and μ with a practical value of P_A in PLC ($P_A = 0.01$).

$10\log_{10}(\tau)$ \ $10\log_{10}(\mu)$	10	20	30
-10	7.73×10^{-5}	0	0
0	0	0	0
10	0	0	0
20	0	0	0

F_R factor defined as:

$$F_R = \frac{R_{\varepsilon_{max}} - R_{\varepsilon_1}}{R_{\varepsilon_{max}}}. \tag{4.36}$$

It can be noted from Table 4.3 that the difference between R_ε at ε very close to one (i.e. $R_{\varepsilon_{max}}$) and ε equal to one (i.e. R_{ε_1}) is negligible.

Figure 4.16 plots the average rate R_ε for $P_A = 0.01$ and different values of τ and μ for PLC channels, where one can notice that the maximum of R_ε is found at $\varepsilon = 1$ in the three cases. For PLC applications, this means that the outage probability ε required to maximize the average rate is almost one, i.e. when none of the impulsive noise-affected symbols are recovered. Hence, in order to optimize the average data rate, designed schemes must transmit using a data rate C_o' defined in Eq. (4.29) with $\alpha_o = 0$. In other words, they must transmit using a data rate C defined in Eq. (4.17), i.e. without taking into account the presence of impulsive noise. Obviously, the above conclusion is valid in the particular case of PLC with impulsive noise characteristics similar to the ones given in Section 4.6.4. Other values of the

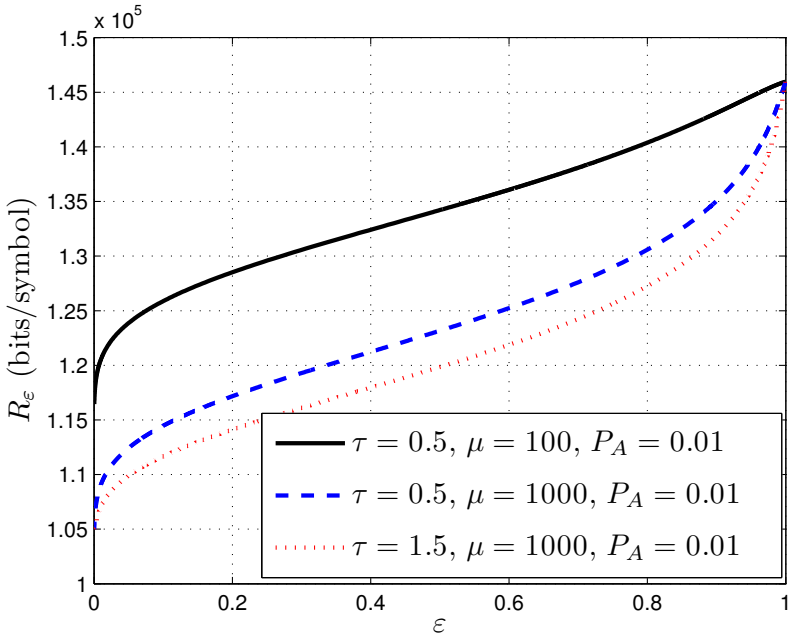

FIGURE 4.16: R_ε for $P_A = 0.01$ and different values of τ and μ for PLC channels.

characteristic parameters P_A, μ and τ (corresponding to other propagation environments) might lead to a different conclusion, but the generic approach proposed here remains correct.

A summary of the proposed outage capacity approach for OFDM-based systems affected by impulsive noise is as follows:

- Based on the impulsive noise characteristics, the values of the parameters τ, μ and P_A can be deduced.
- Based on τ , μ and the CTF, C_ε can be obtained as described in subsection 4.6.3, as well as the curve y_1.
- Based on the value of P_A, the straight line y_2 can be obtained and its intersection with the curve y_1 can be studied.
- If there is only one point of intersection (and the sign of the derivative changes at this point), the abscissa of this point represents the optimal ε that maximizes the average outage rate R_ε.
- If there are more than one point of intersection, only the intersection points of odd rank are considered (the others correspond to minimum rates), as well as the one at $\varepsilon = 1$ if it is of even rank. The ε that maximizes the average outage rate is retained.

4.8 Conclusion

In this chapter, first, we examined the influence of the impulsive noise characteristics on the BER performance in uncoded OFDM PLC systems. This was done by using an easily tractable noise model which can be easily implemented on computer simulations and which well describes the asynchronous impulsive noise. The results showed significant deterioration in the BER performance due to the impulsive noise. Next, we proposed an outage capacity approach in order to optimize the average data rate in OFDM systems affected by impulsive noise. In detail, we studied the outage capacity of OFDM systems affected by impulsive noise by providing the transmitted symbols with a noise margin. We first expressed the channel capacity in terms of the noise margin. Then, we found the outage probability, defined as the probability that the energy of the impulsive noise contained in an OFDM symbol exceeds the noise margin, as a function of the same parameter. Based on the two aforementioned relations, we investigated the outage capacity of the system. Next, we proposed an outage capacity approach that enables to determine the optimal outage probability (or noise margin) needed to maximize the average data rate of the system, and which is based on the statistical distribution of the impulsive noise parameters, namely the impulse power, impulse width and interarrival time. For indoor broadband PLC, it was shown that the optimal outage probability was almost one (i.e. the optimal noise margin was almost zero). Obviously, choosing other values of the impulsive noise characteristic parameters (for other propagation environments) might lead to a different result, but the generic approach proposed here remains the same.

Moreover, an algorithm for computing the capacity of PLC channels was proposed and presented in Appendix C. The proposed algorithm can serve as a basis for low-complexity and efficient bit-loading algorithm for PLC.

Conclusion

As a result of the efforts made to use the electric power distribution grid as data transmission medium, the power-line channel has become nowadays a medium that provides telecommunication services to subscribers in homes or businesses, enabling new and highly convenient networking functions without any additional cables. However, the power-line medium has not been designed for communication purposes and is a challenging environment for reliable and high-speed data communication. Modeling the PLC channel and ensuring maximum data rates and communications reliability in the presence of impulsive noise are two main issues. Recently, MIMO techniques have become an important research field for enhancing the throughput of indoor broadband PLC systems by exploiting the additional protective earth wire. The development of such systems requires an accurate description of the propagation channel. However, due to the considerable variability of PLC network topologies and the lack of common wiring practices, the characteristics of the PLC CTFs are difficult to model, raising an important issue. To get the full variability of the MIMO-PLC channel, random channel generators are of great interest for the design and testing of communication algorithms. Another issue is the noise present over PLC channels which is actually a mixture of colored background noise and impulsive noise. The impulsive noise, and more specifically the asynchronous impulsive noise, is the main cause of transmission errors since it may deform a large amount of data, creating therefore important performance degradation.

In this thesis, we have first addressed the issue of MIMO-PLC random channel generation. Then, the general issue of data rate optimization in OFDM systems affected by impulsive noise, and its application to indoor broadband PLC, have been addressed.

Chapter 1 was dedicated to providing an overview on indoor broadband MIMO PLC. First, we have presented a brief overview on PLC, namely the historical evolution of communications over power lines, the PLC networks, the PLC frequency bands and the major broadband PLC groups and specifications. Then, we have introduced the MIMO-PLC channel. Specifically, the applicability of MIMO techniques in PLC has been described. In addition, the MIMO spatial correlation has been presented based on the European MIMO-PLC

field measurements, which would be further considered as a target measurement campaign of the MIMO-PLC random channel generator proposed in Chapter 3.

In Chapter 2, we have presented the state-of-the-art study on the PLC CTF and noise characterization and modeling. As the mutipath behavior of the power-line channel is commonly accepted, three PLC CTF models based on the "top-down" statistical modeling approach have been presented. Namely, we have described the multipath channel model proposed by Zimmermann, the channel model proposed by France Télécom, where the measured channels were interestingly classified into nine classes according to their capacities, and the random channel generator proposed by Tonello, which is basically a statistical extension of the multipath model proposed by Zimmermann applied to the set of nine channel classes proposed by France Télécom. Next, we turned to MIMO-PLC channels, where different SISO-based MIMO-PLC channel models have been described. Specifically, an approach that is based on assigning a random phase shift to each defined path of the SISO CTF of the Zimmerman-statistically-extended model has been presented. The model was provided for the same-circuit and different-circuit cases; the nine channel classes, however, were not adopted. On the other hand, we have presented the characteristics of the various types of disturbance occurring in PLC transmission, which can be roughly categorized into background noise and impulsive noise. The asynchronous impulsive noise has been presented as the most detrimental noise term among the additive noises since its exhibits the highest PSD and may thus lead to significant performance degradation. Hence, we have described some of literature models of the asynchronous impulsive noise. Specifically, we have considered the asynchronous impulsive noise characterization and modeling approaches proposed by Zimerrmann and Dostert for broadband PLC channels. Therefore, the impulsive noise was modeled through the three exponentially distributed time-domain parameters, namely the impulse power (or amplitude), impulse width and inter-arrival time. Concerning the background noise, the colored Gaussian model for the PSD proposed by OMEGA project has been considered in this study.

Chapter 3 was dedicated to the presentation of a MIMO random channel generator for indoor broadband PLC channels based on the SISO one presented in the literature. We considered that a MIMO channel can be defined as the superposition of correlated SISO channels. Thus, we attempted to describe a MIMO channel, specifically a 2×2 MIMO channel, using the same nine classes obtained with the SISO configuration. We considered that a SISO channel class, characterized by a certain average path loss profile and a certain average coherence bandwidth, can be extended to a MIMO channel class with similar characteristics. An additional parameter, related to the correlation between the spatial channels of each class, was taken into consideration similar to a formalism proposed in the literature. As an example of application, we applied the procedure to the spatial correlation of the European MIMO PLC field measurements. We have shown that when a specific spatial correlation is chosen

for each class, the target spatial correlation can be accurately reproduced by the channel generator. Therefore, the proposed MIMO random channel generator enables to represent the wide variation of MIMO-PLC channels and has a practical value for designing and testing communication systems over PLC channels.

In Chapter 4, first, we have examined the impact of the impulsive noise characteristics on the BER performance in uncoded OFDM PLC systems by using an easily tractable noise model. The noise model, which was derived from the pulse train noise model, can be easily implemented on computer simulations and well represents the asynchronous impulsive noise present over PLC channels. Next, we proposed an information theory-based approach in order to ensure maximum average data rate in OFDM systems affected by impulsive noise. The proposed approach was based on the principle of outage capacity, which is well-known for slow fading channels. We supposed that the temporal variation of the channel characteristics is now due to the impact of impulsive noise on the transmitted symbols, rather than the variation of the CTF due to fading. In detail, we studied the outage capacity of OFDM systems affected by impulsive noise by providing the transmitted symbols with a noise margin (or useful power reserve). We first expressed the channel capacity in terms of the noise margin. Then, we found the analytical expression of the outage probability, defined as the probability that the energy of the impulsive noise contained in an OFDM symbol exceeds the noise margin, as a function of the same parameter (noise margin). Based on the two aforementioned relations, we investigated the outage capacity of the system. Next, we proposed an approach that enables to determine the optimal outage probability (or noise margin) required to maximize the average data rate of the system. For indoor broadband PLC, it was shown that the optimal outage probability was almost one (i.e. the optimal noise margin was almost zero). Obviously, choosing other values of the impulsive noise characteristic parameters (corresponding to other propagation environments) might lead to a different result, but the generic approach proposed here remains the same.

Finally, as perspectives of the present work, we can mention:

- The application of the outage capacity approach to other propagation environments impaired by impulsive noise.
- The BER performance analysis based on the analytical expression of the outage probability of an impulsive noise-affected symbol, provided in Appendix A.
- Proposing a low complexity bit-loading algorithm for PLC systems based on the proportionality noticed between the PSD models of the background noise and impulsive noise (see Appendix C).
- Using the proposed MIMO random channel generator in the context of HD or ultra-high-definition video transmission. In fact, previous studies in our laboratory related to

the joint source-channel optimization for video transmission over MIMO wireless channels have been made [116]. The proposed methods take into account both transmission parameters (such as MIMO channel correlation state) and video coding parameters in order to optimize the system performance. Thus, it would be interesting to apply theses methods to the MIMO-PLC channel in order optimize video transmissions as a function of the channel correlation state, which can well be represented using the proposed random channel generator.

List of Publications

Journal Papers

1. K. Khalil, M. G. Gazalet, P. Corlay, F. X. Coudoux and M. Gharbi, "An MIMO random channel generator for indoor power-line communication," *IEEE Transactions On Power Delivery*, vol. 29, no. 4, pp. 1561–1568, July 2014.
2. K. Khalil, M. G. Gazalet, P. Corlay, M. Gharbi and F. X. Coudoux, "An outage capacity approach for OFDM systems affected by impulsive noise: Application to indoor broadband power-line communications," (to be submitted).

Conference Paper

3. K. Khalil, P. Corlay, F. X. Coudoux, M. G. Gazalet and M. Gharbi, "Analysis of the impact of impulsive noise parameters on BER performance of OFDM power-line communications," *The 7th International Symposium on Signal, Image, Video and Communications (ISIVC)*, Marrakech, Morocco, Nov 2014.

APPENDIX A

Impulsive Noise-Affected Symbol Outage Probability (ε) Integration

In this appendix, we investigate the outage probability (ε) of a symbol (the probability that a symbol is lost), given that it is affected by impulsive noise. We examine in a detailed manner the influence of an impulse on a transmitted symbol. Figure A.1 illustrates the impulsive noise-affected symbol model in our system. An OFDM symbol of duration T_S might be affected by an impulse of time width t_w. The time duration of the overlap is denoted by $t_{overlap}$. The latter represents the duration of the part of OFDM symbol deformed by the impulsive noise. An impulse is characterized by three main parameters: the power ψ_I, the time width t_w and the interarrival time t_{IA}, which is the time between the beginning

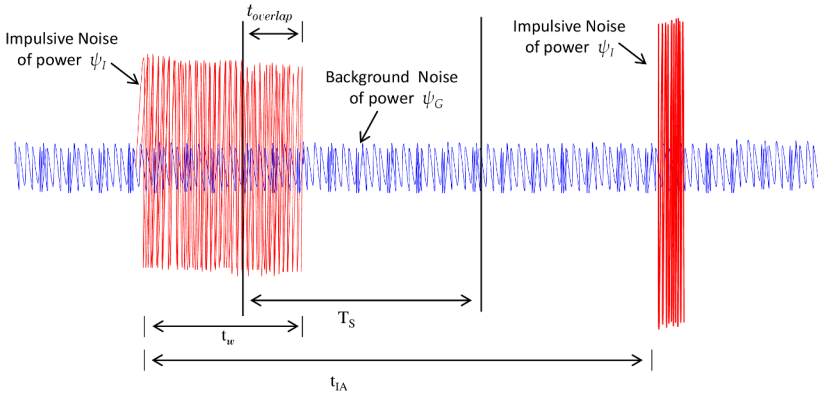

FIGURE A.1: Impulsive noise-affected OFDM symbol model.

of two consecutive impulses. The power of the background noise is denoted by ψ_G. ψ_{I_0}, ψ_{G_0}, t_{w_0}, t_{IA_0} are denoted by the average values of the random parameters ψ_I, ψ_G, t_w, t_{IA}, respectively. The statistical distribution of the impulsive noise parameters, namely t_w and ψ_I, were obtained from [5]. Their PDF are denoted by:

$$p(t_w) = \frac{1}{t_{w_0}} \exp\left(-\frac{t_w}{t_{w_0}}\right)$$

and

$$p(\psi_I) = \frac{1}{\psi_{I_0}} \exp\left(-\frac{\psi_I}{\psi_{I_0}}\right).$$

Please note that the $p(\cdot)$ notation is used for the PDF of several random parameters. The system declares an outage if the energy of the impulsive noise contained in an OFDM symbol exceeds the noise margin α_o. The outage probability of an impulsive noise-affected symbol defined in Eq. (4.22) is given here:

$$\begin{aligned} p_{out} =& \text{prob}\left\{\frac{\xi_I}{\xi_G} > \alpha_o\right\} \\ =& \text{prob}\left\{\frac{\psi_I \cdot t_{overlap}}{\psi_G \cdot T_S} > \alpha_o\right\} \\ =& \text{prob}\left\{\rho > \frac{\alpha_o \cdot \psi_G}{\psi_I}\right\} \\ =& \varepsilon \end{aligned} \tag{A.1}$$

where

- $\rho = \dfrac{t_{\text{overlap}}}{T_S}, \quad 0 \le \rho \le 1$ (see Figure A.1);
- $\xi_I = t_{overlap} \cdot \psi_I$ is the energy of the impulsive noise contained in an OFDM symbol;
- $\xi_G = T_S \cdot \psi_G$ is the energy of the background noise contained in an OFDM symbol.

The outage probability ε can be written in integral form as:

$$\varepsilon = \iint\limits_D \left[\int\limits_{\frac{\alpha_o \psi_G}{\psi_I}}^{1} p(\rho/(t_w, \psi_I))\, \mathrm{d}\rho \right] p(t_w) p(\psi_I)\, \mathrm{d}t_w\, \mathrm{d}\psi_I, \tag{A.2}$$

where the term inside the brackets represents the outage probability ε without taking into account the random aspect of the variables t_w and ψ_I, and is denoted by $\varepsilon(t_w, \psi_I)$,

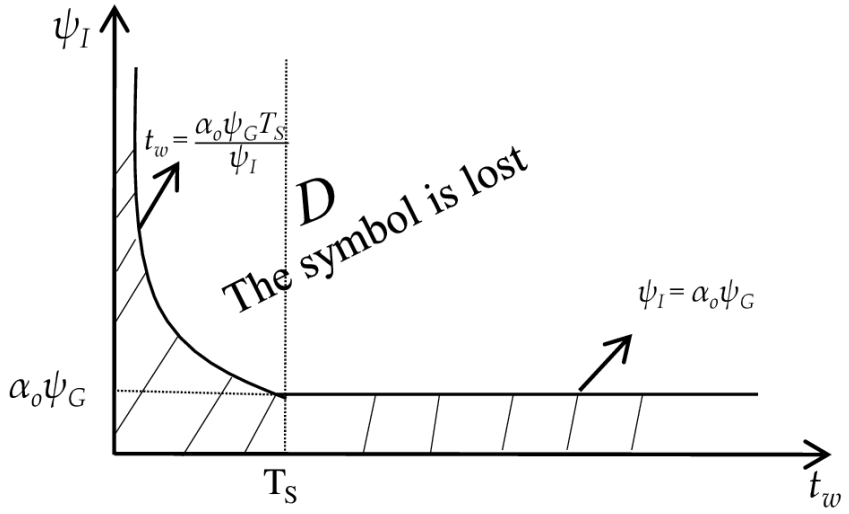

FIGURE A.2: The domain of integration D in the $t_w\psi_I$-plane.

$$\varepsilon(t_w, \psi_I) = \int_{\frac{\alpha_o \psi_G}{\psi_I}}^{1} p(\rho/(t_w, \psi_I))\, \mathrm{d}\rho, \tag{A.3}$$

where $p(\rho/(t_w, \psi_I))$ represents the PDF of ρ for given values of t_w and ψ_I. D is the domain of integration in the $t_w\psi_I$-plane and is depicted in Figure A.2. In order to find D, two cases need to be considered for an impulsive noise-affected symbol:

1. If $t_w \leq T_S$, then $0 \leq \rho \leq \frac{t_w}{T_S}$; by substituting the upper limit of ρ in Eq. (A.1) we get $t_w > \frac{\alpha_o \psi_G T_S}{\psi_I}$.
2. If $t_w > T_S$, then $0 \leq \rho \leq 1$; by substituting the upper limit of ρ in Eq. (A.1) we get $\psi_I > \alpha_o \psi_G$.

Therefore Eq. (A.2) becomes:

$$\varepsilon = \int_{\alpha_o \psi_G}^{\infty} \int_{\frac{\alpha_o \psi_G T_S}{\psi_I}}^{\infty} \varepsilon(t_w, \psi_I)\, p(t_w) p(\psi_I)\, \mathrm{d}t_w\, \mathrm{d}\psi_I. \tag{A.4}$$

Let us now investigate $p(\rho/(t_w, \psi_I))$. If we consider an OFDM symbol defined in the interval $[0 - T_S]$, the overlap between the impulse and the symbol only occurs if the starting time t_0 of the impulse falls within the interval $]-t_w, T_S[$. We assume that t_0 follows a uniform distribution. Two possible cases of impulse width t_w have to be considered:

1. If $t_w \leq T_S$: in this case, if t_0 falls within the interval $]0, T_S - t_w[$, then $\rho = \frac{t_w}{T_S}$, otherwise ρ is less than $\frac{t_w}{T_S}$ with a uniform distribution.

2. If $t_w > T_S$: in this case, if t_0 is within the interval $]-t_w+T_S, 0[$, then $\rho = 1$, otherwise ρ is less than 1 with a uniform distribution.

Therefore $p(\rho/(t_w, \psi_I))$ can be written in equation form as:

$$p(\rho/(t_w,\psi_I)) = \begin{cases} \dfrac{T_S - t_w}{T_S + t_w}\delta\left(\rho - \dfrac{t_w}{T_S}\right) + \dfrac{2T_S}{T_S + t_w} rect\left(\dfrac{\rho - \dfrac{t_w}{2T_S}}{\dfrac{t_w}{T_S}}\right) & \text{if } t_w < T_S \\ \dfrac{t_w - T_S}{T_S + t_w}\delta\left(\rho - 1\right) + \dfrac{2T_S}{T_S + t_w} rect\left(\rho - \dfrac{1}{2}\right) & \text{if } t_w > T_S, \end{cases} \tag{A.5}$$

where $\delta(\cdot)$ and $rect(\cdot)$ are the Dirac function and the rectangular function, respectively. While using this PDF, Eq. (A.3) becomes:

$$\varepsilon(t_w, \psi_I) = 1 - \frac{2T_S}{t_w + T_S}\frac{\alpha_o \psi_G}{\psi_I}. \tag{A.6}$$

Now, let us solve Eq. (A.4), i.e. take into account the random aspect of t_w and ψ_I. To do so, we changed the variables: $x = \frac{t_w}{t_{w_0}}$ and $y = \frac{\psi_I}{\psi_{I_0}}$, and we defined the two parameters: $\tau = \frac{t_{w_0}}{T_S}$ and $\mu = \frac{\psi_{I_0}}{\psi_G}$. Then Eq. (A.4) becomes:

$$\begin{aligned} \varepsilon(\tau,\mu,\alpha_o) &= \int_{\frac{\alpha_o}{\mu}}^{\infty}\int_{\frac{\alpha_o}{\tau\mu y}}^{\infty}\left(1 - \frac{2}{\tau x + 1}\cdot\frac{\alpha_o}{\mu y}\right)e^{-x}e^{-y}\,\mathrm{d}x\,\mathrm{d}y. \\ &= \int_{\frac{\alpha_o}{\mu}}^{\infty}\left[\int_{\frac{\alpha_o}{\tau\mu y}}^{\infty}\left(1 - \frac{2}{\tau x + 1}\cdot\frac{\alpha_o}{\mu y}\right)e^{-x}\mathrm{d}x\right]e^{-y}\,\mathrm{d}y \\ &= \int_{\frac{\alpha_o}{\mu}}^{\infty}\left[e^{\frac{-\alpha_o}{\tau\mu y}} - \frac{2\alpha_o e^{\frac{1}{\tau}}}{\tau\mu y}\mathrm{E}_1\left(\frac{1}{\tau} + \frac{\alpha_o}{\tau\mu y}\right)\right]e^{-y}\,\mathrm{d}y \\ &= \int_{\frac{\alpha_o}{\mu}}^{\infty} e^{-(\frac{\alpha_o}{\tau\mu y} + y)}\,\mathrm{d}y - \frac{2\alpha_o e^{\frac{1}{\tau}}}{\tau\mu}\int_{\frac{\alpha_o}{\mu}}^{\infty}\frac{\mathrm{E}_1\left(\frac{1}{\tau}(1 + \frac{\alpha_o}{\mu y})\right)e^{-y}}{y}\,\mathrm{d}y, \end{aligned} \tag{A.7}$$

where E_1 is the exponential integral function and can be defined for positive real x by:

$$\mathrm{E}_1(x) = \int_x^{\infty}\frac{e^{-u}}{u}\,\mathrm{d}u.$$

APPENDIX B

Numerical Calculation of ε

In the previous appendix, we provided the analytical expression of the probability that a symbol is lost, given that it is affected by impulsive noise. For the purpose of simplicity, we define here the two parameters $a = \frac{1}{\tau}$ and $b = \frac{1}{\mu}$ and rewrite the result as a function of these parameters:

$$\varepsilon(a, b, \alpha_o) = \int_{b\alpha_o}^{\infty} e^{-(\frac{ab\alpha_o}{y} + y)} \, \mathrm{d}y - 2\alpha_o bae^a \int_{b\alpha_o}^{\infty} \frac{\mathrm{E}_1\left(a(1 + \frac{b\alpha_o}{y})\right) e^{-y}}{y} \, \mathrm{d}y. \tag{B.1}$$

For convenience, we change the variable: $t = \dfrac{y}{\alpha_o b}$, then Eq. (B.1) becomes:

$$\varepsilon(a, \alpha_o b) = \alpha_o b \int_{1}^{\infty} e^{-\alpha_o bt} \left(e^{-\frac{a}{t}} - 2ae^a \frac{\mathrm{E}_1\left(a(1 + \frac{1}{t})\right)}{t} \right) \mathrm{d}t. \tag{B.2}$$

The numerical evaluation of ε in Eq. (B.2) causes a problem due the nature of the function that is to be integrated (integrand). Theoretically, for integration to infinity using numerical softwares such as MATLAB, we can simply choose a very high upper limit. However, in the case where the integrand decreases very slowly, choosing such a limit might lead to numerical calculations that exceed the computational capacity of the computer and the software (this is particularly the case for the function studied here when the parameter $\alpha_o b$ is very small). A brief analysis of the integrand shows that it can be framed by two simple functions that are easier to integrate:

$$f_1 < \alpha_o b\, e^{-\alpha_o bt} \left(e^{-\frac{a}{t}} - 2ae^a \frac{\mathrm{E}_1\left(a(1+\frac{1}{t})\right)}{t} \right) < f_2, \tag{B.3}$$

where f_1 and f_2 depend on the boundaries of the two functions $e^{-\frac{a}{t}}$ and $\mathrm{E}_1\left(a(1+\frac{1}{t})\right)$. For a domain of function $\mathcal{D} : t \geq Z$, where $Z \geq 1$, we have:

$$e^{\frac{-a}{Z}} < e^{-\frac{a}{t}} < 1,$$
$$\mathrm{E}_1\left(a(1+\frac{1}{Z})\right) < \mathrm{E}_1\left(a(1+\frac{1}{t})\right) < \mathrm{E}_1(\mathrm{a}).$$

By substituting the lower limit of $e^{-\frac{a}{t}}$ and the upper limit of $\mathrm{E}_1\left(a(1+\frac{1}{t})\right)$ into Eq. (B.3), we get:

$$f_1 = \alpha_o b\, e^{-\alpha_o bt} \left(e^{\frac{-a}{Z}} - 2ae^a \frac{\mathrm{E}_1(a)}{t} \right). \tag{B.4}$$

Similarly, by substituting the upper limit of $e^{-\frac{a}{t}}$ and the lower limit of $\mathrm{E}_1\left(a(1+\frac{1}{t})\right)$ into Eq. (B.3), we get:

$$f_2 = \alpha_o b\, e^{-\alpha_o bt} \left(1 - 2ae^a \frac{\mathrm{E}_1\left(a(1+\frac{1}{Z})\right)}{t} \right). \tag{B.5}$$

Moreover, it can be noticed that the interval width between the two functions, i.e. $f_2 - f_1$, is a function that decreases quickly as a function of t. This leads to the idea of dividing the integral area into two parts:

$$\begin{aligned} \varepsilon(a, \alpha_o b) &= \alpha_o b \int_1^Z e^{-\alpha_o bt} \left(e^{-\frac{a}{t}} - 2ae^a \frac{\mathrm{E}_1\left(a(1+\frac{1}{t})\right)}{t} \right) \mathrm{d}t \\ &+ \quad \alpha_o b \int_Z^\infty e^{-\alpha_o bt} \left(e^{-\frac{a}{t}} - 2ae^a \frac{\mathrm{E}_1\left(a(1+\frac{1}{t})\right)}{t} \right) \mathrm{d}t. \\ &= \varepsilon_1 + \varepsilon_2. \end{aligned} \tag{B.6}$$

Therefore the possible values of ε_2 will be bounded. We denote these boundaries by m and M such as:

$$m < \varepsilon_2 < M,$$

where m and M are the integral functions of f_1 and f_2 over $\mathcal{D}$, respectively. The value of m must be positive, i.e $m = \max(0, m)$. The choice of Z must depend on the error band $M - m$. We note here that we do not calculate directly ε_2, i.e. we do not integrate the integrand over

the interval $[Z : \infty[$, we can only integrate the functions f_1 and f_2. We then choose a large enough value of Z to ensure that the error band $M - m$ is relatively small. We denote the relative error by $\mathrm{err}_{\mathrm{rel}}$ which must be very small compared to one:

$$\mathrm{err}_{\mathrm{rel}} = \frac{M - m}{m + \varepsilon_1} \tag{B.7}$$

Therefore, we do not calculate ε, but two extremes: $\varepsilon_1 + m$ and $\varepsilon_1 + M$. As $M - m$ is very small compared to ε, we will have a very good approximation in estimating ε as:

$$\varepsilon_{\mathrm{est}} = \varepsilon_1 + \frac{m + M}{2}. \tag{B.8}$$

Obviously, the value Z must be determined experimentally.

Calculation of m and M

$$\begin{aligned} m &= \int_{\mathcal{D}} f_1 \,\mathrm{d}t = \int_Z^\infty f_1 \,\mathrm{d}t \\ &= e^{\frac{-a}{Z}} e^{-\alpha_o b Z} - 2ae^a \alpha_o b \,\mathrm{E}_1\,(a)\,\mathrm{E}_1(\alpha_o b Z) \end{aligned} \tag{B.9}$$

with

$$m = \max(0, m),$$

$$\begin{aligned} M &= \int_{\mathcal{D}} f_2 \,\mathrm{d}t = \int_Z^\infty f_2 \,\mathrm{d}t \\ &= e^{-\alpha_o b Z} - 2ae^a \alpha_o b \,\mathrm{E}_1 \left(a(1 + \frac{1}{Z})\right) \mathrm{E}_1(\alpha_o b Z), \end{aligned} \tag{B.10}$$

and finally

$$M - m = e^{-\alpha_o b Z} \left(1 - e^{\frac{-a}{Z}}\right) + 2ae^a\, \alpha_o b \,\mathrm{E}_1(\alpha_o b Z) \left[\mathrm{E}_1(a) - \mathrm{E}_1 \left(a(1 + \frac{1}{Z})\right)\right]. \tag{B.11}$$

Numerical results

Figures B.1, B.2 and B.3 show the relative error ($\mathrm{err}_{\mathrm{rel}}$) for different values of $\alpha_o b$, a and Z. It can be noticed that relative error is small enough compared to one in the three cases.

Relative error							
alpha*b	1,00E-11	1,00E-10	1,00E-09	1,00E-08	1,00E-07	1,00E-06	1,00E-05
a							
0,01	1.0000500e-04	1.0000500e-04	1.0000499e-04	1.0000493e-04	1.0000424e-04	9.9996928e-05	9.9919556e-05
0,02	2.0002000e-04	2.0002000e-04	2.0001999e-04	2.0001986e-04	2.0001850e-04	2.0000401e-04	1.9985035e-04
0,04	4.0008001e-04	4.0008001e-04	4.0007999e-04	4.0007974e-04	4.0007706e-04	4.0004849e-04	3.9974462e-04
0,06	6.0018004e-04	6.0018003e-04	6.0018000e-04	6.0017963e-04	6.0017568e-04	6.0013333e-04	5.9968168e-04
0,08	8.0032008e-04	8.0032008e-04	8.0032004e-04	8.0031956e-04	8.0031435e-04	8.0025846e-04	7.9966102e-04
0,1	1.0005002e-03	1.0005002e-03	1.0005001e-03	1.0004995e-03	1.0004931e-03	1.0004239e-03	9.9968230e-04
0,2	2.0020013e-03	2.0020013e-03	2.0020012e-03	2.0020001e-03	2.0019878e-03	2.0018542e-03	2.0004114e-03
0,4	4.0080107e-03	4.0080107e-03	4.0080105e-03	4.0080084e-03	4.0079853e-03	4.0077305e-03	4.0049495e-03
0,6	6.0180361e-03	6.0180360e-03	6.0180358e-03	6.0180328e-03	6.0179996e-03	6.0176303e-03	6.0135662e-03
0,8	8.0320855e-03	8.0320855e-03	8.0320852e-03	8.0320814e-03	8.0320386e-03	8.0315591e-03	8.0262505e-03
1	1.0050167e-02	1.0050167e-02	1.0050167e-02	1.0050162e-02	1.0050110e-02	1.0049524e-02	1.0043001e-02

FIGURE B.1: Relative error for $Z = 100$.

Relative error							
alpha*b	1,00E-11	1,00E-10	1,00E-09	1,00E-08	1,00E-07	1,00E-06	1,00E-05
a							
0,01	1.0000050e-05	1.0000049e-05	1.0000040e-05	9.9999524e-06	9.9990696e-06	9.9902027e-06	9.9015466e-06
0,02	2.0000200e-05	2.0000198e-05	2.0000181e-05	2.0000005e-05	1.9998241e-05	1.9980521e-05	1.9803320e-05
0,04	4.0000800e-05	4.0000796e-05	4.0000761e-05	4.0000411e-05	3.9996888e-05	3.9961490e-05	3.9607445e-05
0,06	6.0001799e-05	6.0001794e-05	6.0001742e-05	6.0001217e-05	5.9995939e-05	5.9942895e-05	5.9412261e-05
0,08	8.0003199e-05	8.0003192e-05	8.0003123e-05	8.0002424e-05	7.9995393e-05	7.9924728e-05	7.9217718e-05
0,1	1.0000500e-04	1.0000499e-04	1.0000490e-04	1.0000403e-04	9.9995250e-05	9.9906986e-05	9.9023780e-05
0,2	2.0002000e-04	2.0001998e-04	2.0001981e-04	2.0001807e-04	2.0000057e-04	1.9982456e-04	1.9806251e-04
0,4	4.0008001e-04	4.0007997e-04	4.0007963e-04	4.0007617e-04	4.0004132e-04	3.9969070e-04	3.9617840e-04
0,6	6.0018003e-04	6.0017998e-04	6.0017947e-04	6.0017429e-04	6.0012219e-04	5.9959775e-04	5.9434206e-04
0,8	8.0032008e-04	8.0032001e-04	8.0031933e-04	8.0031245e-04	8.0024316e-04	7.9954547e-04	7.9255158e-04
1	1.0005002e-03	1.0005001e-03	1.0004992e-03	1.0004906e-03	1.0004042e-03	9.9953376e-04	9.9080598e-04

FIGURE B.2: Relative error for $Z = 1000$.

Relative error							
alpha*b	1,00E-11	1,00E-10	1,00E-09	1,00E-08	1,00E-07	1,00E-06	1,00E-05
a							
0,01	1.0000004e-06	9.9999950e-07	9.9999052e-07	9.9990070e-07	9.9900250e-07	9.9006053e-07	9.0489204e-07
0,02	2.0000018e-06	2.0000000e-06	1.9999821e-06	1.9998024e-06	1.9980062e-06	1.9801236e-06	1.8097971e-06
0,04	4.0000076e-06	4.0000040e-06	3.9999681e-06	3.9996089e-06	3.9960169e-06	3.9602563e-06	3.6196367e-06
0,06	6.0000174e-06	6.0000120e-06	5.9999582e-06	5.9994195e-06	5.9940321e-06	5.9403966e-06	5.4295087e-06
0,08	8.0000312e-06	8.0000240e-06	7.9999522e-06	7.9992340e-06	7.9920517e-06	7.9205439e-06	7.2394082e-06
0,1	1.0000049e-05	1.0000040e-05	9.9999503e-06	9.9990527e-06	9.9900755e-06	9.9006978e-06	9.0493321e-06
0,2	2.0000198e-05	2.0000180e-05	2.0000001e-05	1.9998206e-05	1.9980258e-05	1.9801558e-05	1.8099257e-05
0,4	4.0000796e-05	4.0000760e-05	4.0000402e-05	3.9996814e-05	3.9960936e-05	3.9603691e-05	3.6200295e-05
0,6	6.0001794e-05	6.0001740e-05	6.0001203e-05	5.9995824e-05	5.9942026e-05	5.9406328e-05	5.4302601e-05
0,8	8.0003192e-05	8.0003121e-05	8.0002404e-05	7.9995235e-05	7.9923525e-05	7.9209449e-05	7.2406000e-05
1	1.0000499e-04	1.0000490e-04	1.0000401e-04	9.9995046e-05	9.9905431e-05	9.9013040e-05	9.0510400e-05

FIGURE B.3: Relative error for $Z = 10000$.

APPENDIX C

An Algorithm for Computing the Capacity of PLC Channels

As it has been reported in Chapter 2, PLC exhibits both a high frequency-selective fading effect and an impulsive behavior. The channel capacity resulted from the water-filling optimal power distribution presented in Section 4.6.1, Eq. (4.17), in the presence of only background noise is rewritten here:

$$C = \sum_{k \in S_u} \log_2 \left(\frac{L}{\eta_k} \right). \tag{C.1}$$

We recall the definition of the parameters:

- k is the subchannel index;
- S_u is the set of indices of the useful subchannels (modulated subchannels);
- L is the water-filling optimization parameter;
- η_k is the subchannel input equivalent noise (in the presence of only background noise):

$$\eta_k = \frac{\psi_k}{|H_k|^2}$$

- ψ_k is the subchannel noise power;
- $|H_k|^2$ is the subchannel gain.

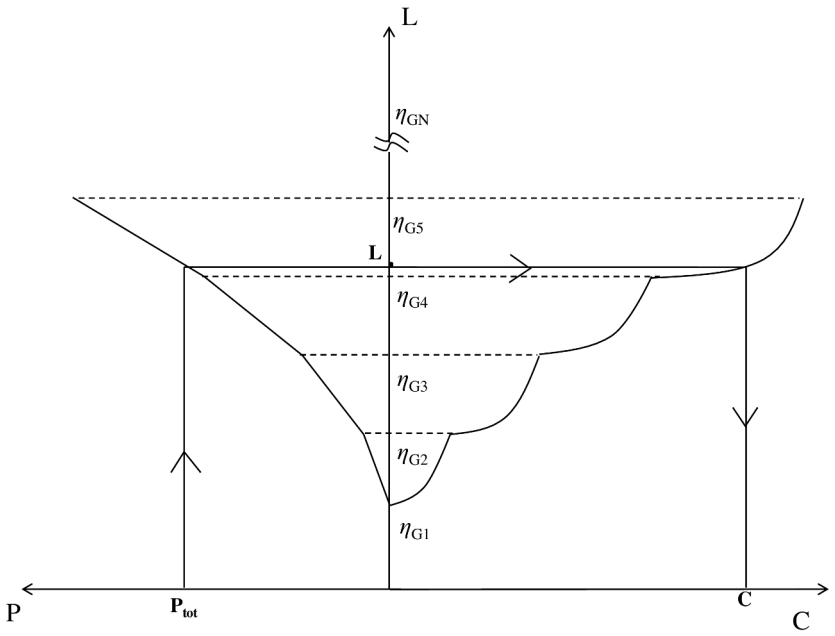

FIGURE C.1: A typical plot of the channel capacity C as a function of water-filling parameter L and the transmission power P in the presence of only background noise.

Figure C.1 depicts the channel capacity C as a function of the water-filling optimization parameter L, which in turn is a function of the transmission power P. According to water-filling algorithm, the channel capacity can be investigated as illustrated graphically in Figure C.1. As indicated by the arrows, for a given total power P_{tot}, its corresponding water-filling optimization parameter L can be obtained, and thus the channel capacity C can be computed.

Taking the impulsive noise into consideration, and based on the proportionality noticed between the two PSD models of the background and impulsive noises, $\eta_k^{'}$ (in the presence of impulsive noise) can be written as:

$$\begin{aligned} \eta_k^{'} &= \eta_{G_k} + \eta_{I_k} \\ &= \eta_{G_k}(1+\alpha) \end{aligned} \tag{C.2}$$

for all the subchannels k. Thus, channel capacity limit in Eq. (C.1) becomes:

$$C' = \sum_{k \in S_u'} \log_2 \left(\frac{L'}{\eta_{G_k}(1+\alpha)} \right). \tag{C.3}$$

We recall the definition of the parameters:

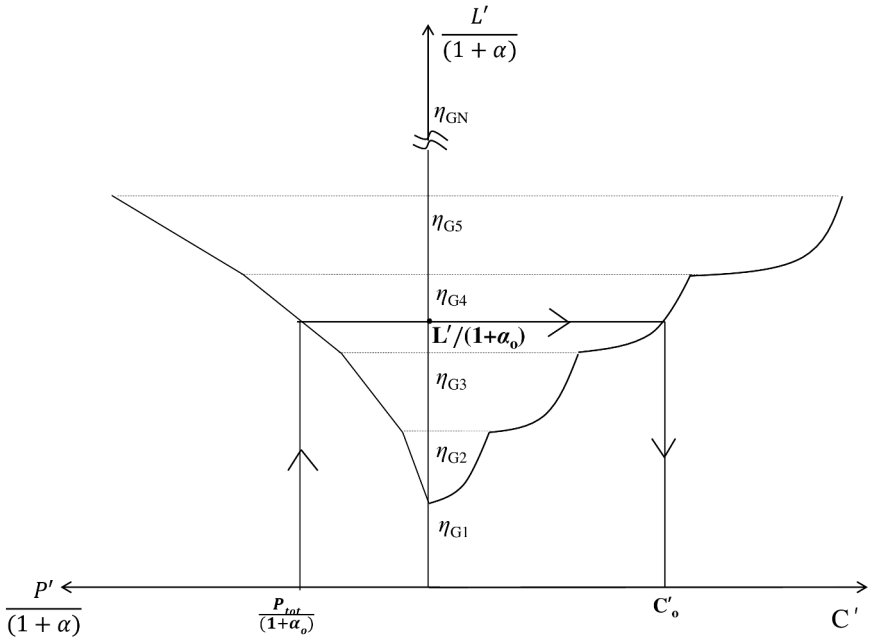

FIGURE C.2: A typical plot of the channel capacity C' as a function of the normalized L' and P' in the presence of impulsive noise.

- $(\cdot)'$ refers to the case where impulsive noise is present;
- S'_u is the set of indices of the useful subchannels in the presence of impulsive noise;
- L' is the water-filling parameter in the presence of impulsive noise;
- η_{G_k} is the subchannel input equivalent noise (background noise):

$$\eta_{G_k} = \frac{\psi_{G_k}}{|H_k|^2},$$

- ψ_{G_k} is the subchannel background noise power;
- $|H_k|^2$ is the subchannel gain;
- α is a power ratio of impulsive noise to background noise, defined as:

$$\alpha = \frac{\sum_{k=1}^{N} \psi_{I_k}}{\psi_G},$$

  (in this case α is constant for all subchannels k)
- ψ_{I_k} is the subchannel impulsive noise power and ψ_G is the background noise power.

The channel capacity C' is a function of the water-filling optimization parameter L' and thus the transmission power P' as illustrated in Figure C.2, where both L' and P' are normalized

by a factor of $(1+\alpha)$. We note here that the resultant curve of Figure C.2 is the same one as in the case where there is no impulsive noise (i.e. the same as in Figure C.1) with coordinates which are P, L and C instead of the normalized $P^{'}$ and $L^{'}$ and the $C^{'}$. In the presence of impulsive noise, for a given P_{tot}, the channel capacity of Eq. (C.3) can be obtained as a function of α as indicated by the arrows. For each value α_o of α, we obtain its corresponding optimization parameter $L^{'}/(1+\alpha_o)$, which corresponds to $C_o^{'}$. This allows us to investigate the channel capacity in the presence of impulsive noise using one parameter, which is α. This algorithm can serve as a basis for a low complexity bit-loading algorithm for PLC systems.

APPENDIX D

Study of the Function $\frac{C_\varepsilon}{\frac{\mathrm{d}C_\varepsilon}{\mathrm{d}\varepsilon}}$

We have mentioned in Chapter 4 that in order to maximize the average rate R_ε, we study the sign of its derivative by comparing the straight line y_2 with the curve y_1. A detailed study of the function $y_1 = \frac{C_\varepsilon}{\frac{\mathrm{d}C_\varepsilon}{\mathrm{d}\varepsilon}}$ is needed to acquire a better understanding of R_ε and specially at $\varepsilon = 1$ (i.e. $\alpha_o = 0$). The function y_1 can be written as:

$$y_1 = \frac{C_\varepsilon}{\frac{\mathrm{d}C_\varepsilon}{\mathrm{d}\varepsilon}} = \frac{C_\varepsilon}{\frac{\mathrm{d}C_\varepsilon}{\mathrm{d}\alpha_o}} \cdot \frac{\mathrm{d}\varepsilon}{\mathrm{d}\alpha_o}. \tag{D.1}$$

So, we investigate the two functions $\frac{\mathrm{d}\varepsilon}{\mathrm{d}\alpha_o}$ and $\frac{\mathrm{d}C_\varepsilon}{\mathrm{d}\alpha_o}$ of Eq. (D.1).

Calculation of the function $\frac{\mathrm{d}\varepsilon}{\mathrm{d}\alpha_o}$

According to Eq. (B.2), the outage probability ε can be defined as:

$$\varepsilon(a, \alpha_o b) = \alpha_o b \int_1^\infty e^{-\alpha_o b t} \left(e^{-\frac{a}{t}} - 2a e^a \frac{\mathrm{E}_1\left(a(1+\frac{1}{t})\right)}{t} \right) \mathrm{d}t. \tag{D.2}$$

Then, its derivative with respect to $\alpha_o b$ is given by:

$$\begin{aligned}\frac{\partial\,\varepsilon(a,\alpha_o b)}{\partial\,\alpha_o b} &= \frac{\varepsilon(a,\alpha_o b)}{\alpha_o b} - \alpha_o b\int_1^{\infty} e^{-\alpha_o bt}\left[te^{\frac{-a}{t}} - 2ae^{a}\mathrm{E}_1\left(a(1+\frac{1}{t})\right)\right] \\ &= \frac{\varepsilon(a,\alpha_o b)}{\alpha_o b} - D,\end{aligned} \tag{D.3}$$

where

$$D = \alpha_o b\int_1^{\infty} e^{-\alpha_o bt}\left[te^{\frac{-a}{t}} - 2ae^{a}\mathrm{E}_1\left(a(1+\frac{1}{t})\right)\right]\,\mathrm{d}t. \tag{D.4}$$

The integral of the function presented in Eq. (D.4) has similar characteristics as the one of $\varepsilon(a,\alpha_o b)$. Thus, when the parameter $\alpha_o b$ tends to zero, the limit of D can not be easily found neither analytically nor numerically. Therefore, we investigate D numerically in a similar way as for $\varepsilon(a,\alpha_o b)$ (see Appendix B). We divide the integral area in D into two parts:

$$\begin{aligned}D = \alpha_o b\int_1^{Z_o} e^{-\alpha_o bt}\left[te^{\frac{-a}{t}} - 2ae^{a}\mathrm{E}_1\left(a(1+\frac{1}{t})\right)\right]\,\mathrm{d}t \\ + \quad \alpha_o b\int_{Z_o}^{\infty} e^{-\alpha_o bt}\left[te^{\frac{-a}{t}} - 2ae^{a}\mathrm{E}_1\left(a(1+\frac{1}{t})\right)\right]\,\mathrm{d}t \\ = D_1 + D_2,\end{aligned} \tag{D.5}$$

and we find the two extremes of D_2 such that $m_2 < D_2 < M_2$. The obtained results are given below:

$$m_2 = e^{\frac{-a}{Z_o}}e^{-\alpha_o bZ_o}\frac{(1+\alpha_o bZ_o)}{\alpha_o b} - 2ae^{a}\mathrm{E}_1(a)e^{-\alpha_o bZ_o}. \tag{D.6}$$

and

$$M_2 = e^{-\alpha_o bZ_o}\frac{(1+\alpha_o bZ_o)}{\alpha_o b} - 2ae^{a}\mathrm{E}_1\left(a(1+\frac{1}{Z_o})\right)e^{-\alpha_o bZ_o}. \tag{D.7}$$

Finally, $\frac{\partial\,\varepsilon(a,\alpha_o b)}{\partial\,\alpha_o b}$ can be found as follows:

$$\frac{\partial\,\varepsilon(a,\alpha_o b)}{\partial\,\alpha_o b} = \frac{\varepsilon(a,\alpha_o b)}{\alpha_o b} - (D_1 + \frac{m_1+M_2}{2}). \tag{D.8}$$

One can note that the limit of $|\frac{\partial\,\varepsilon(a,\alpha_o b)}{\partial\,\alpha_o}|$ tends to infinity as α_o tends to 0.

Calculation of the function $\frac{\mathrm{d}C_\varepsilon}{\mathrm{d}\alpha_o}$

We have seen in Section 4.6.4 (and also in Appendix C) that the capacity of OFDM systems in the presence of impulsive noise can be written as:

$$C^{'} = \sum_{k=1}^{N_u^{'}} \ln\left(\frac{L^{'}}{\eta_{G_k}(1+\alpha_o)}\right) = N_u^{'}\left[\ln(L^{'}) - \ln(1+\alpha_o)\right] - \sum_{k=1}^{N_u^{'}} \ln(\eta_{G_k}) \quad \text{(nats/symbol)} \quad \text{(D.9)}$$

(we note here that the subchannels are sorted in increasing order of the input equivalent noise η_{G_k}), where the level $L^{'}$ is given by the following equation:

$$L^{'} = \frac{1}{N_u^{'}}\left(P_{tot} + \sum_{k=1}^{N_u^{'}} \eta_{G_k}(1+\alpha_o)\right). \quad \text{(D.10)}$$

The derivative of Eq. (D.9) gives:

$$\frac{\mathrm{d}C^{'}}{\mathrm{d}\alpha_o} = N_u^{'}\left[\frac{1}{L^{'}}\frac{\mathrm{d}L^{'}}{\mathrm{d}\alpha_o} - \frac{1}{1+\alpha_o}\right] + \frac{\mathrm{d}N_u^{'}}{\mathrm{d}\alpha_o}\left[\ln\left(\frac{L^{'}}{1+\alpha_o}\right)\right] - \frac{\mathrm{d}}{\mathrm{d}\alpha_o}\left[\sum_{k=1}^{N_u^{'}} \ln(\eta_{G_k})\right]. \quad \text{(D.11)}$$

We can show that the sum of the last two terms in Eq. (D.11) is zero, i.e. we have:

$$\frac{\mathrm{d}C^{'}}{\mathrm{d}\alpha_o} = N_u^{'}\left[\frac{1}{L^{'}}\frac{\mathrm{d}L^{'}}{\mathrm{d}\alpha_o} - \frac{1}{1+\alpha_o}\right]. \quad \text{(D.12)}$$

The result of the derivative of $L^{'}$ with respect to α_o is given by:

$$\frac{\mathrm{d}L^{'}}{\mathrm{d}\alpha_o} = \frac{1}{N_u^{'}}\sum_{k=1}^{N_u^{'}} \eta_{G_k}. \quad \text{(D.13)}$$

Therefore

$$\frac{\mathrm{d}C^{'}}{\mathrm{d}\alpha_o} = N_u^{'}\left[\frac{\sum_{k=1}^{N_u^{'}} \eta_{G_k}}{P_{tot} + (1+\alpha_o)\sum_{k=1}^{N_u^{'}} \eta_{G_k}} - \frac{1}{1+\alpha_o}\right], \quad \text{(D.14)}$$

or in an absolute value form:

$$\left|\frac{\mathrm{d}C^{'}}{\mathrm{d}\alpha_o}\right| = N_u^{'}\frac{P_{tot}}{(1+\alpha_o)\left[P_{tot} + (1+\alpha_o)\sum_{k=1}^{N_u^{'}} \eta_{G_k}\right]}. \quad \text{(D.15)}$$

It can be noted that as α_o tends to 0 the limit of $\left|\frac{\mathrm{d}C^{'}}{\mathrm{d}\alpha_o}\right|$ converges to $N_u\frac{P_{tot}}{P_{tot}+\sum_{k=1}^{N_u} \eta_{G_k}}$ $(= \frac{P_{tot}}{L})$ (nats/symbol).

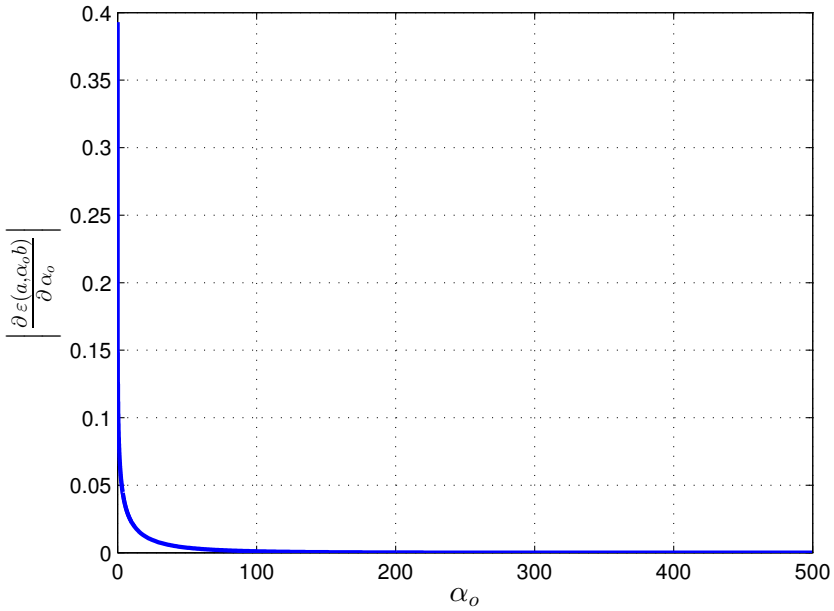

FIGURE D.1: The absolute value of the derivative of $\partial\,\varepsilon(a,\alpha_o b)$ with respect to α_o .

Plotting the results

The function y_1 of Eq. (D.1) can be defined as:

$$y_1 = \frac{C_\varepsilon}{\frac{\mathrm{d}C_\varepsilon}{\mathrm{d}\varepsilon}} = \frac{C_\varepsilon}{\left|\frac{\mathrm{d}C}{\mathrm{d}\alpha_o}\right|} \cdot \left|\frac{\partial\,\varepsilon(a,\alpha_o b)}{\partial\,\alpha_o}\right| \tag{D.16}$$

($\frac{\mathrm{d}C}{\mathrm{d}\alpha_o}$ and $\frac{\partial\,\varepsilon(a,\alpha_o b)}{\partial\,\alpha_o}$ are both negative functions). Figures D.1 and D.2 plot $|\frac{\partial\,\varepsilon(a,\alpha_o b)}{\partial\,\alpha_o}|$ and $\left|\frac{\mathrm{d}C'}{\mathrm{d}\alpha_o}\right|$, respectively, for $\tau = 0.5$, $\mu = 100$ and $P_A = 0.01$. We have seen that as α_o tends to 0 $|\frac{\partial\,\varepsilon(a,\alpha_o b)}{\partial\,\alpha_o}|$ tends to infinity, while $\left|\frac{\mathrm{d}C'}{\mathrm{d}\alpha_o}\right|$ converges to a finite number. Therefore, the limit of y_1 tends to + infinity as α_o tends to 0. Or in other words, the limit of y_1 tends to + infinity as ε tends to 1. Figure D.3 plots y_1 as a function of ε, where it can be noticed that it goes to infinity as ε goes to 1.

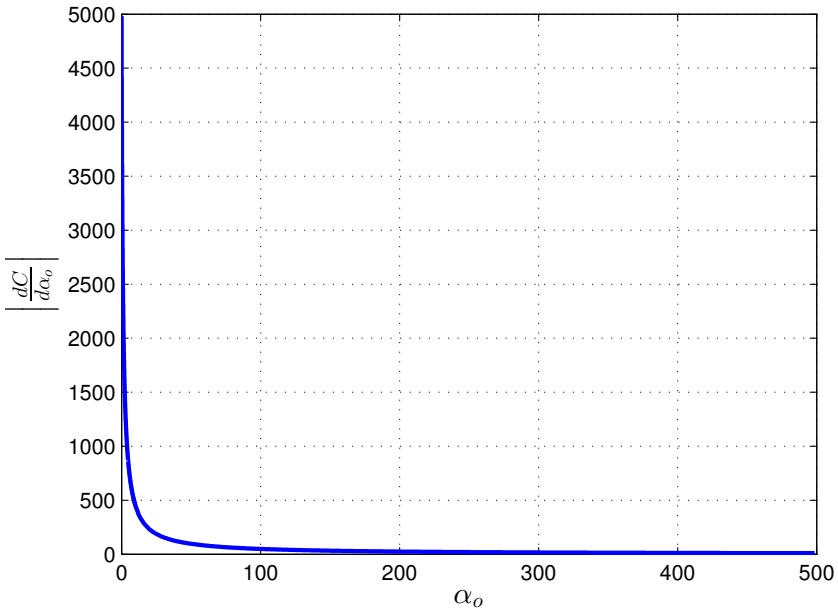

FIGURE D.2: The absolute value of the derivative of C with respect to α_o.

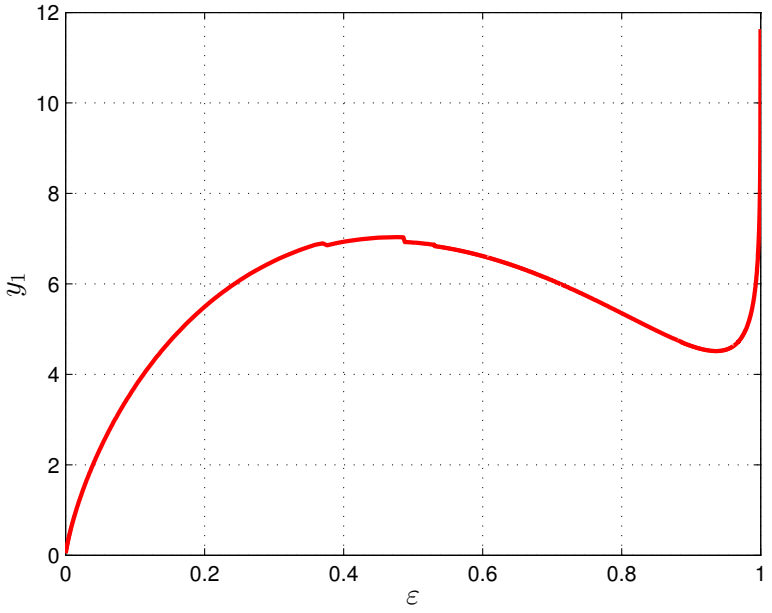

FIGURE D.3: The function y_1.

Bibliography

[1] M. M. Rahman, C. S. Hong, J. Lee, M. A. Razzaque, and J. H. Kim. Medium access control for power line communications: An overview of the IEEE 1901 and ITU-T G.hn standards. *IEEE Commun. Mag*, 49(6):183 – 191, June 2011.

[2] H. C. Ferreira, L. Lampe, J. Newbury, and T. G. Swart. *Power line communications*. John Wiley & Sons, New York, USA, 2010.

[3] A. M. Tonello, F. Versolato, B. Bejar, and S. Zazo. A fitting algorithm for random modeling the PLC channel. *IEEE Trans. Power Del.*, 27(3):1477– 1484, June 2012.

[4] M. Tlich, A. Zeddam, A. Moulin, and F. Gauthier. Indoor power-line communications channel characterization up to 100 MHz - part I: One-parameter deterministic model. *IEEE Trans. Power Del.*, 23(3):1392–1401, 2008.

[5] M. Zimmermann and K. Dostert. Analysis and modeling of impulsive noise in broadband powerline communications. *IEEE Trans. Electromagn. Compat.*, 44(1):249– 258, Feb. 2002.

[6] D. Schneider, A. Schwager, W. Bäschlin, and P. Pagani. European MIMO PLC field measurements: Channel analysis. In *Proc. IEEE Int. Symp. Power Line Commun. Appl. (ISPLC)*, pages 304–309, Beijing, Chine, 2012.

[7] P. A. Brown. Power line communications - past present and future. In *Proc. IEEE Int. Symp. Power Line Commun. Appl. (ISPLC)*, pages 1–8, Lancaster UK, 1999.

[8] K. Dostert. Telecommunications over the power grid - Possibilities and limitations. In *Proc. IEEE Int. Symp. Power Line Commun. Appl. (ISPLC)*, pages 1–9, Essen, Germany, 1997.

[9] *Power line communications*. Prentice Hall, 2001.

[10] M. S. Yousuf and M. El-Shafei. Power line communications: An overview - Part I. In *4th International Conference on Innovations in Information Technology (IIT '07)*, pages 218–222, 2007.

[11] S. Galli, A. Scaglione, and Z. Wang. For the grid and through the grid: The role of power line communications in the smart grid. *Proc. IEEE*, 99(6):998–1027, 2011.

[12] A. Haidine, H. Hrasnica, and R. Lehnert. *Broadband powerline communications networks*. John Wiley & Sons, 2004.

[13] L. T. Berger, A. Schwager, P. Pagani, and D. M. Schneider. *MIMO power line communications*. CRC Press, 2014.

[14] S. Galli and O. Logvinov. Recent developments in the standardization of power line communication within the IEEE. *IEEE Commun. Mag.*, 46(7):64– 71, 2008.

[15] V. Oksman and S. Galli. G.hn: The new ITU-T home networking standard. *IEEE Commun. Mag.*, 47(10):138–145, 2009.

[16] Homeplug powerline alliance website. www.homeplug.org.

[17] HomePlug PowerLine Alliance. HomePlug AV baseline specification. Version 1.0.00, Dec. 2005.

[18] HomePlug AV2 White Paper [Online]. http://www.homeplug.org. 2012.

[19] Homegrid Forum alliance website. www.homegridforum.org.

[20] HD-PLC alliance website. www.hd-plc.org.

[21] Universal powerline association website. www.upaplc.org.

[22] IEEE Std.802.11. Wireless LAN Medium Access Control and Physical Layer Specification. 591-612, 2007.

[23] L. Schumacher, L. T. Berger, and M. J. Ramiro. Recent advances in propagation characterisation and multiple antenna processing in the 3GPP framework. In *Proceedings of XXVIth URSI General Assembly*, 2002.

[24] Seventh Framework Programme: Theme 3 ICT-213311 OMEGA Deliverable D3.2, PLC Channel Characterization and Modelling, Dec. 2008.

[25] C. E. Shannon. A mathematical theory of communication. *Bell System Technical Journal*, 27:379–423, 623–656, 1948.

[26] P. Langfeld and K. Dostert. The capacity of typical powerline reference channels and strategies for system design. In *Proc. IEEE Int. Symp. Power Line Commun. Appl. (ISPLC)*, pages 271– 278, Malm, Sweden, 2001.

[27] E. Liu, Y. Gao, G. Samdani, O. Mukhtar, and T. Korhonen. Broadband power line channel and capacity analysis. In *Proc. IEEE Int. Symp. Power Line Commun. Appl. (ISPLC)*, pages 7–11, Vancouver, BC, Canada, 2005.

[28] M. Kuhn, S. Berger, I. Hammerström, and A. Wittneben. Power line enhanced cooperative wireless communications. *IEEE J. Sel. Areas Commun.*, 24(7):1401–1410, July 2006.

[29] J. Anatory, N. Theethayi, R. Thottappillil, M. M. Kissaka, and N. H. Mvungi. Broadband power-line communications: The channel capacity analysis. *IEEE Trans. Power Del.*, 23(1):164–170, Jan. 2008.

[30] A. Schwager. *Powerline communications: Significant technologies to become ready for integration*. PhD thesis, University of Duisburg-Essen, May 2010.

[31] A. Schwager, D. Schneider, W. Bäschlin, A. Dilly, and J. Speidel. MIMO PLC: theory, measurements and system setup. In *Proc. IEEE Int. Symp. Power Line Commun. Appl. (ISPLC)*, pages 48–53, Udine, Italy, 2011.

[32] D. Schneider, J. Speidel, L. Stadelmeier, D. Schill, and A. Schwager. Potential of MIMO for inhome power line communications. *ITG-Fachtagung, Dortmund*, 2009.

[33] A. Paulraj, R. Nabar, and D. Gore. *Introduction to space-time wireless communications*. Cambridge University Press, Cambridge, U.K., 2003.

[34] L. Stadelmeier, D. Schneiderv, D. Schill, A. Schwager, and J. Speidel. MIMO for inhome power line communications. In *International ITG Conference on Source and Channel Coding*, pages 1–6, Ulm, Germany, 2008.

[35] R. Hashmat, P. Pagani, A. Zeddam, and T. Chonavel. MIMO communications for inhome PLC networks: Measurements and results up to 100 Mhz. In *Proc. IEEE Int. Symp. Power Line Commun. Appl. (ISPLC)*, pages 120–124, Rio de Janeiro, Brazil, 2010.

[36] A. Canova, N. Benvenuto, and P. Bisaglia. Receivers for MIMO-PLC channels: Throughput comparison. In *Proc. IEEE Int. Symp. Power Line Commun. Appl. (ISPLC)*, pages 114–119, Rio de Janeiro, Brazil, 2010.

[37] D. Rende, A. Nayagam, K. Afkhamie, L. Yonge, R. Riva, D. Veronesi, F. Osnato, and P. Bisaglia. Noise correlation and its effect on capacity of in-home MIMO power line channels. In *Proc. IEEE Int. Symp. Power Line Commun. Appl. (ISPLC)*, pages 60–65, Udine, Italy, 2011.

[38] F. Versolatto and A. M. Tonello. A MIMO PLC random channel generator and capacity analysis. In *Proc. IEEE Int. Symp. Power Line Commun. Appl. (ISPLC)*, pages 66–71, Udine, Italy, 2011.

[39] N. Pavlidou, A. J. H. Vinck, J. Yazdani, and B. Honary. Power line communications: state of the art and future trends. *IEEE Commun. Mag.*, 41(4):34 –40, April 2003.

[40] M. Zimmermann and K. Dostert. A multipath model for the powerline channel. *IEEE Trans. Commun.*, 50(4):553– 559, Apr. 2002.

[41] M. Tlich, A. Zeddam, A. Moulin, and F. Gauthier. Indoor power-line communications channel characterization up to 100 MHz–part II: Time-frequency analysis. *IEEE Trans. Power Del.*, 23(3):1402–1409, Jul. 2008.

[42] S. Galli. A novel approach to the statistical modeling of wireline channels. *IEEE Trans. Commun.*, 59(5):332–1345, May 2011.

[43] A. M. Tonello, F. Versolatto, and A. Pittolo. In-Home power line communication channel: Statistical characterization. *IEEE Trans. Commun.*, 62(6):2096–2106, avril 2014.

[44] F. J. Canete, J. A. Cortés, L. Diez, and J. T. Entrambasaguas. Analysis of the cyclic short-term variation of indoor power line channels. *IEEE J. Sel. Areas Commun.*, 24(7):1327–1338, 2006.

[45] F. Gianaroli, F. Pancaldi, and G. M. Vitetta. Broadband system models based on Zadeh's representation for indoor powerline channels: An experimental validation. In *Proc. IEEE ICC*, pages 4304–4309. IEEE, 2013.

[46] S. Galli and T. Banwell. A deterministic frequency-domain model for the indoor power line transfer function. *IEEE J. Sel. Areas Commun.*, 24(7):1304–1316, 2006.

[47] A. M. Tonello and T. Zheng. Bottom-up transfer function generator for broadband PLC statistical channel modeling. In *Proc. IEEE Int. Symp. Power Line Commun. Appl. (ISPLC)*, pages 7–12. IEEE, 2009.

[48] T. Esmailian, F. R. Kschischang, and P. G. Gulak. In-building power lines as high-speed communication channels: Channel characterization and a test channel ensemble. *Int. J. Commun. Syst.*, 16(5):381–400, May 2003.

[49] A. M. Tonello and F. Versolatto. Bottom-up statistical PLC channel modeling-part I: Random topology model and efficient transfer function computation. *IEEE Trans. Power Del.*, 26(2):891–898, 2011.

[50] C. R. Paul. *Analysis of Multiconductor Transmission Lines*. John Wiley & Sons, New York, 1994.

[51] H. Philipps. Modeling of power line communications channels. In *Proc. IEEE Int. Symp. Power Line Commun. Appl. (ISPLC)*, Lancaster, UK, April 1999.

[52] M. Zimmerman and K. Dostert. A multi-path signal propagation model for the powerline channel in the high frequency range. In *Proc. IEEE Int. Symp. Power Line Commun. Appl. (ISPLC).*, pages 45–51, Lucaster, UK, 1999.

[53] H. Philipps. Development of a statistical model for power line communications channels. In *Proc. IEEE Int. Symp. Power Line Commun. Appl. (ISPLC)*, Limerick, Ireland, April 2000.

[54] G. NDO. *Etude et Optimisation de Techniques de Réduction de Bruit Impulsif pour Transmissions Haut Débit sur Lignes à Courants Porteurs en Contexe Résidentiel*. PhD thesis, Thesis at École Nationale Supérieure des Télécommunications de Bretagne, 2010.

[55] A. M. Tonello. Wideband impulse modulation and receiver algorithms for multiuser power line communications. *EURASIP Journal on Advances in Signal Processing*, 2007, 2007.

[56] A. M. Tonello, S. D'Alessandro, and L. Lampe. Cyclic prefix design and allocation in bit-loaded OFDM over power line communication channels. *IEEE Trans. Commun.*, 58(11):3265–3276, 2010.

[57] A. M. Tonello, F. Versolatto, B. B. Haro, and S. Z. Bello. A top-down random generator for the in-home PLC channel. In *Proc. IEEE GLOBECOM*, pages 1–5, Houston, TX, USA, 2011.

[58] D. Anastasiadou and T. Antonakopoulos. Multipath characterization of indoor power-line networks. *IEEE Trans. Power Del.*, 20(1):90–99, 2005.

[59] T. Banwell and S. Galli. A novel approach to the modeling of the indoor power line channel part I: circuit analysis and companion model. *IEEE Trans. Power Del.*, 20(2):655–663, 2005.

[60] S. Galli and T. Banwell. A novel approach to the modeling of the indoor power line channel-Part II: transfer function and its properties. *IEEE Trans. Power Del.*, 20(3):1869–1878, 2005.

[61] F. Versolatto and A. M. Tonello. An MTL theory approach for the simulation of MIMO power-line communication channels. *IEEE Trans. Power Del.*, 26(3):1710–1717, 2011.

[62] D. Veronesi, R. Riva, P. Bisaglia, F. Osnato, K. Afkhamie, A. Nayagam, D. Rende, and L. Yonge. Characterization of in-home mimo power line channels. In *Proc. IEEE Int. Symp. Power Line Commun. Appl. (ISPLC)*, pages 42–47. IEEE, 2011.

[63] R. Hashmat, P. Pagani, A. Zeddam, and T. Chonavel. A channel model for multiple input multiple output in-home power line networks. In *Proc. IEEE Int. Symp. Power Line Commun. Appl. (ISPLC)*, pages 35– 41, Udine, Italy, 2011.

[64] A. Schwager, W. Baschlin, H. Hirsch, P. Pagani, N. Weling, J. L. G. Moreno, and H. Milleret. European MIMO PLT field measurements: Overview of the ETSI STF410 campaign & EMI analysis. In *Proc. IEEE Int. Symp. Power Line Commun. Appl. (ISPLC)*, pages 298–303. IEEE, 2012.

[65] M. Babic, M. Hagenau, K. Dostert, and J. Bausch. OPERA deliverable D4, Theoretical postulation of PLC channel model. OPERA-IST Integrated Project No. 507667, funded by EC, Mar. 2005.

[66] P. Kyritsi, D. C. Cox, R. A. Valenzuela, and P. W. Wolniansky. Correlation analysis based on MIMO channel measurements in an indoor environment. *IEEE Journ. on Selec Areas in Comm.*, 21(5):713–720, 2003.

[67] A. Tomasoni, R. Riva, and S. Bellini. Spatial correlation analysis and model for in-home mimo power line channels. In *Proc. IEEE Int. Symp. Power Line Commun. Appl. (ISPLC)*, pages 286–291, 2012.

[68] J. P. Kermoal, L. Schumacher, K. I. Pedersen, P. E. Mogensen, and F. Frederiksen. A stochastic MIMO radio channel model with experimental validation. *IEEE J. Sel. Areas Commun.*, 20(6):1211–1226, 2002.

[69] O. G. Hooijen. A channel model for the residential power circuit used as a digital communications medium. *IEEE Trans. Electromagn. Compat.*, 40(4):331– 336, Nov. 1998.

[70] H. Meng, Y. L. Guan, and S. Chen. Modeling and analysis of noise effects on broadband power-line communications. *IEEE Trans. Power Del.*, 20(2):630– 637, Apr. 2005.

[71] J. A. Cortés, L. Diez, F. J. Cañete, and J. J. Sánchez-Martínez. Analysis of the indoor broadband power-line noise scenario. *IEEE Trans. Electromagn. Compat.*, 52(4):849–858, Sep. 2010.

[72] Y. Hirayama, H. Okada, T. Yamazato, and M. Katayama. Noise analysis on wide-band PLC with high sampling rate and long observation time. In *Proc. IEEE Int. Symp. Power Line Commun. Appl. (ISPLC)*, pages 142–147., Kyoto, Japan, Mars 2003.

[73] E. Liu, Y. Gao, G. Samdani, O. Mukhtar, and T. Korhonen. Broadband characterization of indoor powerline channel and its capacity consideration. In *Proc. IEEE ICC*, volume 2, pages 901–905. IEEE, 2005.

[74] D. Middleton. *An introduction to statistical communication theory*, volume 960. McGraw-Hill New York, 1960.

[75] D. Middleton. Statistical-physical model of electromagnetic interference. *IEEE Trans. Electromagn. Compat.*, EMC-19(3):106–126, Aug. 1977.

[76] T. Shongwey, A. J. Vinck, and H. C. Ferreira. On impulse noise and its models. In *Proc. IEEE Int. Symp. Power Line Commun. Appl. (ISPLC)*, pages 12–17, 2014.

[77] R. Pighi, M. Franceschini, G. Ferrari, and R. Raheli. Fundamental performance limits of communications systems impaired by impulse noise. *IEEE Trans. Commun.*, 57(1):171–182, 2009.

[78] T. Oberg and M. Mettiji. Robust detection in digital communications. *IEEE Trans. Commun.*, 43(5):1872–1876, 1995.

[79] X. Wang and H. V. Poor. Robust multiuser detection in non-Gaussian channels. *IEEE Trans. Signal Process.*, 47(2):289–305, 1999.

[80] S. V. Vaseghi. *Advanced Digital Signal Processing and Noise Reduction, 4th ed.* John Wiley & Sons, 2009.

[81] Y. H. Ma, P. L. So, and E. Gunawan. Performance analysis of OFDM systems for broadband power line communications under impulsive noise and multipath effects. *IEEE Trans. Power Del.*, 20(2):674– 682, Apr. 2005.

[82] G. Ndo, P. Siohan, and MH. Hamon. Adaptive noise mitigation in impulse environment: Application to power-line communications. *IEEE Trans. Power Del.*, 25(2):647–656, Jan. 2010.

[83] J. Mitra and L. Lampe. Convolutionally coded transmission over Markov-Gaussian channels: Analysis and decoding metrics. *IEEE Trans. Commun.*, 58(7):1939 –1949, Jul. 2010.

[84] G. Ndo, F. Labeau, and M. Kassouf. A Markov-Middleton model for bursty impulsive noise: Modeling and receiver design. *IEEE Trans. Power Del.*, 28(4):2317–2325, Oct. 2013.

[85] K. Khalil, M. G. Gazalet, P. Corlay, F. X. Coudoux, and M. Gharbi. An MIMO random channel generator for indoor power-line communication. *IEEE Trans. Power Del.*, 29(4):1561–1568, July 2014.

[86] S. Galli. A simplified model for the indoor power line channel. In *Proc. IEEE Int. Symp. Power Line Commun. Appl. (ISPLC)*, pages 13–19, Dresden, Germany, 2009.

[87] S. Galli. A simple two-tap statistical model for the power line channel. In *Proc. IEEE Int. Symp. Power Line Commun. Appl. (ISPLC)*, pages 242–248. IEEE, 2010.

[88] F. J. Canete, J. A. Cortés, L. Diez, and J. L. G. Moreno. On the statistical properties of indoor power line channels: Measurements and models. In *Proc. IEEE Int. Symp. Power Line Commun. Appl. (ISPLC)*, pages 271– 276, Udine, Italy, 2011.

[89] F. Versolatto and A. M. Tonello. On the relation between geometrical distance and channel statistics in in-home PLC networks. In *Proc. IEEE Int. Symp. Power Line Commun. Appl. (ISPLC)*, pages 280–285. IEEE, 2012.

[90] F. Versolatto and A. M. Tonello. PLC channel characterization up to 300 MHz: Frequency response and line impedance. In *Proc. IEEE GLOBECOM*, pages 3525–3530, 2012.

[91] M. Ghosh. Analysis of the effect of impulse noise on multicarrier and single carrier QAM systems. *EEE Trans. Commun.*, 44(2):145 – 147, Feb. 1996.

[92] N. Andreadou and F. N. Pavlidou. Modeling the noise on the OFDM power-line communications system. *IEEE Trans. Power Del.*, 25(1):150–157, 2010.

[93] N. Andreadou and A. M. Tonello. On the mitigation of impulsive noise in power-line communications with LT codes. *IEEE Trans. Power Del.*, 28(3):1483–1490, May 2013.

[94] H. Goldman. Performance of Turbo-TCM over a noise burst channel. *Trans. Emerg. Telecommun. Technol.*, 13(6):583– 588, 2008.

[95] D. Umehara, H. Yamaguchi, and Y. Morihiro. Turbo decoding in impulsive noise environment. In *Proc. IEEE GLOBECOM*, pages 194–198, Dallas, Texas ,USA, 2004.

[96] V. N. Papilaya and A. J. H. Vinck. Investigation on a new combined impulsive noise mitigation scheme for OFDM transmission. In *Proc. IEEE Int. Symp. Power Line Commun. Appl. (ISPLC)*, pages 86–91, Johannesburg, South Africa, 2013.

[97] A. M. Hmidat, B. S. Sharif, W. L. Woo, and M. A. S. Hassan. Fuzzy-based multiuser detector for impulsive CDMA channel. *Trans. Emerg. Telecommun. Technol.*, 18(7):769– 776, 2007.

[98] C. H. Yih. Iterative interference cancellation for OFDM signals with blanking nonlinearity in impulsive noise channels. *IEEE Signal Process. Lett.*, 19(3):147–150, 2012.

[99] G. Avril, F. Moulin, A. Zeddam, M. Tlich, and F. Nouvel. Impulsive noise detection on masked carriers. In *Proc. IEEE Int. Symp. Power Line Commun. Appl. (ISPLC)*, pages 369– 373, Jeju Island, Korea, 2008.

[100] M. Sliskovic. Impulse noise detection algorithms for multicarrier communication systems - Performance analysis. In *Proceedings of IEEE ISPA*, 2001.

[101] J. Rinne and A. Hazmi. Impulse burst position detection and channel estimation schemes for OFDM systems. *IEEE Trans. Consum. Electron.*, 49(3):539–545, 2003.

[102] M. R. Ahadiat, P. Azmi, and A. Haghbin. Impulsive noise estimation and suppression in OFDM systems over in-home power line channels. *Int. J. Commun. Syst.*, 2014.

[103] T. Y. Al-Naffouri, A. A. Quadeer, and G. Caire. Impulse noise estimation and removal for OFDM systems. *IEEE Trans. Commun.*, 62(3):976–989, Feb. 2014.

[104] S.V. Zhidkov. Analysis and comparison of several simple impulsive noise mitigation schemes for OFDM receivers. *IEEE Trans. Commun.*, 56(1):5 – 9, January 2008.

[105] S. V. Zhidkov. Impulsive noise suppression in OFDM-based communication systems. *IEEE Trans. Consum. Electron.*, 49(4):944 – 948, Nov. 2003.

[106] H.-M. Oh, Y.-J. Park, S. Choi, J.-J. Lee, and K.-C. Whang. Mitigation of performance degradation by impulsive noise in LDPC coded OFDM system. In *Proc. IEEE Int. Symp. Power Line Commun. Appl. (ISPLC)*, pages 331–336, Orlando, Florida, USA, Mar. 2006.

[107] Jing Lin, Marcel Nassar, and Brian L. Evans. Impulsive noise mitigation in powerline communications using sparse bayesian learning. *IEEE J. Sel. Areas Commun.*, 31(7):1172–1183, JULY 2013.

[108] Lutz Lampe. Bursty impulsive noise detection by compressed sensing. In *Proc. IEEE Int. Symp. Power Line Commun. Appl. (ISPLC)*, pages 29 – 34, Udine, Italy, 2011.

[109] H. V. Vu, N. H. Tran, T. V. Nguyen, and S. I. Hariharan. On the capacity of Bernoulli-Gaussian impulsive noise channels in Rayleigh fading. In *Proc. IEEE PIMRC*, pages 1281– 1285, London, UK, 2013.

[110] S. P. Herath, N. H. Tran, and T. Le-Ngoc. On optimal input distribution and capacity limit of Bernoulli-Gaussian impulsive noise channels. In *Proc. IEEE ICC*, pages 3429–3433, Ottawa, Canada, 2012.

[111] M. Sheikh-Hosseini, G. A. Hodtani, and M. Molavi-Kakhki. Capacity analysis of power line communication point-to-point and relay channels. *Trans. Emerg. Telecommun. Technol.*, 2014.

[112] L. D. Bert, P. Caldera, D. Schwingshackl, and A. M. Tonello. On noise modeling for power line communications. In *Proc. IEEE Int. Symp. Power Line Commun. Appl. (ISPLC)*, pages 283–288, Udine, Italy, 2011.

[113] A. Goldsmith. *Wireless communication*. Cambridge University Press, 2005.

[114] C. Goudemand, M. G. Gazalet, F. X. Coudoux, P. Corlay, and M. Gharbi. Reduced complexity power minimization algorithm for DMT transmission —application to layered multimedia services over DSL. In *Proc. IEEE ICECS*, pages 728–731, Nice, France, 2006.

[115] J. Haring and A. Vinck. OFDM transmission corrupted by impulsive noise. In *Proc. IEEE Int. Symp. Power Line Commun. Appl. (ISPLC)*, pages 9–14, Limerick, Ireland, 2000.

[116] I. F. E. Fatani. *Contribution à l'étude de l'optimisation conjointe source-canal d'une transmission vidéo dans un contexte MIMO sans fil: Application à la vidéo surveillance embarquée pour les transports publics*. PhD thesis, Université de valenciennes, Octobre 2010.

Titre : Contributions à l'étude des communications numériques sur le réseau électrique à l'intérieur des bâtiments : modélisation du canal et optimisation du débit

Résumé : Au cours de ces dernières années, le réseau électrique est devenu un candidat incontournable pour la transmission de données à haut débit à l'intérieur des bâtiments. De nombreuses solutions sont actuellement à l'étude afin d'optimiser ces technologies connues sous le nom Courants Porteurs en Ligne (CPL) ou PLC (Power-Line Communications). La technique MIMO (Multiple-Input Multiple-Output) a été tout récemment transposée au réseau filaire électrique pour lequel différents modes d'alimentation peuvent être envisagés entre la phase, le neutre et la terre. Dans le cadre de cette thèse, nous proposons deux contributions originales à l'étude des communications numériques sur le réseau électrique à l'intérieur des bâtiments. La première contribution concerne la modélisation du canal MIMO-PLC. En repartant d'un modèle du canal paramétrique SISO (Single-Input Single-Output) connu dans la littérature, nous proposons un modèle du canal MIMO en considérant un nouveau paramètre caractérisant la corrélation spatiale. Le modèle proposé permet de représenter fidèlement la corrélation spatiale des mesures effectuées à l'échelle européenne. La deuxième contribution concerne le bruit impulsif présent sur le réseau électrique domestique qui constitue un problème majeur dans les systèmes de communications. Nous proposons une méthode basée sur la notion de capacité de coupure afin d'optimiser le débit moyen dans les systèmes OFDM (Orthogonal Frequency Division Multiplexing) soumis aux bruits impulsifs. D'abord, nous étudions la capacité du système en fonction d'une marge de bruit fournie aux symboles transmis. Ensuite, nous déterminons l'expression analytique de la probabilité de coupure (outage) d'un symbole OFDM en fonction de cette marge, en étudiant de manière détaillée l'interaction entre l'impulsion de bruit et le symbole. A partir de ces deux calculs, nous déduisons la capacité de coupure. Puis, nous proposons une approche qui maximise l'espérance mathématique du débit reçu. Finalement, nous présentons les résultats obtenus dans le cas particulier d'une transmission à haut débit sur PLC en présence de bruits impulsifs.

Mots clés : *Courants porteurs en ligne, MIMO, OFDM, bruit impulsif, modélisation du canal, capacité de coupure.*

Title: Contributions to indoor broadband power-line communications: Channel modeling and data rate optimization

Abstract: In recent years, the electrical network has become an essential candidate for high-speed data transmission inside buildings. Many solutions are currently underway in order to optimize these technologies known under the name of in-home Power-Line Communications (PLC). Multiple-Input Multiple-Output (MIMO) technique has recently been transposed into power-line networks for which different signal feeding possibilities can be considered between phase, neutral and earth wires. In this thesis, we propose two original contributions to indoor broadband PLC. The first contribution concerns the MIMO-PLC channel modeling. Based on a Single-Input Single-Output (SISO) parametric channel model presented in the literature, we propose a MIMO one by considering a new parameter which characterizes the spatial correlation. The proposed model enables an accurate description of the spatial correlation of European MIMO PLC field measurements. The second contribution is related to the impulsive noise present in power-line networks which constitutes a major problem in communications systems. We propose an outage capacity approach in order to optimize the average data rate in Orthogonal Frequency Division Multiplexing (OFDM) systems affected by impulsive noise. First, we study the channel capacity as a function of a noise margin provided to the transmitted symbols. Then we determine the analytical expression of the outage probability of an OFDM symbol in terms of the noise margin, by studying in detail the interaction between the noise impulse and the symbol. Based on the two aforementioned relations, we deduce the outage capacity. Then we propose an approach that enables to maximize the average system data rate. Finally, we present the results in the particular case of indoor broadband PLC in the presence of impulsive noise.

Key words: *Power-line communications, MIMO, OFDM, impulsive noise, channel modeling, outage capacity.*